

## TOPICAL REVIEW

# Low-energy positron interactions with atoms and molecules

C M Surko<sup>1</sup>, G F Gribakin<sup>2</sup> and S J Buckman<sup>3</sup><sup>1</sup> Department of Physics, University of California, San Diego, La Jolla, CA 92093, USA<sup>2</sup> Department of Applied Mathematics and Theoretical Physics, Queen's University, Belfast BT7 1NN, UK<sup>3</sup> Research School of Physical Sciences and Engineering, Australian National University, Canberra, ACT 0200, Australia

Received 22 November 2004, in final form 11 January 2005

Published 8 March 2005

Online at [stacks.iop.org/JPhysB/38/R57](http://stacks.iop.org/JPhysB/38/R57)**Abstract**

This paper is a review of low-energy positron interactions with atoms and molecules. Processes of interest include elastic scattering, electronic and vibrational excitation, ionization, positronium formation and annihilation. An overview is presented of the currently available theoretical and experimental techniques to study these phenomena, including the use of trap-based positron beam sources to study collision processes with improved energy resolution. State-resolved measurements of electronic and vibrational excitation cross sections and measurement of annihilation rates in atoms and molecules as a function of incident positron energy are discussed. Where data are available, comparisons are made with analogous electron scattering cross sections. Resonance phenomena, common in electron scattering, appear to be less common in positron scattering. Possible exceptions include the sharp onsets of positron-impact electronic and vibrational excitation of selected molecules. Recent energy-resolved studies of positron annihilation in hydrocarbons containing more than a few carbon atoms provide direct evidence that vibrational Feshbach resonances underpin the anomalously large annihilation rates observed for many polyatomic species. We discuss open questions regarding this process in larger molecules, as well as positron annihilation in smaller molecules where the theoretical picture is less clear.

**Contents**

1. Introduction	58
2. Theoretical overview	62
2.1. Atoms	62
2.2. Molecules	68
2.3. Positron annihilation on atoms	70
2.4. Positron annihilation on molecules	73

3. Experimental techniques	74
3.1. Positron sources and moderators	74
3.2. Detection techniques	75
3.3. Electrostatic beams	75
3.4. Scattering experiments using electrostatic beams	77
3.5. Buffer-gas positron traps and trap-based beams	82
3.6. Scattering experiments using a trap-based beam	85
3.7. Annihilation experiments	88
4. Positron scattering	91
4.1. Grand total cross sections	91
4.2. Elastic differential cross sections	95
4.3. Vibrational excitation	97
4.4. Electronic excitation	99
4.5. Direct ionization	101
4.6. Positronium formation	102
5. Positron annihilation	105
5.1. Annihilation on atoms	105
5.2. Annihilation on molecules	109
6. Summary and a look to the future	116
Acknowledgments	120
References	120

## 1. Introduction

This paper is a review of the present state of understanding of the interaction of low-energy positrons with atoms and molecules. Emphasis is placed upon recent developments, driven by new capabilities. The use of high-resolution trap-based positron beams for scattering and annihilation experiments is discussed, as well as theoretical advances, such as predicting positron binding to neutral species and the understanding of the effects of virtual positron states and resonances. The reader is referred to previous review material for a discussion of earlier work and aspects of the field not covered here [1–5].

There is an increasing appreciation of the importance of low-energy antimatter for both scientific and technological applications. Fundamental uses of positrons include the formation of neutral antihydrogen atoms, which in turn can be used for testing of QED, the action of gravity on antiatoms, and tests of the CPT theorem [6–8]. Recent predictions of positron bound states with neutral atoms (which are the positron analogues of negative ions) [9] have important implications for positron and positronium chemistry. Interesting predictions for many-body states of antimatter include those for the  $\text{Ps}_2$  molecule [10], Bose-condensed gases of Ps atoms [10] and electron–positron plasmas [11–16]. In astrophysical settings, the annihilation radiation from positrons provides an important tool with which to study a wide range of phenomena [17]. Technological applications of positrons are numerous and increasing. They include PET (positron emission tomography) [18] to study metabolic processes, and the characterization of materials [19, 20], such as low-dielectric-constant insulators for chip manufacture. Positrons offer new ways to study a wide range of other phenomena including plasmas [21], atomic clusters and nanoparticles [16], and a new method to ionize molecules, such as those of biological interest, for mass spectrometry [22].

Many, if not most, of these uses of positrons depend on a quantitative understanding of the basic interactions of positrons with matter. The interaction of positrons with atoms and molecules is a cornerstone of this knowledge. Processes of interest include electronic

excitation, positronium formation, ionization and annihilation for both atoms and molecules, and vibrational and rotational excitation of molecules. From a fundamental point of view, the interaction of a light positively charged particle free from the Pauli exclusion principle and therefore the exchange interaction characteristic of electrons, with the added richness of a positronium channel, provides new tests of our understanding of basic atomic physics.

In the decades following the prediction of the positron by Dirac [23] and its discovery in cosmic rays by Anderson [24], positron atomic physics (e.g., in the range of positron energies  $\lesssim 1 \text{ Ryd} = 13.6 \text{ eV}$ ) progressed relatively slowly. While positrons can be obtained from both radioisotopes and from electron accelerators, the yields of positron sources are weak as compared, for example, to sources of electrons. Furthermore, positrons from either radioisotopes or accelerators typically have a broad spectrum of energies up to and above the electron rest energy,  $mc^2 = 511 \text{ keV}$ , where  $m$  is the electron mass and  $c$  is the speed of light. Thus the spectral weight in the range of interest for low-energy atomic physics studies is small. When positrons interact with matter, they slow down rapidly. While many important phenomena occur that involve the resulting low-energy positrons, these processes proved difficult to study in a precise way before the advent of efficient methods to create low-energy positron beams.

In the late 1940s and early 1950s, Deutsch and collaborators [25, 26] investigated the rate of annihilation of positrons in atomic and molecular gases at atmospheric pressure. These studies can in some sense be regarded as the beginning of modern positron atomic physics. In these experiments, the test gas itself was used to slow an appreciable fraction of the positrons from a radioisotope source to energies characteristic of the temperature of the ambient gas. In this way, the interaction of a thermalized, Maxwellian distribution of positrons with a test gas could be studied. In the course of this work, Deutsch and collaborators discovered the positronium (Ps) atom, which is the bound state of a positron and an electron, and they measured the lifetime of orthopositronium (ortho-Ps). This ortho-Ps atom, which is the spin  $S = 1$  state of the electron–positron pair, decays predominantly by the emission of three gamma quanta and has a lifetime  $\tau_{\text{o-Ps}} = 142 \text{ ns}$ , while para-Ps with spin  $S = 0$  decays into two quanta, each with an energy of  $511 \text{ keV}$ , in a time  $\tau_{\text{p-Ps}} = 0.125 \text{ ns}$ . Deutsch and collaborators also verified, at least in an approximate way, the basic predictions of Dirac [27] for the annihilation rate,  $\lambda$ , of positrons in the presence of a uniform, uncorrelated gas of electrons, namely

$$\lambda = \pi r_0^2 n c, \quad (1)$$

where  $r_0 = e^2/mc^2$  is the classical electron radius (in cgs units), and  $n$  is the electron number density. Since  $r_0 \sim 10^{-4} a_0$ , where  $a_0$  is the Bohr radius, the cross section for annihilation is thus expected to be much smaller than that for a typical atomic scattering process.

Even in Deutsch's work, there were strong indications of other important effects determining the annihilation rate, including the notion that positrons might attach to polyatomic molecules such as freon ( $\text{CCl}_2\text{F}_2$ ). The decay of positrons in molecular gases was further investigated by Paul and Saint-Pierre [28], who studied alkane molecules as large as butane. They found departures from the Dirac annihilation rate by factors as large as 500, and speculated that this might be caused by the formation of positron–molecule bound states. The idea that some of these large annihilation rates might be caused by low-lying virtual states or weakly bound states of a positron and a target was discussed theoretically by Goldanskii and Sayasov [29]. Later, annihilation on molecules was further analysed by Smith and Paul [30], who explored the possibility that these large rates might be caused by vibrational resonances. Work continued in the late 1960s and 1970s using variants of Deutsch's technique to study annihilation rates and the fraction of positrons creating positronium in positron collisions

with atoms and selected molecules. The results of these studies are discussed in detail in the excellent review by Griffith and Heyland [1]. Measurements of positron annihilation processes in gases were also made as a function of test-gas density and temperature and in the presence of an applied electric field [31–36].

However, the separation of specific atomic physics processes and studying them with precision required sources of monoenergetic positrons. Beginning with Cherry [37] and then Groce [38], materials were developed to ‘moderate’ the broad energy spectrum of the positrons to produce beams with appreciable fluxes and energy spreads of a few electron volts or less. These initial technological breakthroughs were followed by many subsequent improvements, one of which was a more efficient MgO moderator [39]. Moderator efficiencies, defined as the number of slow positrons emitted per fast positron, improved from  $10^{-7}$  [38] to  $10^{-3}$  for single-crystal metals such as tungsten [40]. Later, solid noble-gas moderators were developed with efficiencies exceeding 1% [41, 42]. Use of these moderators enabled a wide range of important cross section measurements.

In spite of these developments, the typical energy resolution in these experiments was  $\geq 0.5$  eV. This precluded studies of many important phenomena, including precise studies of threshold effects, study of vibrational and rotational transitions in molecules and other state-resolved positron-impact cross sections. Also precluded were studies of annihilation as a function of positron energy. Recently, such measurements have been made possible by the development of efficient positron accumulators to trap and cool positron plasmas [14, 43]. These cold plasmas are used, in turn, to create beams with much smaller energy spreads (i.e.,  $\Delta\varepsilon \sim 20$  meV) [44, 45]. The success of these experiments is one motivation for the present review.

This review focuses on the current state of understanding of positron interactions with atoms and molecules in the range of energies from  $\sim 0.05$  eV to 100 eV. At these energies positron collisions are expected to be significantly different from the analogous collisions involving electrons. Factors contributing to these differences include the repulsive short-range positron–atom interaction, in contrast to the attractive electron–atom interaction; the absence of exchange interaction for positrons; and the positronium channel, which appears to have many important consequences for low-energy positron scattering.

For targets with ionization potentials  $E_i < 6.8$  eV (i.e., the ground-state binding energy of positronium), the Ps-formation channel is open at all energies. Even for targets with  $E_i > 6.8$  eV the Ps-formation threshold is never far away. Hence, taking into account this process (either virtual or real) is mandatory in positron scattering calculations. It leads to stronger correlation effects in positron scattering (i.e., as compared with electron scattering), caused by the *attractive* electron–positron Coulomb interaction. Rigorous treatment of this process is difficult, especially for many-electron targets. This remains one of the most significant challenges for positron scattering theory.

In this review we discuss elastic, quasi-elastic, vibrational and electronic excitation, ionization and positronium-formation cross sections. Emphasis is placed on recent developments, such as the first state-resolved studies of vibrational and electronic excitation processes. The current state of understanding regarding selected differential scattering cross sections is also discussed.

Where data are available for both electron and positron scattering processes, comparisons of the cross sections are made. From these comparisons, some qualitative features are evident. At low energies, the magnitudes of electron and positron cross sections can be quite different with perhaps a surprising result that, in many cases, positron cross sections are larger. On the other hand, while resonance phenomena, in which a projectile binds to the target for a short period of time, are ubiquitous in electron scattering, they appear to be much less common in

positron scattering. Finally, it is of interest to note that the integral, positron-impact cross sections for vibrational excitation of molecules studied thus far have a sharp rise at onset, possibly indicating some kind of resonant enhancement. The underlying physics of this process has yet to be elucidated.

Another area in which a significant progress has been made is the study of positron annihilation on atoms and molecules below the threshold for positronium formation. As indicated by equation (1), the cross section for annihilation on a free electron (neglecting the electron–positron Coulomb interaction) is  $\sigma = \pi r_0^2(c/v)$ , where  $v$  is the relative velocity of the annihilating pair. Even allowing for possible enhancements due to resonances, typical annihilation cross sections are very small and therefore difficult to measure. The development of efficient positron traps enabled new kinds of measurements for dilute atomic and molecular gases (including gases of large molecules) *in situ* in the presence of an ambient temperature positron gas. In particular, the spectra of gamma quanta from annihilation in binary collisions and the dependence of annihilation rates on positron temperature (for a Maxwellian distribution of positrons in a trap) have been measured.

Subsequent to these measurements, the development of a tunable, trap-based positron beam enabled high-resolution studies of annihilation for atoms and molecules as a function of positron energy. These experiments provide the first direct evidence of positron binding to molecules and the first measurements of the binding energies of these complexes [46, 47]. The experiments and complementary theoretical work explain in a natural way the four-decade-old puzzle concerning very large annihilation rates observed for certain classes of molecules such as hydrocarbons. These large rates arise from the population of positron–molecule quasi-bound states or vibrational Feshbach resonances. Therefore in molecules, the annihilation process provides a unique way to monitor the interaction between the degrees of freedom associated with the quantal motion of the light electrons and positron and those associated with the nuclear motion. While a qualitative picture of this process has been developed, many open questions remain, and we discuss possible new experiments and calculations to address these issues. We hope that an increased understanding achieved in the positron case may help to elucidate open questions in the important area of low-energy electron collisions with molecules, such as the formation of long-lived molecular negative ions and the process of dissociative attachment.

There are areas of positron atomic physics not covered in this review. For example, experiments in atmospheric and higher pressure gases show evidence of density-dependent effects, indicative of positron interactions with several atoms or molecules [4, 48]. Another important area is *positronium* scattering from atomic and molecular targets [5, 49]. The technical challenges involved in positronium scattering experiments are even more severe than those in positron scattering. In addition to producing a monoenergetic positron beam, one must then convert the positrons to Ps atoms, which is typically accomplished by the relatively inefficient process of charge exchange in a gas cell.

Finally, it is of interest to put this review in historical perspective. The argument is frequently made that recent developments in positron technology have led to new insights in positron atomic physics. However, while the technology has progressed, our standards for precise understanding and our appreciation of what can be done have also continued to progress. As pointed out by Griffith and Heyland in 1978 [1], Bransden made the following insightful observation a decade earlier [50]:

‘The points of contact between theory and experiment are not as many as could be wished and are somewhat indirect. The reason for this is that there are at present no controlled mono-energetic beams of low-energy positrons.’

With some qualification, we can make the same statement today: the current state of the art in positron atomic physics experiments is still not comparable with what can be done with electrons. At the time of Griffith and Heyland's review, beams with 1 eV resolution were just becoming available. At this writing, beams with  $\sim 20$  meV resolution are now in use. The next frontier of 1 meV and sub-millivolt resolution positron beams still awaits us. We have some confidence that this frontier can also be achieved [16], and expect that it will open new perspectives on positron atomic physics.

This review is organized in the following way. An overview is presented of the theory of positron interactions with atoms and molecules, and then the experimental techniques used to study positron scattering and annihilation processes are described. The current state of the knowledge of positron scattering processes is reviewed, followed by a review of positron annihilation phenomena involving atoms and molecules. The review concludes with a summary of key results and a discussion of open questions that will benefit from further work.

## 2. Theoretical overview

### 2.1. Atoms

*2.1.1. Low energy scattering, virtual and bound states—a many-body theory approach.* We begin by discussing the physics of the positron–atom interaction at low energies. Because of the repulsion between the positron and atomic nucleus, the static, short-range atomic potential is repulsive. As a result, the positron does not penetrate far inside the atom. When the positron is outside the atom, it polarizes the electron cloud, giving rise to a long-range, attractive *polarization potential*,  $V(r) = -\alpha_d e^2 / 2r^4$ , where  $\alpha_d$  is the dipole polarizability of the atom. This asymptotic form is identical for electrons and positrons. At low positron energies, for which large separations play a dominant role, this polarization potential can overcome the effects of the short-range repulsion, resulting in a net positron–atom attraction.

For energies below the Ps-formation threshold there is an additional mechanism that contributes to the positron–atom attraction. It originates from virtual Ps formation, whereby one of the atomic electrons joins the positron temporarily to form Ps. The resulting short-range attractive interaction is similar to covalent molecular bonding, where the system can be thought of as a superposition of  $A + e^+$  and  $A^+ + \text{Ps}$  states. Due to the light mass of the positron, this attraction does not necessarily lead to a stable  $e^+A$  ‘molecule’. However, for atoms with larger dipole polarizabilities, the net attraction is strong enough to produce either low-lying positron–atom virtual states or weakly bound states [9, 51, 52].

Many-body theory provides a method to compare quantitatively the relative importance of various correlation contributions to the positron–atom interactions. This approach has its origin in Feynman's work on quantum electrodynamics [53], where the now-famous ‘diagrams’ were first introduced. These diagrams serve as a short hand for lengthy algebraic expressions, and they provide a universal bookkeeping tool for the terms in perturbation-theory expansions. While completely rigorous, this technique also facilitates the use of intuition and provides unique physical insights into quantum processes.

Within the formalism of many-body theory, the scattering of a positron (or electron) from an atom in the ground state can be described by the *Dyson equation* (see, for example, [54]),

$$H_0 \psi(\mathbf{r}) + \int \Sigma_\varepsilon(\mathbf{r}, \mathbf{r}') \psi(\mathbf{r}') d\mathbf{r}' = \varepsilon \psi(\mathbf{r}), \quad (2)$$

where  $H_0$  is the Hamiltonian of the positron (electron) moving in the static field of the target (usually described in the Hartree–Fock approximation),  $\psi(\mathbf{r})$  is the quasiparticle wavefunction



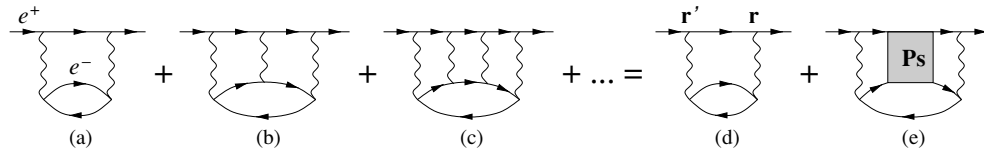


**Figure 1.** Many-body theory expansion of the correlation potential,  $\Sigma$ . Diagram (a) describes a process where the positron (upper line) acts on the target by means of its Coulomb potential (wavy lines) and produces an electron–hole pair (the excited electron is shown by a line with an arrow to the right, and a hole in one of the ground-state orbitals by a line with an arrow to the left). This *polarization* of the target acts back on the positron, giving rise to the long-range polarization potential. Diagrams (b), (c) and higher order terms, that include more Coulomb interactions between the positron and excited electron, describe the effect of (virtual) Ps formation. Their sum,  $\Sigma^{(\text{Ps})}$ , is shown by diagram (e) with a shaded block to indicate virtual Ps.

of the projectile,  $\varepsilon$  is its energy, and  $\Sigma_\varepsilon(\mathbf{r}, \mathbf{r}')$  is a nonlocal energy-dependent correlation potential. This correlation potential accounts for the interaction between the target and projectile beyond the static approximation. It can be expressed as a perturbation series in the residual electron–positron and electron–electron interactions. Although equation (2) has the form of a single-particle Schrödinger equation, it incorporates all of the many-body effects via  $\Sigma_\varepsilon(\mathbf{r}, \mathbf{r}')$ . At large distances  $\Sigma_\varepsilon(\mathbf{r}, \mathbf{r}')$  has the behaviour of the (local) polarization potential,

$$\Sigma_\varepsilon(\mathbf{r}, \mathbf{r}') \approx -\frac{1}{2}\alpha_d e^2 / r^4 \delta(\mathbf{r} - \mathbf{r}'). \quad (3)$$

If the static field of the target is included in the zeroth-order Hamiltonian,  $H_0$ , the perturbation expansion of  $\Sigma$  starts with the second-order diagram shown in figure 1(a). This diagram (together with some higher order corrections to the electron–hole loop) is responsible for the long-range behaviour of equation (3), and we denote its contribution to the correlation potential by  $\Sigma^{(\text{pol})}$ . With the corresponding exchange diagrams added, this approximation gives a good description of the electron–atom interaction (see below).

In positron–atom scattering, the approximation based on  $\Sigma^{(\text{pol})}$  is found to be deficient [55–57]. The physical reason for this is that  $\Sigma^{(\text{pol})}$  does not account for the contribution of virtual Ps to the positron–target interaction. To include this effect, one needs to consider an infinite series of diagrams with repeated electron–positron interactions (i.e., the diagrams (b) and (c) in figure 1 and similar higher order terms). The sum of this series gives the virtual Ps contribution to the correlation potential,  $\Sigma^{(\text{Ps})}$ . While in earlier works it was obtained by using an approximate Ps propagator [51, 52, 57], it can now be calculated consistently by summing an infinite series of electron–positron ladder diagrams [58–60]. The strength of  $\Sigma^{(\text{Ps})}$  is comparable to that of  $\Sigma^{(\text{pol})}$ . In contrast, the ladder diagram series in electron–atom scattering is sign-alternating (because of the Coulomb *repulsion* between the electrons), and it represents only a small correction to  $\Sigma^{(\text{pol})}$ .

The role of the correlation potential in low-energy positron and electron scattering is illustrated by figure 2, which shows the  $s$ -wave phase shifts for Ar. In the static approximation (short-dashed curves), the positron and electron phase shifts are negative and rather similar, indicating net repulsion in both cases. For the positron, this is a result of the repulsive static potential, while for the electrons, this is a manifestation of the Pauli principle. The latter requires the scattering electron’s wavefunction to be orthogonal to the wavefunctions of the atomic electrons, and this effect tends to expel the extra electron from the atomic core. The inclusion of the polarization potential,  $\Sigma^{(\text{pol})}$ , makes the phase shifts positive at low momenta, indicating that polarization overcomes the static repulsion. Accordingly, the scattering lengths,  $a$ , defined by the  $s$ -wave phase shift  $\delta_0 \approx -ak$  (in the limit that the particle’s wave number  $k \rightarrow 0$ ), become negative in both cases. As a result, the  $s$ -wave phase shift now passes through

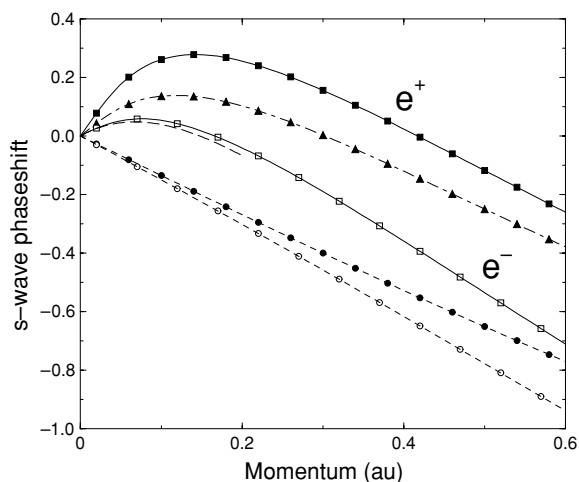


**Figure 2.** The  $s$ -wave phase shifts for scattering from Ar: electrons (open symbols) and positrons (full symbols): dashed curve with circles, static target field (including exchange, for the electron case); solid curve with squares, correlation potential included (i.e.,  $\Sigma^{(\text{pol})}$  for the electron [61], and  $\Sigma^{(\text{pol})} + \Sigma^{(\text{Ps})}$  for the positron [58, 59]); dot-dash curve with triangles,  $\Sigma^{(\text{pol})}$  only included for the positron. Thick long-dashed curve at low momenta is the electron  $s$ -wave phase shift from a fit to measured total cross sections [64].

zero at a small but nonzero projectile momentum, a behaviour which manifests itself in the Ramsauer–Townsend minima in the elastic scattering cross sections. Note that the effect of  $\Sigma^{(\text{pol})}$  is greater for the positron than the electron, because in the electron case,  $\Sigma^{(\text{pol})}$  contains some ‘repulsive’ exchange diagrams. Note also that the electron phase shift obtained with  $\Sigma^{(\text{pol})}$  is close to that inferred from experiment, and the use of  $\Sigma^{(\text{pol})}$  for the electron yields accurate elastic cross sections at low energies, see, e.g., [61–63].

As can be seen in figure 2, when the virtual Ps contribution is included in the positron correlation potential,  $\Sigma = \Sigma^{(\text{pol})} + \Sigma^{(\text{Ps})}$ , the positron phase shift becomes considerably larger, indicating a much greater attraction to the target. This can also be seen from the magnitude of the corresponding scattering lengths, namely  $a = -4.4a_0$  for the positron as compared with  $a = -1.5a_0$  for the electron. As mentioned above, the inclusion of  $\Sigma^{(\text{Ps})}$  is crucial in obtaining the correct scattering and annihilation cross sections for the positron (see also [52, 60]).

Thus the effects of polarization and virtual Ps formation overcome the static positron–target repulsion. For targets with large dipole polarizabilities, this leads to a strong attractive potential for the positron. As shown in table 1, this manifests itself, in particular, in large negative values of the scattering lengths in heavier noble gases. For Ar, Kr and Xe, the scattering lengths are negative, and their magnitudes are much larger than the mean radii of the corresponding atoms, i.e.,  $|a| \gg a_0$ . In this situation, the elastic scattering cross sections at low energy,  $\sigma_{\text{el}} \approx 4\pi a^2$ , are much greater than the geometric sizes of the targets. This enhancement can be viewed as arising from the existence of a *virtual level* for the projectile, at an energy given by  $\varepsilon = \hbar^2/(2ma^2) = 1/2a^2$ .<sup>4</sup> These virtual levels also lead to enhanced positron annihilation cross sections [29, 52, 56].

Based upon their many-body theory analysis of the role of  $\Sigma^{(\text{pol})}$  and  $\Sigma^{(\text{Ps})}$  in positron–atom attraction in noble gases, Dzuba *et al* [51] predicted positron binding to neutral atoms and calculated the positron binding energies for Mg, Zn, Cd and Hg. While this calculation did

<sup>4</sup> In section 2, atomic units,  $\hbar = m = e^2 = 1$ , are used.



**Table 1.** Positron scattering lengths and energies of positron–atom virtual or bound states.

Atom	He	Ne	H	Ar	Kr	Xe	Be	Zn	Cu	Cd	Mg
$\alpha_d$ (au) <sup>a</sup>	1.38	2.68	4.5	11.1	16.7	27.1	38	38	41	49	72
$E_i$ (eV)	24.6	21.6	13.6	15.8	14.0	12.1	9.32	9.39	7.73	8.99	7.64
$a$ (au) <sup>b</sup>	−0.42	−0.43	−	−4.4	−10.1	−81	12.6	11.6	9.45	9.05	5.6
	−0.53	−0.61	−	−5.3	−10.4	−45					
	−0.48		−2.1								
$\varepsilon$ (eV) <sup>c</sup>				0.70	0.13	$2 \times 10^{-3}$	−0.086	−0.101	−0.152	−0.166	−0.439
								−0.23	−0.170	−0.35	−0.87

<sup>a</sup> Dipole polarizabilities for noble gases and Mg [65], and for other atoms [66].

<sup>b</sup> Scattering lengths for atoms with bound states (Be–Mg) are estimated from the relation  $\varepsilon = -1/2a^2$ . For noble gases: first row, from many-body calculations [58–60]; second row, from polarized-orbital calculations [67]; third row, values for hydrogen and helium from Kohn variational calculations [68] and [69] respectively.

<sup>c</sup> Energies of positron–atom virtual states for heavier noble gases are estimated as  $\varepsilon = 1/2a^2$ ; bound state energies are calculated for Be–Mg: first row, stochastic variational method or configuration interaction (CI) [9]; second row, many-body theory [51], and a combination of CI and many-body theory for Cu [70].

not constitute a proof of binding, it indicated that many atoms with large dipole polarizabilities should be capable of binding positrons<sup>5</sup>. Two years later, positron binding to Li was proved by a calculation that employed the stochastic variational method (SVM, see below) [71]. Since then many atoms have been shown to form bound states with positrons (see [9] for a review). The binding energies of some of these states are listed in table 1, where the entries are ordered according to the strengths of their dipole polarizabilities. Here one can observe the evolution from positron virtual states to weakly bound states as the inverse scattering length,  $a^{-1}$ , passes through zero and changes sign between Xe and Be.

While there are differences between the predictions of the binding energies found using various methods (e.g., the use of an approximate  $\Sigma^{(\text{Ps})}$  in [51] may have led to an overestimate of the positron–atom attraction), the very fact of positron binding with neutral atoms is now firmly established theoretically. However, experimental verification of positron binding to atoms is still lacking. (As discussed below, the situation for positron–*molecule* bound states is quite different in that annihilation experiments provide strong evidence for these states.) Suggestions to study positron–atom bound states experimentally include measuring the charge transfer reaction  $A^- + e^+ \rightarrow e^+A + e^-$  and detecting either the positive ions  $A^+$  produced by positron annihilation in  $e^+A$  or the electrons produced by the reaction [72, 73], or by measuring the forward–backward asymmetry of the low-energy positron–atom differential cross section, which is sensitive to the *sign* of the scattering length [74].

The values of the positron scattering lengths for the noble-gas atoms obtained in the many-body theory calculations are generally in agreement with those obtained using the simpler *polarized-orbital* (PO) method. This method, which was proposed in [75], entails calculating the response of an atom in the Hartree–Fock approximation to a perturbation due to an external Coulomb potential of a point charge at a fixed position  $r$ , in the linear approximation. One then calculates the effect of the distorted atomic charge distribution on the point charge, which produces a local PO potential,  $V_{\text{PO}}(r)$ . This contribution is then added to the static potential of the target (e.g., see [76]). Since  $V_{\text{PO}}(r)$  is of second order in the charge of the projectile, it does not depend on the sign of the charge and is the same for the electron

<sup>5</sup> For atoms with  $E_i > 6.8$  eV, positron binding ensures that the system is stable with respect to dissociation into a positive ion and Ps.

and the positron. In practice, the contribution of the monopole part of the Coulomb potential is discarded, and only the dipole term is retained in  $V_{\text{PO}}(r)$  for the electron; in contrast, all multipoles are included for the positron. While this procedure lacks rigour, it produces elastic scattering cross sections in better agreement with the experimental data (see, e.g., [77]).

From the point of view of many-body theory,  $V_{\text{PO}}(r)$  corresponds to a calculation of the correlation potential  $\Sigma_\varepsilon(\mathbf{r}, \mathbf{r}')$  from diagram (d) in figure 1, with additional corrections which account for correlations within the target and correspond to a description of the atomic polarization in the random phase approximation. The assumption of a fixed position  $r$  in the PO method means that the energies of the intermediate, virtual states of the projectile are neglected. Mathematically, this leads to an *overestimation* of  $\Sigma^{(\text{pol})}$  and a contraction of the vertices  $\mathbf{r}$  and  $\mathbf{r}'$  in figure 1(d), thus producing a *local* potential. This *adiabatic* approximation might be appropriate for a heavy particle, but it is more difficult to justify in the case of electrons or positrons.

When the PO method is used for electrons (where there is no additional strong correlation contribution analogous to  $\Sigma^{(\text{Ps})}$ ), this overestimation is mitigated by omitting all multipoles higher than the dipole in  $V_{\text{PO}}(r)$ . Similarly, in the case of positrons, comparison of PO calculations with and without higher multipoles [78] shows that *the dipole term alone* produces results close to those obtained using  $\Sigma^{(\text{pol})}$  (with all multipoles included). Remarkably, the addition of higher multipoles, as per [76], and the overestimation of  $\Sigma^{(\text{pol})}$  by the PO method mimics the effect of including  $\Sigma^{(\text{Ps})}$  in the correlation potential [52]. This explains a largely fortuitous accord between the results of the PO method and more sophisticated many-body theory positron–atom calculations.

### 2.1.2. Variational and coupled-channel methods—Ps formation and other inelastic processes.

Positron scattering from simple targets, such as hydrogen, helium or alkali-metal atoms (considered as systems of one electron in the field of the ion core) can be treated successfully using few-body methods. A common feature of these approaches is that, unlike the many-body theory, they operate with the total wavefunction of the system. For H and He the most accurate results have been obtained using Kohn variational and similar methods, with the paper by Schwartz [68] setting the standard for decades thereafter. Thus, for *s*-wave scattering from a one-electron target below the Ps-formation threshold, the total wavefunction can be represented as

$$\Psi(\mathbf{r}_1, \mathbf{r}) = \frac{\chi(r)}{\sqrt{4\pi kr}} \Phi_0(\mathbf{r}_1) + \sum_{l,m,n \geq 0} C_{lmn} \exp(-\alpha r - \beta r_1 - \gamma |\mathbf{r} - \mathbf{r}_1|) r^l r_1^m |\mathbf{r} - \mathbf{r}_1|^n, \quad (4)$$

where  $\chi(r)$  is a positron scattering wavefunction ( $\chi(r) \propto \sin(kr + \delta_0)$  at large distances),  $\Phi_0(r_1)$  is the target ground-state wavefunction,  $l$ ,  $m$  and  $n$  are integers, and  $\alpha$  and  $\beta$  are positive constants. The second term on the right-hand side represents correlations.

To solve the scattering problem one can adopt a particular form of the scattering wavefunction, e.g.,  $\chi(r) = \sin kr + \tan \delta_0^t \cos kr (1 - e^{-\lambda r})$ , and find the trial phase shift  $\delta_0^t$  and the coefficients  $C_{lmn}$  by varying Kohn's expression,

$$\tan \delta_0 = \tan \delta_0^t + 2k \int \Psi(E - H) \Psi \, d\mathbf{r}_1 \, d\mathbf{r}, \quad (5)$$

where  $E$  and  $H$  are the total energy and Hamiltonian of the system. To ensure convergence the calculation is run for a range of  $N$ , which limits the number of correlation terms,  $|l + m + n| \leq N$  [68, 79]. This method was also used to study positron–He scattering [80] and generalized to positron energies above the Ps-formation threshold but below any other inelastic scattering threshold (i.e., the so-called Ore gap) for H and He [81–84].

In the latter case, the wavefunction in equation (4) will also contain an extra term proportional to  $R^{-1}\phi_0(\mathbf{r} - \mathbf{r}_1) \cos KR$  (at large distances), where  $\phi_0$  is the ground-state Ps wavefunction, and  $K$  and  $R$  are the Ps momentum and centre of mass coordinate, respectively. A similar term,  $R^{-1}\phi_0(\mathbf{r} - \mathbf{r}_1) e^{-\kappa R}$ , where  $\frac{1}{2}k^2 - E_i = -\frac{1}{4}\kappa^2 - \frac{1}{4}$ , is known to improve the convergence of positron–atom calculations below the Ps-formation threshold, which demonstrates the importance of virtual Ps [85].

Another approach based on equation (4) uses the Feshbach projection operator formalism and converts the scattering problem into a single-particle Schrödinger equation for the positron wavefunction  $\chi(r)$  with an *optical potential*, similar to equation (2) [86]. Its advantage is that the phase shift thus obtained provides a lower bound for the true phase shift (achieved for  $N \rightarrow \infty$ ). Recently, the Kohn variational method was used to calculate positron scattering and annihilation from Cu- and H-like ions, using a configuration-interaction-type representation of the second term in equation (4) [87, 88]. While such calculations are limited to simple targets with one or two active electrons, they provide useful benchmarks for other theoretical approaches.

A class of *coupled-channel* or *close-coupling* methods is based on representation of the total wavefunction as an expansion over the states of the target,  $\alpha$ , and if Ps formation is treated explicitly, the states of the Ps atom and ionic residue,  $\beta$ ,

$$\Psi(\mathbf{r}_i, \mathbf{r}) = \sum_{\alpha} \Phi_{\alpha}^N(\mathbf{r}_i) F_{\alpha}(\mathbf{r}) + \sum_{\beta} \hat{A} \Phi_{\beta}^{N-1}(\mathbf{r}_{i \neq j}) \phi_{\beta}(\rho_j) f_{\beta}(\mathbf{R}_j). \quad (6)$$

Here  $\mathbf{r}_i$  stands for the set of  $N$  target electron coordinates,  $\Phi_{\alpha}^N(\mathbf{r}_i)$  are the wavefunctions of the target,  $\mathbf{r}$  is the positron coordinate,  $F_{\alpha}(\mathbf{r})$  are the positron channel functions,  $\Phi_{\beta}^{N-1}(\mathbf{r}_{i \neq j})$  are the wavefunctions of the target without an electron  $j$ ,  $\phi_{\beta}(\rho_j)$  are the internal states of Ps ( $\rho_j = \mathbf{r} - \mathbf{r}_j$ ),  $f_{\beta}(\mathbf{R}_j)$  are the Ps channel functions,  $\mathbf{R}_j = (\mathbf{r} + \mathbf{r}_j)/2$  is the Ps centre of mass coordinate, and  $\hat{A}$  is the antisymmetrization operator. The Schrödinger equation,  $H\Psi = E\Psi$ , is then projected onto the target states and converted into a set of coupled single-particle equations for  $F_{\alpha}$  and  $f_{\beta}$ . These equations can then be solved using  $R$ -matrix methods (see, e.g., [89–91]). The asymptotic behaviour of  $F_{\alpha}(\mathbf{r})$  as  $r \rightarrow \infty$  yields the amplitudes of elastic scattering ( $\alpha = 0$ ) as well as those of target excitation ( $\alpha > 0$ ), while the asymptotic behaviour of  $f_{\beta}(\mathbf{R}_j)$  yields ground- and excited-state Ps-formation amplitudes. An alternative approach is to use a momentum-space representation of the positron and Ps motion, and solve the coupled-channel Lippmann–Schwinger equations for the scattering amplitudes (e.g., see [92–94]).

To treat the excitation of target electrons into the continuum and to provide convergence, target pseudostates  $\Phi_{\alpha}^N(\mathbf{r}_i)$  have been used (e.g., see [95–97]), including those obtained by diagonalizing the target Hamiltonian in the space of square-integrable functions (the so-called convergent close-coupling method, or CCC) [98]. Pseudostates that lie above the target ionization limit represent the continuum, and the cross section for populating these states describes positron-impact ionization.

In principle, if one used a complete set of target states  $\Phi_{\alpha}^N(\mathbf{r}_i)$ , the wavefunction of the system could be formally represented by the first (single-centre) term on the right-hand side of equation (6) alone, without including the Ps channels. This understanding has been tested by a convergent-close-coupling method calculation below the Ps-formation threshold [98]. The inclusion of Ps channels introduces an explicit dependence on the electron–positron separation and makes the calculation of the interaction matrix elements more involved. The ability to include sets of target and Ps pseudostates represented a major advance [91, 94, 97]. Such calculations yield converged results with a much smaller total number of channels [96].

Of course, the Ps channels are also necessary to obtain Ps-formation cross sections. The inclusion of these channels is crucial in situations such as positron scattering from alkali-metal atoms, where the Ps-formation channel is open at all energies [99, 100]. Apart from the calculations of elastic, electronic excitation, Ps-formation and direct ionization cross sections for hydrogen [94, 97, 98, 101, 102] and quasi-one-electron alkali atoms [99, 100], the coupled-channel method has been applied to positron elastic and inelastic scattering from He [103, 104]. Coupled-channel approaches provide total and Ps-formation cross sections for alkali atoms from Li to Cs in good overall agreement with those measured by the Detroit group (see [105] and references therein). In particular, the calculations show a pronounced growth of Ps formation in excited states in the alkali-atom sequence. It correlates with the decrease of the ionization potential of the target atom and increasingly diffuse character of the valence electron orbital [103].

Another approach uses the total wavefunction in the form of a linear combination of explicitly correlated Gaussians,

$$\Psi(\mathbf{r}_i, \mathbf{r}) = \sum_n C_n \exp\left(-\frac{1}{2}\mathbf{x}^T \mathbf{A}_n \mathbf{x}\right) \chi_S, \quad (7)$$

where  $\mathbf{x}$  is the vector of Jacobi coordinates,  $\mathbf{A}_n$  are the matrices of nonlinear variational parameters,  $C_n$  are the linear variational parameters, and  $\chi_S$  is the spin function. The wavefunction in equation (7) allows one to compute the Hamiltonian matrix elements quickly; it has been instrumental in predictions of positron bound states in few-active-electron systems using the SVM (e.g., He  $2^3S$ , Li, Be, Na, Mg, Cu, Zn and Ag) (see [71] and the review [9]). This method was also used to calculate low-energy Ps-atom scattering [106, 107]. The values of Ps–H and Ps–Ps scattering lengths from these calculations are probably the most precise to date.

The positive value of 2.95 au, predicted for the scattering length in the system of two ortho-Ps atoms with parallel spins, deserves special mention. It indicates that the atoms repel each other. This then implies the existence of a long-lived Bose–Einstein condensate (BEC) of spin-polarized Ps atoms. This novel many-electron–many-positron state is predicted to form at or near room temperature (depending upon the atom density), with its lifetime limited only by the annihilation of the ortho-Ps atoms [108, 109].

## 2.2. Molecules

The interaction of a low-energy positron with molecules containing few atoms has much in common with positron–atom interactions. When the de Broglie wavelength or inverse wavenumber of the positron is greater than the size of the target (e.g., for thermalized positrons at 300 K,  $\varepsilon \sim 25$  meV and  $k^{-1} \sim 20a_0$ ), the positron does not discern the internal structure of the molecule. Besides the static interaction, polarization and virtual Ps formation are the important effects that must be considered. In addition, if the molecule possesses a permanent electric dipole moment  $\mu$ , the long-range  $\mu \cdot \mathbf{r}/r^3$  interaction can have a significant effect, especially if the dipole moment is large. Thus, calculations predict that positrons can form bound states with strongly polar diatomic molecules, as indicated in table 2. This result is quite natural, given that their dipole moments exceed the critical value of 1.625 Debye, beyond which a dipole potential supports an infinite sequence of bound states [110]. Even a static Hartree–Fock calculation yields positive positron affinities, although correlations lead to much larger binding energies (see table 2). Hartree–Fock calculations also predict positron binding to larger polar molecules, such as urea,  $\text{CON}_2\text{H}_4$  ( $\mu = 3.99$  Debye) and acetone  $\text{C}_3\text{H}_6\text{O}$  ( $\mu = 3.26$  Debye) [111].

**Table 2.** Positron affinities (PA) of small polar molecules.

Property	LiH	BeO	LiF
$\mu$ (Debye)	5.88	6.26	6.33
$E_i$ (eV)	7.7	10.1	11.3
PA <sup>a</sup> (eV)	0.906	0.762	0.473
	0.161	0.299	0.181

<sup>a</sup> Positron affinities (binding energies): first row, diffusion Monte Carlo calculations [112] (the value for LiH is close to those obtained using SVM [113], and explicitly correlated Gaussians [114]); second row, self-consistent-field (Hartree–Fock) calculations [115].

Turning to positron–molecule scattering, the multicentred nature of the problem and the need to consider several valence electrons, in addition to strong correlation effects, make it a difficult problem to treat *ab initio*. Even for the hydrogen molecule, which to date has received most attention from theorists, there is a lack of definitively converged results. Here positron scattering again proves to be a greater challenge than its electron counterpart. At low energies ( $\sim 1$  eV), the best calculations for  $H_2$  are probably those done using the Kohn variational method [116, 117]. For example, the lowest  $\Sigma_g^+$  partial-wave cross section calculated using this approach is in agreement with experimental data below 2 eV (see section 4).

*R*-matrix calculations [118] demonstrate the importance of short- and long-range correlation effects, but still underestimate the elastic scattering cross sections at low energies by a factor of 2 due to inadequate representation of ‘short-range polarization’ effects (i.e., virtual Ps formation). The Kohn and *R*-matrix methods have also been applied to positron scattering from  $N_2$  [119, 120]. The latter work also considered vibrationally inelastic cross sections *ab initio*. The elastic cross sections predicted by both calculations are, however, considerably smaller than the experimental values at energies below 3 eV.

Another *ab initio* approach to positron–molecule scattering is based on the Schwinger multichannel variational method [121]. This technique calculates the scattering amplitude in the following form:

$$f(\mathbf{k}_f, \mathbf{k}_i) = -\frac{1}{2\pi} \sum_{m,n} \langle S_{\mathbf{k}_f} | V | \chi_m \rangle (A^{(+)-1})_{mn} \langle \chi_n | V | S_{\mathbf{k}_i} \rangle. \quad (8)$$

Here,  $\mathbf{k}_i$  and  $\mathbf{k}_f$  are the initial and final positron momenta,  $S_{\mathbf{k}}$  is the product of a target state and a plane wave,  $V$  is the positron–target interaction potential,  $\chi_n$  are the  $(N + 1)$ -particle configurations determined variationally, and  $A^{(+)} = PVP + Q\hat{H}Q - VG_p^{(+)}V$ , where  $P$  and  $Q$  are projection operators onto open and closed channels, respectively,  $\hat{H}$  is the energy minus the total Hamiltonian of the system, and  $G_p^{(+)}$  is the noninteracting positron Green’s function in the  $P$  space. The advantage of this method is that the configuration functions,  $\chi_n$ , can be constructed from electron and positron orbitals using a convenient Gaussian basis. It has been applied to elastic scattering calculations for  $H_2$ ,  $CH_4$ ,  $N_2$ ,  $C_2H_2$ ,  $C_2H_4$ ,  $CO_2$  and  $SF_6$  [121–124], and electronic excitation of  $H_2$  and  $N_2$  by positrons [125, 126]. These calculations also highlight the greater difficulty of the positron scattering problem compared to the electron case [121]. It was found that adding extra orbitals centred just outside the target improved the results [127, 128]. Physically, such orbitals allow one to have a better description of virtual-Ps-type correlations. Good agreement was obtained for the total scattering cross sections at energies between 1 and 10 eV for many-electron targets such as  $N_2$ ,  $C_2H_2$  and  $C_2H_4$  [122, 123]. Large values of the elastic scattering cross sections for  $C_2H_2$  and  $C_2H_4$  at zero energy obtained in these calculations indicate the presence of positron virtual states (see also [129]).

*Ab initio* treatment of correlation effects in positron–molecule interactions becomes increasingly more difficult for polyatomic targets and processes involving nuclear degrees of freedom, such as vibrational excitation. However, a calculation becomes feasible if the positron–molecule interaction is approximated by means of a local potential (see, e.g., [130]),

$$V(\mathbf{r}) = V_{\text{st}}(\mathbf{r}) + V_{\text{pol}}(\mathbf{r}), \quad (9)$$

where  $V_{\text{st}}(\mathbf{r})$  is the (repulsive) static potential of the molecule, and  $V_{\text{pol}}(\mathbf{r})$  is the correlation–polarization potential. This approach is similar to the polarized-orbital method where one uses  $V_{\text{pol}}(\mathbf{r}) = V_{\text{PO}}(r)$ , but many other different forms for  $V_{\text{pol}}(\mathbf{r})$  have also been used. A popular choice for a ‘parameter-free’ potential is based on the positron–electron-gas model for the short-range part  $V_{\text{pol}}(\mathbf{r}) = V_{\text{corr}}(\mathbf{r})$  at  $r < r_c$ , joined with the long-range asymptotic form  $V_{\text{pol}}(\mathbf{r}) = -\alpha/2r^4$  at  $r = r_c$  [131], where  $r_c$  is the radius at which the two expressions are equal. In this form, the method was applied to positron scattering from CO, CH<sub>4</sub> and SiH<sub>4</sub> [131, 132], and more recently to larger polyatomic targets, such as C<sub>2</sub>H<sub>2</sub>, C<sub>2</sub>H<sub>4</sub>, C<sub>2</sub>H<sub>6</sub>, NH<sub>3</sub>, H<sub>2</sub>O, CF<sub>4</sub> and SF<sub>6</sub> [133, 134]. In many cases, the results are in good agreement with experimental integral cross sections at few-eV positron energies.

The potential thus constructed depends on the nuclear coordinates as parameters. It therefore provides coupling between the positron motion and molecular vibration (or rotation). Separating the angular and radial parts of the positron wavefunction, one can then set up a body-fixed vibrational close-coupled set of equations (see, e.g., [135]),

$$\left[ \frac{d^2}{dr^2} - \frac{l(l+1)}{r^2} + k_v^2 \right] u_{vl, \nu_0 l_0}^\Lambda(r) = 2 \sum_{v'l'} V_{vl, v'l'}^\Lambda(r) u_{v'l', \nu_0 l_0}^\Lambda(r), \quad (10)$$

where  $u_{vl, \nu_0 l_0}^\Lambda(r)$  are the positron channel functions with symmetry  $\Lambda$ ,  $\nu$  enumerates the vibrational states,  $k_v$  is the positron wave number in channel  $\nu$ ,  $V_{vl, v'l'}^\Lambda(r)$  are the matrix elements of the positron–molecule potential (9) between the vibrational states, which also couple the positron angular momenta  $l$  and  $l'$ , and  $\nu_0 l_0$  denotes the initial-state channel. This and similar methods have been used to investigate the role of nuclear dynamics on positron scattering and calculate vibrational excitation cross sections for H<sub>2</sub>, N<sub>2</sub>, CO, CO<sub>2</sub> [136, 137]. These calculations show that vibrations have a relatively small effect on the elastic scattering cross sections. On the other hand, the vibrational excitation cross sections in H<sub>2</sub>, CO and CO<sub>2</sub> obtained by this method have prominent maxima close to threshold, in agreement with recent experimental data (see section 4.3).

In recent years positron interactions with larger polyatomic systems, such as clusters and fullerenes, have also been explored theoretically, predicting giant resonances in positron capture by metallic clusters [138] and trapped positron states in cage-like C<sub>60</sub> structures [139].

### 2.3. Positron annihilation on atoms

In the non-relativistic Born approximation, the electron–positron annihilation cross section averaged over the particle spins is given by (see, e.g., [140]),

$$\bar{\sigma}_{2\gamma} = \pi r_0^2 (c/v), \quad (11)$$

where  $v$  is the relative velocity. The cross section in equation (11) obeys a pure  $1/v$ -law, which characterizes the near-threshold behaviour of inelastic processes with fast particles in the final state. At the instant of annihilation, the electron–positron separation,  $r \sim \hbar/mc$ , is much smaller than typical atomic distances (e.g., the Bohr radius). Hence the annihilation can be regarded as taking place at a point where the electron and positron coordinates are equal. The cross section for positron annihilation on a many-electron target is then obtained



**Table 3.** Experimental and theoretical values of  $Z_{\text{eff}}$  at room temperature for atoms.

Atom	H	He	Ne	Ar	Kr	Xe
$Z_{\text{eff}}^{\text{a}}$	–	3.94	5.99	26.7	65.7	320, 400–450
$Z_{\text{eff}}^{\text{b}}$	–	–	–	33.8	90.1	401
$Z_{\text{eff}}^{\text{c}}$	8.39	3.88	6.98	30.5	56.3	202
$Z_{\text{eff}}^{\text{d}}$	7.96	3.78	5.52	25.9	64.1	406

<sup>a</sup> Room-temperature measurements in a dense gas for He, Ne and Ar [149], Kr and Xe [150], with the larger values for Xe obtained by the addition of a small amount of H<sub>2</sub> to facilitate positron cooling.

<sup>b</sup> Room-temperature measurements in a positron trap (see [148] and references therein).

<sup>c</sup> Kohn variational calculations for H (see, e.g., [85]) and He [151], and polarized-orbital calculations for Ne, Ar, Kr and Xe (see [67] and references therein).

<sup>d</sup> Many-body theory calculations ([58–60]).

by multiplying the right-hand side of equation (11) by the average positron density at the positions of all  $Z$  target electrons [141], namely

$$\sigma_a = \pi r_0^2 (c/v) Z_{\text{eff}}, \quad (12)$$

where

$$Z_{\text{eff}} = \int \sum_{i=1}^Z \delta(\mathbf{r} - \mathbf{r}_i) |\Psi(\mathbf{r}_1, \dots, \mathbf{r}_Z, \mathbf{r})|^2 d\mathbf{r}_1 \dots d\mathbf{r}_Z d\mathbf{r} \quad (13)$$

is the *effective* number of electrons that contribute to the annihilation process, and  $\Psi(\mathbf{r}_1, \dots, \mathbf{r}_Z, \mathbf{r})$  is the total wavefunction of the  $Z$  electron and one positron coordinates. It is normalized to the positron plane wave,  $\Psi(\mathbf{r}_1, \dots, \mathbf{r}_Z, \mathbf{r}) \cong \Phi_0(\mathbf{r}_1, \dots, \mathbf{r}_Z) e^{i\mathbf{k}\cdot\mathbf{r}}$  at large positron–target separation where  $\Phi_0$  is the target ground-state wavefunction and  $\mathbf{k}$  is the positron momentum.

Equation (13) implies that annihilation is a weak process compared with elastic scattering. In principle, annihilation can be incorporated into the theory as an inelastic channel open from threshold on an equal footing with scattering. In particular, this leads to complex values of the scattering length [142]. Such a treatment becomes mandatory close to the positronium-formation threshold, where annihilation is inseparable from Ps formation. This can be described by introducing an imaginary absorbing potential [143, 144] or by including the outgoing Ps wave damped by Ps annihilation, in the wavefunction  $\Psi(\mathbf{r}_1, \dots, \mathbf{r}_Z, \mathbf{r})$  [145].

If one neglects the positron–target interaction and substitutes the asymptotic, plane wave function into equation (13), one obtains  $Z_{\text{eff}} = Z$ . This is, of course, a very crude approximation. For example, the experimental values of  $Z_{\text{eff}}$  obtained by measuring the annihilation rate,  $\lambda = \pi r_0^2 c Z_{\text{eff}} n_m$  (where  $n_m$  is the number density of the gas), for thermalized positrons in room-temperature rare gases, can be quite different from the numbers of target electrons (see table 3). Even more puzzling is the fact that, for many polyatomic molecules,  $Z_{\text{eff}}$  exceeds  $Z$  by orders of magnitude [28, 146–148], e.g.,  $Z_{\text{eff}} = 3500, 11\,300, \text{ and } 37\,800$  for C<sub>3</sub>H<sub>8</sub>, C<sub>4</sub>H<sub>10</sub> and C<sub>5</sub>H<sub>12</sub>, respectively (see section 5.2).

A number of effects are important in determining the magnitude of  $Z_{\text{eff}}$ . First, the strong repulsion by the nucleus means that a low-energy positron has a small probability of penetrating inside the atom and annihilating with inner-shell electrons. Hence, only the valence and sub-valence electrons contribute effectively, suggesting that  $Z_{\text{eff}}$  might be smaller than  $Z$ .

On the other hand, the long-range attraction between the positron and the target increases the positron density at the target. In particular, when the positron possesses a virtual (or a

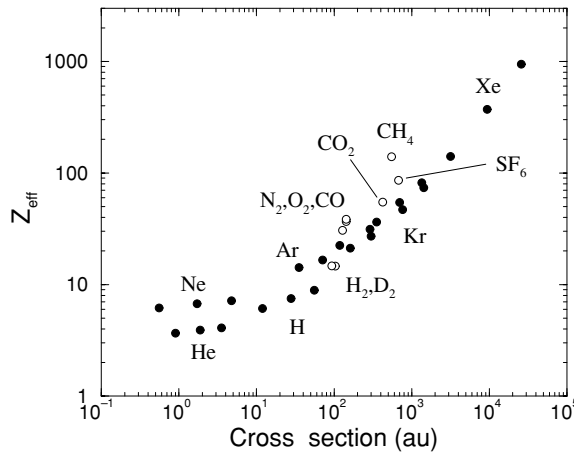


**Figure 3.**  $Z_{\text{eff}}$  and  $\sigma_{\text{el}}$  for atoms (●) and small molecules (○). Values for atoms from theory: hydrogen [153], rare gases (see [67] and references therein). For molecules, room-temperature  $Z_{\text{eff}}$  and (momentum transfer) cross sections are from experiment [146, 148, 154].

weakly bound) state, its quasiparticle wavefunction is enhanced at small separations (yet still outside the target), as  $\psi(\mathbf{r}) \sim 1 + f/r$ , since the scattering amplitude  $f$  ( $f = -a$  at  $\varepsilon = 0$ ) is large [29, 52, 56]. In this case, both  $Z_{\text{eff}}$  and  $\sigma_{\text{el}}$  are enhanced as  $|f|^2$ . Indeed, as shown in figure 3, there is a strong correlation between these two quantities for atoms and simple molecules [152]. The presence of virtual levels also leads to a strong energy dependence of  $f$ ,  $Z_{\text{eff}}$  and  $\sigma_{\text{el}}$  [52, 152].

There is also an important short-range correlation effect due to the Coulomb attraction of the annihilating electron and positron that further increases the contact density (i.e., the electron density at the position of the positron) [52, 152]. This short-range enhancement of the contact density involves high-lying virtual excitations, and as a result, it has only a weak dependence on positron energy [60]. The magnitude of this effect is larger for systems with lower ionization potentials and diffuse valence electron orbitals. As discussed below, this understanding is supported by model-potential calculations [142].

The importance of both the long- and short-range correlation effects makes  $Z_{\text{eff}}$  a difficult quantity to calculate. Unlike the scattering problem, which probes the asymptotic part of the wavefunction  $\Psi(\mathbf{r}_1, \dots, \mathbf{r}_Z, \mathbf{r})$ , the calculation of  $Z_{\text{eff}}$  requires accurate knowledge of the wavefunction at small electron–positron separations. In the language of many-body theory, this means that, besides the positron–target potential  $\Sigma_\varepsilon(\mathbf{r}, \mathbf{r}')$ , one needs to evaluate the large correlation corrections to the electron–positron annihilation vertex  $\delta(\mathbf{r} - \mathbf{r}_i)$  [52, 56, 60].

At present, precise theoretical values of  $Z_{\text{eff}}$  have been obtained for H and He, where accurate variational wavefunctions are available (see section 2.2), or through a  $T$ -matrix calculation (for H) which avoids an explicit calculation of the wavefunction [155]. The values of  $Z_{\text{eff}}$  for rare-gas atoms are given reasonably well by PO calculations (see [67] and references therein), and even more accurately by recent many-body calculations [58, 59].

For atoms that have weakly bound positron states, low-energy  $Z_{\text{eff}}$  values are also enhanced; for example,  $Z_{\text{eff}} = 119, 96$  and  $36$  at  $\varepsilon = 0$ , for Be, Cu and Mg, respectively [142]. For such systems, there is an estimate that links  $Z_{\text{eff}}$  at zero energy with the annihilation rate in the positron bound state,  $\Gamma_a$ ,

$$Z_{\text{eff}} \approx \Gamma_a \varepsilon_B^{-3/2} / (\sqrt{2} r_0^2 c), \quad (14)$$

**Table 4.** Room-temperature  $Z_{\text{eff}}$  for diatomic and small polyatomic molecules.

Molecule	H <sub>2</sub>	N <sub>2</sub>	O <sub>2</sub>	CO	CO <sub>2</sub>	NH <sub>3</sub>	C <sub>2</sub> H <sub>2</sub>	CF <sub>4</sub>	CH <sub>4</sub>	CCl <sub>4</sub>
$Z_{\text{eff}}^{\text{a}}$	14.6	30.5	36.7	38.5	54.7	1600	3160	54.4	142	9530
$Z_{\text{eff}}^{\text{b}}$	10.2	9.3	–	–	–	–	145	–	–	–
$Z_{\text{eff}}^{\text{c}}$	2	48	65	33	51	565	37	98.5	64.7	1141

<sup>a</sup> Measured values from dense gas [146, 157] and positron trap [148] experiments.

<sup>b</sup> *Ab initio* calculations using the Kohn variational method for H<sub>2</sub> [158] and the Schwinger multichannel method [123, 159].

<sup>c</sup> Correlation–polarization potential calculations [133, 160, 161], including vibrational close coupling for diatomic molecules and CO<sub>2</sub>.

where  $\varepsilon_B$  is the binding energy [142, 156]. Reference [142] also demonstrates that a simple model-potential positron–atom calculation yields the correct energy dependence of  $Z_{\text{eff}}$ , as long as the potential is tuned to reproduce positron–atom elastic scattering.

Therefore, the role of positron–atom virtual levels in producing large  $Z_{\text{eff}}$  is by now well understood (i.e., the increase in  $Z_{\text{eff}}$  for noble gas atoms in table 3 follows the change in the scattering lengths in table 1). However, it is important to note that for room-temperature positrons, this type of enhancement is limited to values up to  $Z_{\text{eff}} \sim 10^3$  [152].

#### 2.4. Positron annihilation on molecules

The situation regarding calculations of  $Z_{\text{eff}}$  for molecules is much less clear. As seen from table 4 and figure 3, the measured  $Z_{\text{eff}}$  values for diatomic and small polyatomic species are similar to those found in atoms. However, even for H<sub>2</sub>, the calculated value is noticeably smaller than that measured. The results of Schwinger multichannel calculations underestimate  $Z_{\text{eff}}$  considerably, yet as discussed above, this same method produces reasonable positron–molecule scattering cross sections. This indicates that the main difficulty with this procedure is in describing the short-range electron–positron correlation (which is also the case for positron–atom  $Z_{\text{eff}}$  calculations). This correlation is completely neglected in the correlation–polarization potential calculations where the total wavefunction is given by a product of the wavefunctions for the positron and the molecular electrons. When applied to atoms, such approximations typically underestimate  $Z_{\text{eff}}$  by factors of 3 to 6 [52]. It is therefore surprising that large  $Z_{\text{eff}}$  are obtained, often exceeding the experimental values (see table 4). While some of them are close to experiment, the data for H<sub>2</sub>, CF<sub>4</sub> and CH<sub>4</sub> highlight the inconsistency of the results.

The gap between theory and experiment is even greater for molecules with  $Z_{\text{eff}} > 10^3$ . To understand these huge annihilation rates one needs to consider a new mechanism [30, 147, 152, 156], whereby positrons annihilate after attaching themselves to a molecule. This mechanism operates for molecules that can form bound states with the positron. Given that positron binding with neutral atoms is now firmly established, it is natural to expect that many molecules can also bind positrons. As discussed in section 5.2.1 below, recent experimental results confirm that this is the case. Assuming that the binding energy,  $\varepsilon_B$ , of such states is a fraction of an electron volt, the positron energy released in the process of binding is sufficient to excite molecular vibrations. Since the vibrational motion is quantized, this is only possible for selected incident positron energies  $\varepsilon$ , such that  $\varepsilon + \varepsilon_B = E_\nu$ , where  $E_\nu$  is the energy of  $\nu^{\text{th}}$  vibrational excitation. Thus, the positron becomes temporarily captured in a vibrational Feshbach resonance (VFR), and this greatly enhances the probability of annihilation.

For polyatomic molecules, the density of vibrational excitations can be very high. Averaging  $Z_{\text{eff}}$  over the closely spaced VFR, one obtains the following estimate for the resonant contribution at low positron momenta  $k$  [152, 156]

$$Z_{\text{eff}}^{(\text{res})} = \frac{2\pi^2 \rho_{\text{ep}} \Gamma^{(\text{e})}}{k \Gamma} \rho(\varepsilon + \varepsilon_B), \quad (15)$$

where  $\rho_{\text{ep}}$  is the electron–positron contact density in the positron–molecule bound state,  $\Gamma^{(\text{e})}$  is the average VFR width with respect to positron emission,  $\Gamma = \Gamma^{(\text{e})} + \Gamma^{(\text{a})}$  is its total width (where  $\Gamma^{(\text{a})} = \pi r_0^2 c \rho_{\text{ep}}$  is the annihilation width), and  $\rho(E_v)$  is the vibrational spectrum level density. Given that  $\rho(E_v)$  increases rapidly with the size of the molecule and is sensitive to its atomic composition, equation (15) and the VFR annihilation mechanism explain qualitatively the main features of the experimental data [152, 156, 162]. For example, the huge difference between  $Z_{\text{eff}}$  for  $\text{CH}_4$  and  $\text{CCl}_4$  (table 4) is interpreted as being due to the presence of low frequency modes in the latter and its ability to bind positrons.

This progress notwithstanding, a detailed quantitative understanding of the interaction of positrons with the vibrational degrees of freedom and large values of  $Z_{\text{eff}}$  observed for many large molecules is still lacking. The only dynamical calculation to date that has shown the effect of VFR, is a simple zero-range potential model for  $\text{Kr}_2$  [163]. A possible interplay between the vibrations and positron virtual states has been explored in [164]. Given the similarity between electron and positron scattering at low energies, one hopes that deciphering the information contained in positron annihilation rates may provide insights into the dynamics of electron–molecule VFR. This would be a valuable development, since resonances underpin many processes in low-energy electron–molecule collisions [165].

### 3. Experimental techniques

#### 3.1. Positron sources and moderators

Positrons can be obtained from radioisotopes or from electron–positron pair-production sources such as electron accelerators [166]. The isotope  $^{22}\text{Na}$  ( $\tau_{1/2} = 2.6$  years) was used in Deutsch’s experiments, and it still remains the isotope of choice for most atomic physics experiments. It is now available commercially in sealed capsules with high-transparency windows in activities up to  $\sim 100$  mCi [167].

There is an ongoing effort to develop positron sources with larger fluxes. One approach is to use short-lived positron-emitting isotopes that can be produced by accelerators [168–171]. As an alternative, electron–positron pair-production sources create positrons by impinging fast electrons (e.g., from a linear electron accelerator (LINAC)) on high- $Z$  targets (so called ‘converters’) [172]. This process produces high-energy gamma rays that, in turn, interact with the target nuclei to produce pairs. The high-energy gamma rays for positron production can also be obtained from the radioactive decay of short-lived, reactor-produced isotopes created by neutron capture on targets such as  $^{113}\text{Cd}$  [173].

Regardless of whether the positrons are obtained using isotopes or pair production, they have a broad spectrum of energies (typically hundreds of keV) and must be decelerated to lower energies before they can be used in atomic physics experiments. This can be accomplished using a solid, liquid or gaseous material as ‘moderator.’ Many such moderator materials have been used to produce slow positrons in vacuum, including blocks or foils of single-crystal or polycrystalline metals (e.g., tungsten, copper or nickel) or a layer of a rare-gas solid at cryogenic temperatures [19]. The positrons lose energy in the moderating material. They are re-emitted with a spectrum of energies of width  $\sim 0.5$  eV from metals and  $\sim 2$  eV from rare-gas solids. Low moderator efficiencies hindered early positron atomic physics

research. Fortunately, moderator efficiencies have improved dramatically over the decades since Cherry and Groce's pioneering experiments. They are now typically  $10^{-4}$ – $10^{-3}$  for metals [40] and  $10^{-2}$  for rare-gas solids [41]. Using a relatively convenient 100 mCi  $^{22}\text{Na}$  source and a solid neon moderator, positron fluxes of  $\sim 10^7 \text{ s}^{-1}$  can be obtained [42]. There are several higher flux positron facilities in the world at reactors and electron accelerators. While these intense positron sources have the potential for studying a range of atomic physics processes, particularly where scattering cross sections are small, to date, they have not yet had a particularly significant impact on the field.

### 3.2. Detection techniques

A number of methods are available to detect positrons [5]. For larger positron fluxes, the charge to a collector plate can be measured. Positrons can also be collected on a metal plate and the characteristic 511 keV gamma rays detected with a scintillator (e.g., NaI) and photomultiplier tube. For small positron fluxes, individual positrons can be detected using a channel electron multiplier (CEM).

One method used to reduce background noise is to make coincidence measurements by correlating the arrival of a positron detected using a CEM or the annihilation gamma rays, with a signal from the emission of the fast positron from the source. This fast positron can be detected using a thin scintillator inserted between the source and moderator. Alternatively, if the positron source is  $^{22}\text{Na}$ , positron emission (90% branching ratio) is accompanied by a 1.27 MeV gamma ray that can be easily detected.

The annihilation gamma rays from positron interactions with matter can be analysed by measuring their Doppler-broadened energy spectrum or by measuring the angular correlation of the annihilation radiation (ACAR technique) [5]. Both techniques provide important information about the momentum distribution of the annihilating electrons. The Doppler shift due to the centre of mass motion of the annihilating electron–positron pair is measured using a detector with high-energy resolution, such as intrinsic germanium, and a multichannel analyser. In ACAR, the momentum of the annihilating pair, in the plane perpendicular to momenta of the two gamma rays, results in gamma emission at angles slightly different from  $180^\circ$ , thereby providing a measure of the pair momentum. The gamma rays are recorded using NaI detectors and slits at large distances from the test species to define the angle more precisely. Alternatively, the gamma rays can be detected by large, two-dimensional detector arrays for higher collection efficiency and data rate.

Larger solid angles can be used in the Doppler-broadening technique, but the resolution is limited to  $\sim 1$  keV, even when using the highest resolution detector available. The ACAR technique has superior resolution (e.g., equivalent Doppler shift  $\sim 0.2$  keV), but because the technique requires detectors far separated, it has relatively low detection efficiency. In the typical case of the annihilation of a thermal positron (i.e., with a small energy), a 1 keV Doppler shift corresponds to the positron annihilating with an electron having 4 eV of kinetic energy. The ACAR technique can distinguish centre of mass motions in specific directions in the laboratory frame. This is advantageous for studying anisotropic systems (e.g., crystalline materials). For the case of un-oriented atoms or molecules, such as those studied here, this is not an advantage.

### 3.3. Electrostatic beams

A number of groups have used electrostatic beams to study low-energy positron collisions with atoms and molecules. In the majority of cases, these experiments have involved the

measurement of total scattering cross sections and have also involved some form of (relatively) weak magnetic field to confine and guide the positron beam. Nonetheless, to distinguish these techniques from those described in the following section, where high magnetic fields are used, we shall treat these beams as essentially electrostatic in nature.

The most common source used for these beams is the  $^{22}\text{Na}$  isotope, although other radioactive sources such as  $^{58}\text{Co}$  have been used. In all such cases moderators are required before forming the resulting slow positrons into a beam. In a small number of cases proton bombardment sources have also been used. For example, Stein *et al* [174] obtained positrons from a carbon radioisotope created by proton bombardment on boron. While the efficiency of this source was very low, the energy width of the beam was relatively narrow ( $\sim 100$  meV), and so it was used for studies of low-energy total scattering cross sections in a search for resonance features. In several other cases, LINAC-based positron sources have been used.

The first detailed efforts to study positron interactions with atoms and molecules using electrostatically guided beams came in the early to mid-1970s. A common feature of almost all such early experiments was the use of electrostatic extraction and acceleration/deceleration combined with weak guiding magnetic fields and time-of-flight techniques. Many of the features of these experiments are summarized in detail in previous review articles (see, in particular, [2, 175]), and we will not repeat those discussions here.

In order to investigate many state-specific collision processes (elastic scattering, excitation, ionization), and to do so as a function of scattering angle, it is necessary in most cases to produce and scatter the positrons in an environment free of magnetic fields. Below we shall briefly describe some examples of such experiments. The first technique was used by the Detroit group [176] for differential elastic scattering measurements from argon. They used electrostatic fields to transport, focus and energy analyse a positron beam from a moderated  $^{22}\text{Na}$  source, and they carried out the first crossed beam experiment with positrons. Channel electron multipliers were used to detect both the primary positron beam ( $10^5$  positrons/s at 200 eV with an energy width of  $\sim 2$  eV) and those that had been elastically scattered through angles between  $30^\circ$  and  $135^\circ$ . Scattered positron count rates were substantially less than 1 Hz and significant effort was invested in background reduction. A similar approach was employed by the Bielefeld group [177] for elastic differential cross section (DCS) measurements in argon. They produced a low-energy beam, at 8.5 and 30 eV, which had an intensity of about  $6 \times 10^3$  positrons/s at the point where it intersected an atomic beam. Long data accumulation times were required. The results of these experiments are discussed in greater detail in section 4.

More recently, the University College London group has used a variety of electrostatically guided beams for a range of differential (in both energy and angle) scattering measurements on atomic and molecular targets. Köver *et al* [178] employed a  $^{58}\text{Co}$  source, producing  $\sim 10^4$  positrons/s, which were accelerated and focused by electron optics consisting of a simple gun and a three-element, einzel focusing lens. A schematic diagram of this apparatus is shown in figure 4. Final focusing and setting the beam energy was achieved with an electrostatic lens separated from the gun stage by a double cylindrical deflector in order to remove high-energy positrons and gamma rays from the low-energy beam. Several detectors (channel electron multipliers) were used to measure the primary beam flux as well as the elastic scattering, positronium-formation and ionization cross sections. A modified version of this apparatus was developed by Gao *et al* [179] and used for differential elastic scattering.

The final example we discuss is the apparatus, shown schematically in figure 5, that was used by the Aarhus group for measurements of ionization in atoms and molecules [180–182]. About  $3 \times 10^4$  positrons/s are transported electrostatically from a moderated  $^{22}\text{Na}$  source to a gas-filled collision cell. The beam undergoes a  $90^\circ$  bend in a cylindrical mirror analyser after being extracted from the moderator, in order to provide filtering for high-energy positrons and



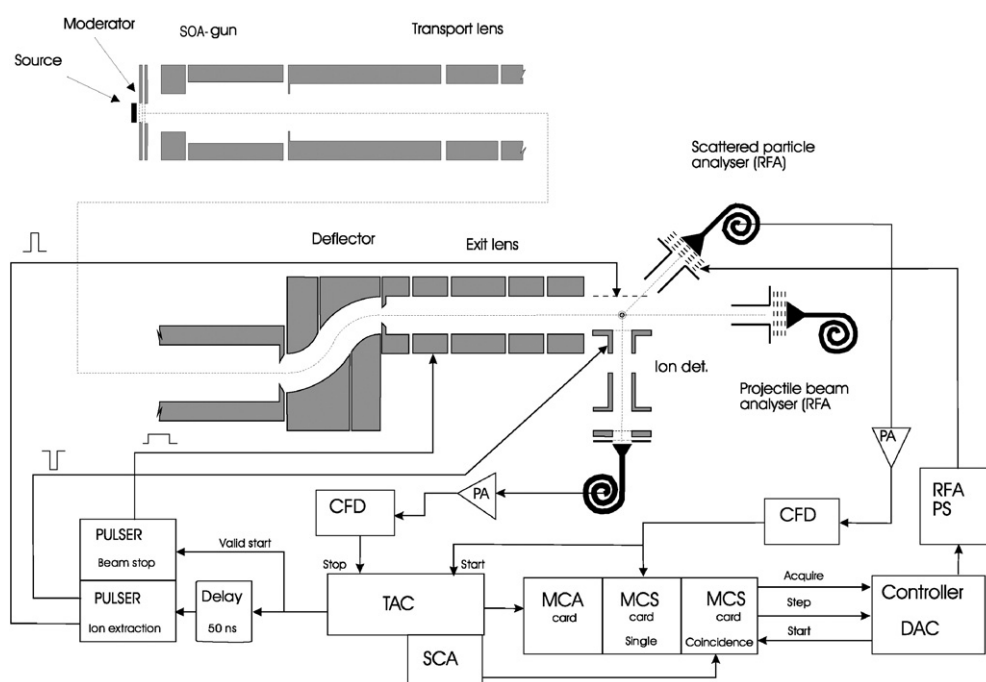


**Figure 4.** The apparatus of Köver *et al* that was used for doubly differential ionization studies on Ar. Reprinted with permission from [178]; copyright 1994 by Institute of Physics Publishing.

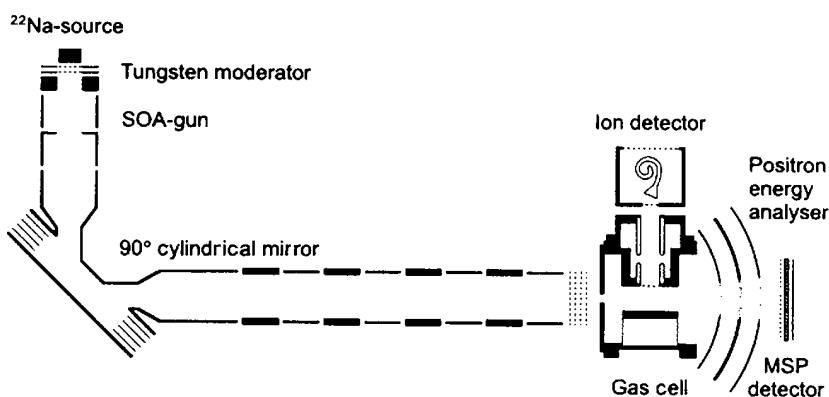


**Figure 5.** A schematic of the apparatus of Bluhme *et al* that was used for ionization studies of the rare gases. Reprinted with permission from [180]; copyright 1999 by Institute of Physics Publishing.

gamma rays. The cylindrical mirror is also used to chop the positron beam into short bursts,  $\sim 1 \mu s$  in duration, at a repetition rate of  $\sim 100$  kHz. Ions are extracted from the collision cell and detected with a CEM.

### 3.4. Scattering experiments using electrostatic beams

There have been many positron scattering experiments using ‘electrostatic’ beams and they have been applied to measurements of essentially all possible processes, ranging from elastic

scattering to ionization and dissociation. We limit our discussion to the most broadly applied and/or successful techniques for the main scattering channels that have been investigated.

*3.4.1. Grand total cross sections.* These types of measurements were some of the earliest experiments that were undertaken with positron beams. An excellent summary of the work in this area prior to the mid-1980s is given in the review article by Charlton [175]. More recent references to work on polyatomic molecules can be found in the extensive review of Kimura *et al* [183]. A common element of most of these experiments is the use of a gas cell, with the total scattering cross section obtained by measuring the attenuation of a beam of positrons, and the subsequent application of the Beer–Lambert law to determine the grand total cross section. Many of these experiments used time-of-flight techniques to obtain the energy of the individual positrons as they traversed the scattering cell. Typically, a pulse obtained when a fast positron from the source passes through a thin scintillator crystal is used to start a timing clock, and detection of the scattered positron with a channel electron multiplier stops the clock. The energy distribution of the recorded positron flux is then measured with and without the target species in the gas cell. The total cross section is obtained from the relationship<sup>6</sup>

$$\sigma_{\text{T}}(E) = \frac{1}{n_m l} \ln \frac{I_0(E)}{I_g(E)}, \quad (16)$$

where  $I_g(E)$  and  $I_0(E)$  are the transmitted intensities of positrons of energy  $E$ , with and without gas in the cell,  $l$  is the length of the gas cell, and  $n_m$  is the number density of gas in the cell.

The main experimental issues with these types of experiments relate to the accurate determination of the quantities  $n_m l$  and the transmitted (unscattered) positron flux  $I_g(E)$ . The first quantity requires an accurate pressure measuring device, together with an accurate knowledge of the effective length of the scattering cell. The second, the measured transmitted flux of positrons with gas in the scattering cell, should be a measure of only the primary (unscattered) beam. However, the nature of these experiments, which usually have some form of exit aperture on the scattering cell, means that including some forward scattering of both elastic and inelastic positrons in  $I_g(E)$  is unavoidable. In most cases, steps are taken to correct this by (i) reducing the effective solid angle for forward scattering by using a long scattering cell and small exit aperture, and (ii) using a retarding potential device prior to the positron detector to repel any inelastically scattered positrons which may pass through the exit aperture. The usual effect of inadequate discrimination against forward scattering is an increase in  $I_g(E)$  which results in a reduction in the value of the measured total cross section.

Most of the work on total scattering measurements was carried out during the 1980s, but several groups have remained active in the measurement of total scattering cross sections, mainly for large molecules. One example of such an experimental system is that used by the Yamaguchi group (see, e.g., [184, 185]) and shown in figure 6. Positrons from a  $^{22}\text{Na}$  source are moderated with a tungsten ribbon, and their energy is set by electrostatic acceleration as they exit the moderator region. The energy of the individual positrons is determined by measuring their time of flight, and the positron beam is transported through the gas cell to the detector by an axial magnetic field typically  $\sim 9$  G. The energy width of the positron beam is typically 1.5 eV. The effective length of the scattering cell and the stability of the pressure measurement are established by normalizing measurements in  $\text{N}_2$  to those of Hoffman *et al* [186]. As the exit aperture of the scattering cell is relatively large (3 mm diameter), a correction is required for the effects of forward elastic scattering. Where possible, this group used data from the literature on the forward scattering DCS for each atom or molecule in order

<sup>6</sup> For consistency with previous literature, energies in section 3 are denoted by the symbol  $E$ , in contrast to the symbol  $\varepsilon$  used elsewhere.

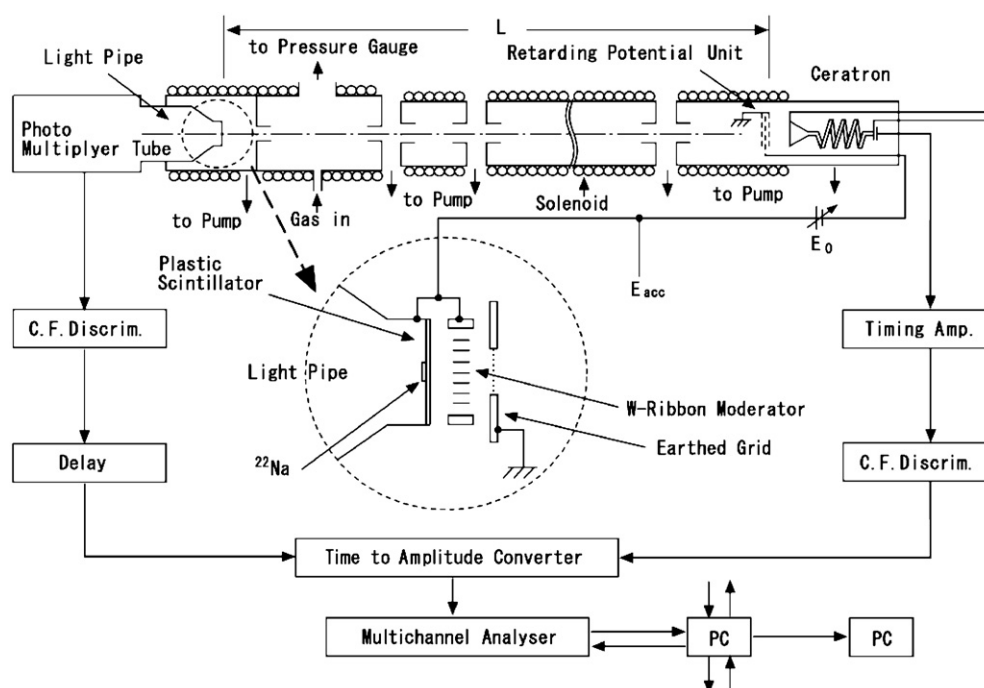


**Figure 6.** Schematic diagram of the time-of-flight apparatus used by the Yamaguchi group for total cross section measurements [184, 185]. Reprinted with permission from [185]; copyright 2001 by the American Institute of Physics.

to calculate these corrections. Typical uncertainties for the total cross sections measured using this technique range from 5 to 15%.

A similar attenuation technique was used by the Wayne State group, who made many of the earlier total cross section measurements, and later, the first measurements of the total scattering cross section for alkali atoms [187, 188] and atomic hydrogen [189, 190]. Examples of the data obtained using these and other methods are discussed in section 4.1.

The Trento group of Zecca, Karwasz and colleagues were also active in the 1980s and early 1990s making measurements of positron total cross sections for a range of atoms and molecules, mainly in the intermediate energy range. This work is described in [191] and references therein. Their more recent work on the convergence of total scattering cross sections for electrons and positrons is discussed in section 4.1.

**3.4.2. Differential elastic scattering cross sections.** The first measurements of elastic DCS for positron scattering were made for argon by Coleman and McNutt [192]. They used a time-of-flight technique, in conjunction with scattering in a magnetic field of 140 G, to obtain the elastic DCS for positrons at energies between 2.2 and 8.7 eV. They used the fact that, for a fixed energy, scattering through angles up to  $90^\circ$  produces an increase in the measured flight times of the scattered positrons. In this way, they used the long-time ‘tail’ of their timing spectra to extract elastic DCS for scattering angles between  $20$  and  $60^\circ$ . Absolute values for the DCS were obtained from the knowledge of the total scattering cross section at each energy.

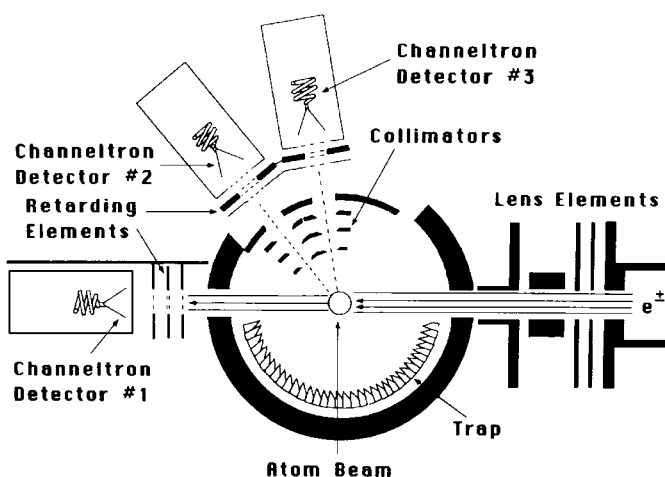


**Figure 7.** Schematic diagram of the apparatus used at Wayne State University for differential positron scattering measurements. Reprinted with permission from [193]; copyright 1992 by the American Physical Society.

Since these experiments, there have been relatively few differential scattering measurements made with electrostatic beams, with most of them made by the group at Wayne State University. They have covered a wide range of atomic and molecular species (Ne, Ar, Kr, Xe, N<sub>2</sub>, CO, O<sub>2</sub>, N<sub>2</sub>O, CO<sub>2</sub>, CH<sub>4</sub>, C<sub>2</sub>H<sub>2</sub> and SF<sub>6</sub>), in the energy range between 4 and 300 eV and for scattering angles between 30° and 135°. An example of the experimental apparatus used for these studies is shown in figure 7. A beam of moderated positrons of variable energy from a <sup>22</sup>Na source is crossed with an atomic or molecular beam from a capillary array source. Both the primary positron beam and positrons scattered by the gas target are detected using channeltron electron multiplier detectors. The scattered particles are detected in two such electron multipliers that rotate about the axis of the gas beam. Each detector has a retarding potential device to discriminate against inelastically scattered particles and an acceptance angle of  $\sim \pm 8^\circ$ . This apparatus can also be used for electron DCS measurements. In this case, the extensive data sets for intermediate energy electron–atom scattering from the literature were used to establish the accuracy of the technique.

Using this and similar apparatus, the Wayne State group measured relative angular distributions for elastic positron scattering. In some cases, these measurements could be placed on an absolute scale by normalization to theoretical predictions. A semi-independent technique that they used involved measuring the ratios of positron to electron scattering at a fixed energy and angle and then normalizing these electron measurements to other experimental or theoretical values. Measurements of the energy dependence of the positron signal were then used to place measurements at all energies and angles on an absolute scale. Some of the data from this extensive series of measurements will be discussed in section 4.2.

Other examples of elastic DCS experiments are the work of the Bielefeld group [177] and the UCL group [194], both of whom studied argon. The measurements of Floeder *et al* are notable in that the group established the absolute scale of their data by measuring and/or estimating all of the required experimental parameters. This included the density of the gas beam, which they estimated from attenuation measurements of the primary beam, together with the known total scattering cross section.

3.4.3. *Inelastic vibrational and electronic excitation.* There have been very few measurements of inelastic scattering of positrons from atoms or molecules using electrostatic beams. Those that do exist are generally not state-specific measurements, but rather measurements of a combination of excitation and/or ionization processes. This is perhaps not surprising given the low beam intensities and modest energy resolutions. Indeed, the difficulty in making any measurements of this type using such an electrostatic beam should not be underestimated.

All the measurements of this type have been done using time-of-flight (TOF) techniques. Early examples include those of the UCL group [195] and the University of Texas group [196] for the excitation and ionization of He atoms. The former work partitioned the inelastic processes into excitation, ionization and positronium formation. They concluded that, at intermediate energies, ionization was the dominant channel. On the other hand, the latter work indicated that at near-threshold energies, excitation of the  $2^1S$  state appeared to dominate [196].

The Yamaguchi group used TOF techniques to measure cross sections for the Schumann–Runge continuum in  $O_2$  [197] and total excitation and ionization in helium, neon and argon atoms [198]. They also used similar techniques to study vibrational excitation of polyatomic targets, such as  $CO_2$  and  $OCS$  [137, 199].

One difficulty in using such TOF methods to study inelastic scattering in a magnetic field is that of separating the time delay due to elastic scattering at an angle to the incident beam from the time delay produced by an inelastic scattering event. As a result, this technique is unlikely to yield definitive, state-selected inelastic scattering measurements, particularly when the energy loss is small.

3.4.4. *Positronium formation.* While positronium formation leads ultimately to a positive ion (and two or three gamma rays not present in conventional ionization), techniques for the measurement of this process are different than those for conventional ionization, and so we discuss the two separately. A number of techniques have been used to deduce or measure absolute cross sections for the formation of positronium in positron scattering from atoms and molecules. Initial attempts to establish these cross sections (e.g., for noble gases) involved extrapolating the total elastic cross section, based on its shape below the positronium threshold, to energies above the positronium threshold. This extrapolated cross section was then subtracted from the total to yield the estimate of the Ps cross section. The uncertainties of the extrapolation procedure aside, the utility of this technique was limited, however, by the unknown contributions from the electronic excitation and ionization channels.

Charlton *et al* [200] made the first direct measurement of the energy dependence of the positronium-formation cross section by detecting, in triple coincidence, the three photons that arise from the decay of ortho-positronium. These were not absolute measurements, but they did provide the first direct indication of the shape of the positronium-formation cross section in the Ore gap for Ar, He,  $H_2$  and  $CH_4$ . In a subsequent and improved experiment [201], they estimated the absolute cross sections for all of the rare-gas atoms from threshold to 150 eV. Using a different technique, which involved measuring the loss of positrons from a scattering cell, Fornari *et al* [202] and Diana *et al* [203] measured the Ps-formation cross section for He, Ar and  $H_2$  at energies up to 250 eV.

Fromme *et al* [204] used a technique where positrons and positive ions were detected in coincidence in order to determine both the ionization cross section and Ps-formation cross section for helium. Absolute values were obtained by measuring electron impact ionization, with the same technique at an energy of 750 eV, and then normalizing to values from the

literature for the electron cross sections. Sperber *et al* [205] used a similar approach, but with positrons from a high-flux reactor, to study Ps formation in atomic hydrogen.

Stein *et al* [206] developed a technique to measure upper and lower limits on the positronium-formation cross sections for a range of gases, including metal vapour targets. The lower limits were imposed by coincident measurements of the two-photon decay of the para-positronium formed in the gas cell and three-photon coincident measurements of that fraction of the ortho-positronium that reaches the walls of the cell and annihilates. The upper limit to the cross section was derived from transmission measurements where most of the scattered positrons were detected except those that formed positronium in the cell.

Finally, a comprehensive set of Ps-formation cross sections, for the heavier rare gases (Ne–Xe), has recently been obtained by Laricchia *et al* [207]. Using an apparatus described by Moxom *et al* [208], they measured *total* ionization cross sections up to energies which were considered high enough to enable direct normalization of these positron measurements to the corresponding electron-impact ionization cross sections. Using these measured cross sections, and data from the literature for the various other components of the total ionization cross section, they were then able to extract the cross section for Ps formation. These recent measurements and others discussed above are presented in section 4.6.

*3.4.5. Ionization.* The first measurements of positron-impact ionization were conducted in the late 1970s and early 1980s (e.g., [195, 209]). In these experiments ionization cross sections were deduced from time-of-flight spectra. The first fully resolved ionization measurements were made by Fromme *et al* [204] who used time-correlation techniques to measure He<sup>+</sup> ions in coincidence with scattered positrons in order to obtain the single ionization cross section for He.

During the 1990s ionization cross sections were measured for a broad range of targets. They include H [210–213], the noble gases [178, 180, 181, 207, 208, 214–220], H<sub>2</sub> [204, 208, 215, 221], and a number of other diatomic and polyatomic molecules (e.g., see [182, 222, 223]). As these experiments have become increasingly sophisticated, measurements of doubly and triply differential cross sections have also been made by the UCL group, as have measurements of dissociative ionization by both the Aarhus and Oak Ridge groups.

One of the significant advances during the 1990s was the ability to perform absolute measurements on atomic hydrogen, and thus provide data against which scattering theory could be compared for a fundamental atomic system. An example of such an experimental approach is shown schematically in figure 8.

In this experiment, positrons from an enriched <sup>64</sup>Cu source, produced by the high-flux beam reactor at the Brookhaven National Laboratory, were moderated using solid krypton. The resulting positron beam had a relatively broad energy width (6 eV). It was crossed at 90° with a beam of hydrogen atoms from a Slevin-type, rf discharge source. Positrons scattered into a forward cone of about 30° were detected by a channel electron multiplier. Ions formed in the scattering region were extracted, mass analysed and detected using another CEM. The ionization cross section (not including positronium formation) is then proportional to the positron–ion coincidence rate. Absolute normalization of the cross section is obtained by measuring the coincidence rate for electron impact ionization and normalizing to known electron cross sections at high energies where the positron and electron cross sections merge.

### *3.5. Buffer-gas positron traps and trap-based beams*

The most successful technique to accumulate positrons uses the Penning–Malmberg trap because of its excellent confinement properties [14]. This device consists of a uniform



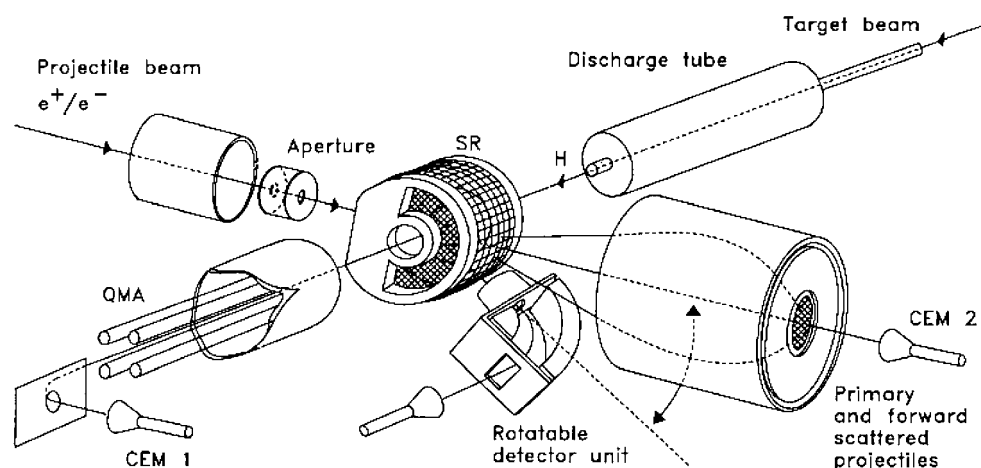


**Figure 8.** Schematic of the experimental apparatus of Hofmann *et al* used for measurements of positron-impact ionization of H. Reprinted with permission from [213]; copyright 1997 by Institute of Physics Publishing.

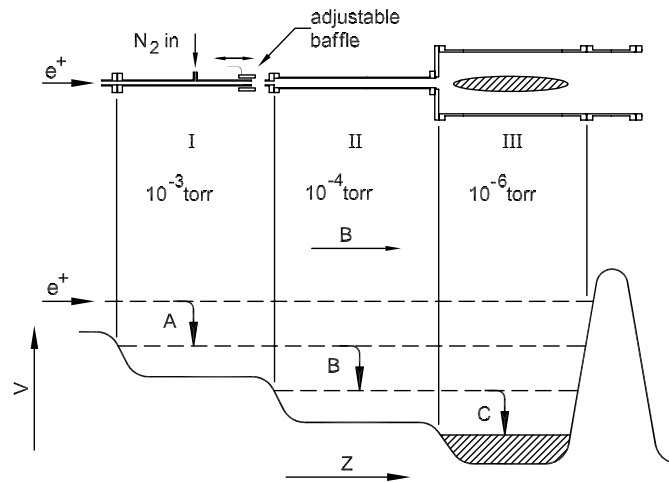
magnetic field (e.g.,  $B \sim 0.05\text{--}0.15$  T) and electrical potentials on cylindrical electrodes to create a potential well along the direction of  $B$ . The most efficient method to trap positrons in this potential well is the use of a buffer gas. First developed in 1988, the buffer-gas positron trap has become increasingly useful for positron atomic physics experiments.

Figure 9 illustrates the operating principle of a three-stage buffer-gas accumulator [14, 147, 224]. Positrons are injected into the trap that has a stepped potential profile to create three stages (I, II and III), each with a different electrical potential and pressure of buffer gas. Using a continuous gas feed and differential pumping, a relatively high pressure ( $\sim 10^{-3}$  Torr) is maintained in stage I. Positrons are trapped by a series of inelastic scattering collisions (marked A, B and C in the figure). They accumulate in stage III, where they are in a low-pressure environment (to reduce annihilation) and cool to the electrode temperature (typically 300 K).

The highest trapping efficiency has been obtained using molecular nitrogen, with the potential arranged so that the trapping collisions in each stage occur at  $\sim 9$  eV. Subsequent positron cross section measurements [225] indicate that this energy corresponds to a peak (possibly a resonance) in the cross section for the lowest lying electronic excited state of  $\text{N}_2$ , while the dominant loss process, positronium formation, is relatively small at these energies.

The positron lifetime in stage III is typically  $\sim 60$  s at a pressure in this stage of  $\sim 5 \times 10^{-7}$  Torr. A small amount of carbon tetrafluoride added to stage III (e.g.,  $10^{-7}$  Torr) assists in cooling and decreases the thermalization time (cooling time,  $\tau_c \sim 0.1$  s) [226]. Using a solid neon moderator and such a three-stage trap, trapping efficiencies of 10–30% can be achieved. With a 100 mCi  $^{22}\text{Na}$  source and solid neon moderator, positrons can be accumulated at a rate  $\sim 3 \times 10^6 \text{ s}^{-1}$ . The trapped positron plasma can be used *in situ* for atomic physics experiments (e.g., studies of positron annihilation) or to make a beam of cold positrons.

The formation of a magnetic positron beam and the apparatus to use it in scattering experiments are illustrated in figure 10 [227, 228]. The bottom of the confining potential well (i.e., stage III in figure 9) is carefully raised, forcing the positrons over the potential barrier,  $V$ , which sets the beam energy,  $E = eV$ , where  $e$  is the positron charge. The parallel energy spread of the beam,  $\Delta E_{\parallel}$ , can be as low as, or lower than, that of the cooled positron cloud (i.e.,



**Figure 9.** Schematic diagram of a three-stage buffer-gas positron accumulator. Above: the electrode structure that produces three regions with different pressures by differential pumping. Below: the corresponding electrical potential profile,  $V(z)$ .

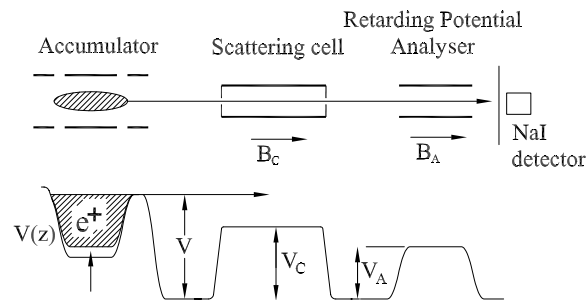


**Figure 10.** The formation of a trap-based positron beam and the arrangement to use it in scattering experiments. Above: the positron accumulator, scattering cell, retarding potential analyser (RPA), and detector. Below: typical potential profile. The positron beam energy in the scattering cell is  $E = e(V - V_C)$ .

$\Delta E_{\parallel} \leq 0.025$  eV). For high-resolution atomic physics experiments, it is convenient to operate the beam in a pulsed mode, using small pulses of positrons to avoid space-charge broadening. Positron fluxes are typically restricted to approximately  $1\text{--}3 \times 10^4$  positrons per pulse, with pulse widths of  $\sim 3$   $\mu\text{s}$  and repetition rates  $\sim 4$  Hz.

Figure 11 shows an example of a retarding potential analyser (RPA) measurement of the parallel energy spread of a 1.7 eV positron beam [44]. In a magnetic field of strength  $B$ , the positron energy,  $E$ , can be separated into a component,  $E_{\parallel}$ , parallel to the field, and a component,  $E_{\perp}$ , perpendicular to the field and associated with the gyromotion of the positron in the plane perpendicular to  $B$ . The energy spread,  $\Delta E_{\parallel}$ , is set by the rate of ejection of the positrons from the potential well, while  $E_{\perp}$  is unchanged by this ejection process, and so its magnitude is set by the temperature of the trapped positron plasma (i.e.,  $E_{\perp} \sim k_B T = 300$  K, or 25 meV). To date, positron annihilation experiments have been done with the beam tunable from 50 meV to many electron volts, and scattering experiments have been done at beam

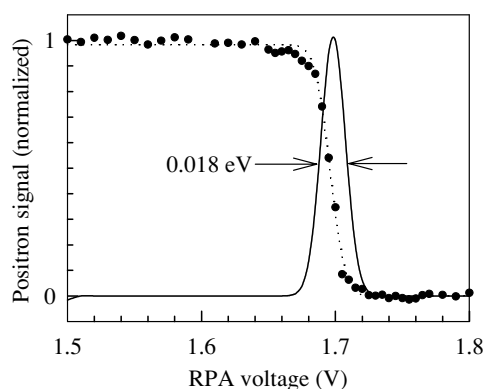


**Figure 11.** Parallel energy spread of a trap-based beam created from a 300 K positron plasma, using the experimental arrangement shown in figure 10. Typical parallel energy spreads are  $\sim 18\text{--}30$  meV (FWHM).

energies from  $\sim 0.2$  eV to 100 eV [44, 225, 229]. Factors that presently limit the useful range of beam energies are discussed below.

### 3.6. Scattering experiments using a trap-based beam

**3.6.1. Experimental arrangement.** The experimental arrangement to study scattering using a magnetically guided trap-based beam is shown in figure 10. The beam is guided through a gas cell containing the target species. All positrons except those backscattered in the gas cell are guided through the RPA to a collector plate. The backscattered particles reflect off the exit gate of the positron accumulator and are guided back through the scattering cell and RPA to the collector plate. The transmitted intensity is measured by monitoring the annihilation gamma rays produced when the positrons strike the collector plate. An important advantage of the technique is that the two key parameters involved in making absolute cross section measurements, namely the path length and test-gas pressure, can be measured with precision. The gas cells used in the experiments have small entrance and exit apertures, so the path length is well defined and the pressure is, to a good approximation, constant in the cell. Target gas pressures typically vary from  $\sim 0.05$  to 1.0 mTorr, measured to an accuracy  $\sim 1\%$  using a capacitance manometer.

Typical cells used in scattering experiments [44, 225, 228, 229] were constructed of gold-plated copper, cylindrical in shape, 40 cm long with an internal diameter of 7 cm, with 5 mm apertures at each end. One important consideration is accurate knowledge of the positron beam energy inside the gas cell. Experience has shown that there are offsets between the applied and actual potentials on the elements of the system, ranging from tens to hundreds of meV. The origin of these stray potentials is not presently understood and is under investigation<sup>7</sup>. To quantify these variations, measurements of the cutoff potential of the various elements and combinations of elements are compared with the results of time-of-flight measurements using the pulsed positron beam [228]. The latter procedure measures the *average* beam energy in the gas cell. The difference between the cutoff potential and the path-averaged value is a

<sup>7</sup> This effect appears to be due to material close to the positron beam (e.g., at the entrance and exit of the gas cell). Tests indicate that it is insensitive to the particular cell material. Calculations indicate that it is not due to non-adiabatic contributions to the positron gyromotion in the magnetic field, nor is it due to variations in the value of the magnetic field in the proximity of the gas cell [230].

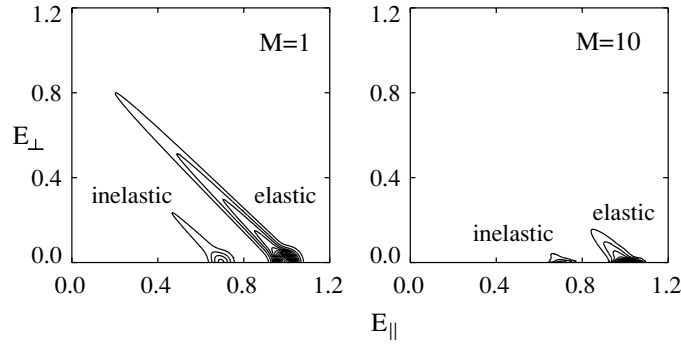


**Figure 12.** Simulation of scattering in a magnetic field for the case where there is both elastic scattering and inelastic scattering. Energy units are arbitrary. The incident beam has a small energy spread ( $\Delta E \approx 0.04$ ), centred at energy  $E_{\parallel} = 1.0$ ,  $E_{\perp} = 0$ ; and there is one open inelastic channel with excitation energy  $E_{\text{ex}} = 0.3$ . (a) At  $M = 1$ , elastic scattering and inelastic scattering produce scattered positrons distributed along two lines, oriented at  $45^{\circ}$  to the abscissa. (b) At  $M = 10$ ,  $E_{\perp}$  decreases by a factor of 10, and the inelastic scattering can be distinguished and measured by the RPA.

measure of the maximum potential variation in the gas cell and therefore provides a measure of the quality of a given cell.

**3.6.2. Cross section measurements.** Cross sections measurements can be made by analysing the parallel energies of the transmitted (i.e., both scattered and unscattered) positrons [225, 227–229]. This technique is intimately connected with the motion of positrons in a magnetic field. At the typical magnetic field strengths used,  $B \sim 0.1$  T and for  $0.025 \leq E_{\perp} \leq 100$  eV, the corresponding gyroradius,  $\rho$ , of the positron is in the range,  $4 \leq \rho \leq 200$   $\mu\text{m}$ . Thus, it is large compared to the scale of atomic interactions and small compared to the spatial scale of the scattering cell, RPA, and collector plate.

For a slowly varying magnetic field, the quantity  $E_{\perp}/B$  is an adiabatic invariant. As a result, changing the ratio of the magnetic field strengths,  $M = B_C/B_A$ , between the scattering cell and the RPA region permits measurement of the total energy of the scattered positron. Namely, the perpendicular component of the energy,  $E_{\perp}$ , is reduced to  $E_{\perp}/M$ , while the energy component,  $E_{\parallel}$ , of the positrons parallel to  $B$  is increased by this same amount,

$$E_{\parallel A} = E_{\parallel C} + E_{\perp C}(1 - 1/M) \approx E_{T,A}, \quad (17)$$

and

$$E_{\perp A} = E_{\perp C}/M \ll E_{\parallel A}, \quad (18)$$

where the subscripts A, C and T denote the energies in the RPA region, scattering cell and total positron energy, respectively. A key point is that, for values of  $M \gg 1$ , to a very good approximation, the RPA measures the *total* positron energy. This is illustrated in figure 12 for the case where  $M = 1$  and  $M = 10$ , and a target atom or molecule that produces both elastic and inelastic scattering, the latter from a single channel with excitation energy,  $E_{\text{ex}} = 0.3$  (arbitrary units).

**Integral inelastic cross sections.** When inelastic channels are open and separated in energy from the incident beam and from each other by an amount greater than the beam energy resolution, the integral cross sections for these processes can be measured. This is

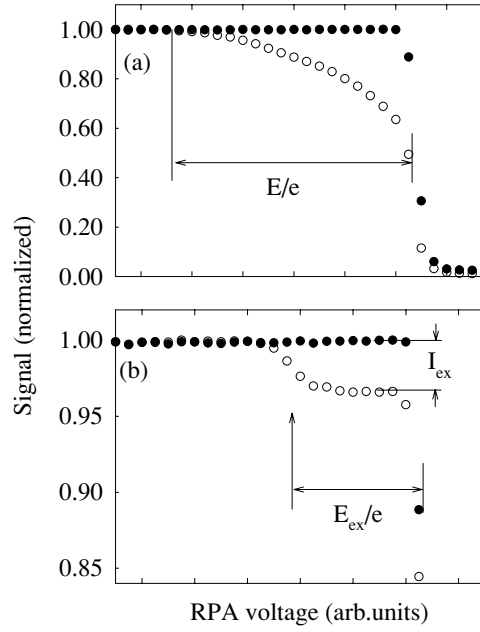


**Figure 13.** RPA curves for scattering of 0.5 eV positrons from CO: (○) test gas in, (●) cutoff of the main beam with no gas: (a)  $M = 1$  and (b)  $M = 35$ . The amplitude of the step in (b) is proportional to the cross section for excitation of the  $\nu_1$  vibrational mode at 0.27 eV.

illustrated in figure 13(b) for one open channel, positron scattering from CO at  $M = 35$ . In this case, the cross section,  $\sigma_{\text{ex}}$ , is given by [228],

$$\sigma_{\text{ex}} = \frac{I_{\text{ex}}}{I_0 n_m l}, \quad (19)$$

where  $n_m$  is the number density of target molecules,  $l$  is the path length in the cell,  $I_0$  is the intensity of the incident positron beam, and  $I_{\text{ex}} \ll I_0$  is the step-change in intensity of the collected positron current indicated in figure 13. In equation (19) and subsequent expressions for cross sections, we assume a linear approximation to the Beer–Lambert law. By varying  $M$  and the RPA voltage, a wide range of cross sections can be measured.

*Differential elastic cross sections.* Another limit is the case where  $M = 1$ . For this value of  $M$  and when no inelastic channels are open (or the scattering from them is negligibly small), an RPA measurement provides a measure of the differential elastic scattering cross section. In particular, for only elastic scattering,  $E = E_{\parallel} + E_{\perp}$ , and the scattering angle is given by

$$\theta = \cos^{-1} \sqrt{E_{\parallel}/E}. \quad (20)$$

In this case, the differential cross section is given by [228]

$$\left. \frac{d\sigma}{d\Omega} \right|_{E,\theta} = -\frac{\sqrt{E E_{\parallel}}}{\pi n_m l I_0} \frac{dI_C}{dE_A}, \quad (21)$$

where  $E_{\parallel}$  is the parallel energy of the scattered positron,  $E_{\parallel} = E \cos^2 \theta$ ,  $I_C$  is the intensity of the collected positron beam, and  $E_A$  is the RPA cutoff energy. In experiments done to date, backscattering is not distinguished from forward scattering, and so the measurements

represent the differential cross section folded about  $90^\circ$ , namely the measured cross section corresponds to

$$\frac{d\sigma}{d\Omega} = \left. \frac{d\sigma}{d\Omega} \right|_{\theta} + \left. \frac{d\sigma}{d\Omega} \right|_{\pi-\theta}. \quad (22)$$

*Grand total cross sections.* Referring to figure 13(a), if the magnetic field ratio is set to  $M = 1$  (uniform field), the grand total cross section can be measured by setting the RPA to an energy  $E - \delta E$ , just below the energy of the incident positron beam (to reject all scattered particles). Positrons that are either scattered in angle or have appreciable energy loss will not be transmitted. The decrease in beam intensity is thus proportional to the grand total scattering cross section, namely [228],

$$\sigma_T(E) = \frac{I_0 - I_C(E - \delta E)}{I_0 n_{ml}}. \quad (23)$$

In a typical experiment [228], the positron beam has an energy resolution  $\Delta E_{\parallel} = 25$  meV (FWHM), and  $\delta E$  is chosen to be  $\sim 40$  meV, corresponding to the  $3\sigma$  point on the cutoff curve for the main beam (which has an approximately Gaussian energy distribution).

*Positronium formation.* To measure the cross section for positronium formation, the RPA is set to pass all energies,  $E$ , and the transmitted beam intensity,  $I_C(E)$ , is measured as a function of the positron energy in the gas cell. The decrease in beam intensity relative to  $I_0$  (i.e., the intensity measured at energies below the positronium-formation threshold) is then proportional to the positronium-formation cross section.

$$\sigma_{Ps}(E) = \frac{1}{n_{ml}} \frac{I_0 - I_C(E)}{I_0}. \quad (24)$$

*Ionization.* To measure ionization cross sections, the field ratio,  $M$ , is set to  $M \gg 1$ , and the RPA set to reject any positron with energy smaller than  $E - E_i$ , where  $E_i$  is the ionization energy of the test species, and  $E$  is the energy of the unscattered positron. The decrease in beam intensity relative to that of the intensity of the transmitted beam at low energies then yields the ionization cross section,

$$\sigma_I(E) = \frac{1}{n_{ml}} \frac{I_0 - I_C(E - E_i)}{I_0}. \quad (25)$$

### 3.7. Annihilation experiments

Annihilation in positron interactions with atoms and molecules can occur in a number of ways [5]. Above the threshold for positronium formation, the positron can carry away one of the target electrons in a neutral positronium atom, which subsequently decays by either two- or three-gamma emission depending on its spin state. Measurement of the cross section for this process in scattering experiments is described above. Annihilation also occurs at energies below the threshold for positronium formation, where the positron annihilates with one of the bound target electrons. The cross section of this process is small compared to atomic scales<sup>8</sup>. It has been studied in a number of ways. The earliest method, used by Deutsch and coworkers in their seminal experiments [25, 232], involves study of the annihilation process at amat test-gas densities<sup>9</sup>. In this case, the test gas itself moderates fast positrons from a radioactive source. Following the development of positron traps another method became available, namely to introduce the test gas at low pressure in the presence of a cloud of trapped

<sup>8</sup> As a result of annihilation in virtual Ps, the cross section shows a rise  $\propto (\epsilon_{thr} - \epsilon)^{-1/2}$  below the Ps-formation threshold,  $\epsilon_{thr}$  [143, 231].

<sup>9</sup> 1 amat is the number density of an ideal gas at the standard temperature and pressure,  $2.69 \times 10^{19} \text{ cm}^{-3}$ .



positrons [147, 224]. This helps to avoid density-dependent effects due to the interaction of the positron with more than one atom. Finally, following the development of tunable-energy trap-based positron beams, it has become possible to study the annihilation process, resolved as a function of positron energy [46].

*3.7.1. Experiments in high-density gases.* Annihilation for a variety of target atoms and molecules has been studied in gases at amagat densities by variants of the technique used by Deutsch [5, 25, 149, 232, 233]. The gas is made sufficiently dense to moderate the fast positrons, and the information is contained in the time distribution of the annihilation signal. In this technique, a  $^{22}\text{Na}$  source is placed in close proximity to a gas cell filled with the test gas. The ‘start’ signal for timing is obtained by detecting the 1.27 MeV gamma ray that accompanies positron emission. Several processes can be distinguished by analysing the details of the time distribution of the annihilation events. They include prompt annihilation due to the fast positrons as they slow down; annihilation of slow (or if thermalization occurs, a Maxwellian distribution) of positrons; and a long-time tail due to ortho-positronium decay. Subsequent to its initial development, many refinements to this technique have been made by a number of workers [5, 233, 234].

In addition to annihilation rate measurements, much effort was devoted to the study of annihilation in the presence of a static electric field. One aim of that work was to obtain information about the momentum transfer and annihilation cross sections at low positron energies [1, 5, 233]. This type of experiment was also extended to the study of positron many-atom phenomena, such as self-trapping in helium gas at cryogenic temperatures [235, 236].

The first measurements of the *gamma-ray spectra* from gaseous media were made in high-pressure gases by Heinberg and Page [237] using the two-dimensional (2D) ACAR technique. However, these experiments focused on positronium formation, and the signal level was insufficient to study in detail annihilation from the test species. Using this same technique and a 2D detector, Coleman *et al* [238] made the first quantitative study of the annihilation of free thermalized positrons with atomic gases at atmospheric densities.

*3.7.2. In situ annihilation experiments in traps.* In these experiments, positrons are typically trapped and cooled to 300 K. Then the buffer gas is removed, a low pressure (e.g.,  $\sim 10^{-6}$  Torr) of the test gas is introduced, and the annihilation rate is measured as a function of time [147, 148, 224, 239, 240]. Figure 14 shows a diagram of the apparatus used in these experiments.

A cold trap is located in close proximity to the positron plasma to reduce impurities. Positrons are allowed to annihilate for various times, then the remaining positrons are dumped on the collector and measured. Measurements are made as a function of test-gas pressure. The slope of the plot of the annihilation rate as a function of test-gas pressure provides a measure of the (normalized) rate.

The dependence of the annihilation rate on *positron temperature* was investigated in the range of temperatures of 0.1–0.5 eV for atoms and 0.1–0.3 eV for molecules [240, 241]. In this case, after the introduction of a test gas, the positrons are heated by a burst of radio-frequency noise. As the positrons cool (by collisions with the test gas), the annihilation rate is obtained from the time dependence of the annihilation signal. The time dependence of the positron temperature is measured independently, as a function of elapsed time from the end of the heating pulse [241].

The annihilation *gamma-ray energy spectra* for atoms and molecules were studied using the apparatus shown in figure 14 [151, 239, 242, 243]. The experiment consists of repeated

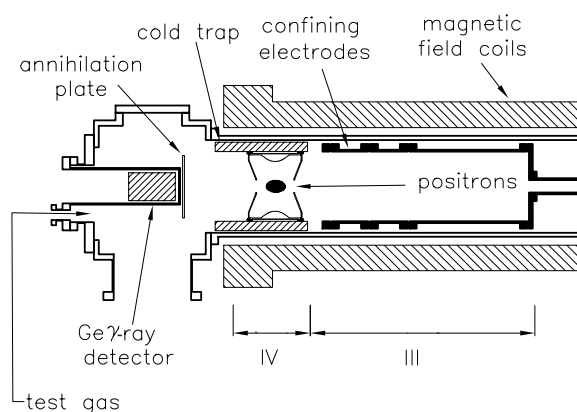


**Figure 14.** Arrangement to study positron annihilation, *in situ*, in a positron trap. Positrons from the three-stage accumulator located on the right are shuttled to a fourth trapping stage that is in close proximity to a collector plate and gamma-ray detector for high collection efficiency.

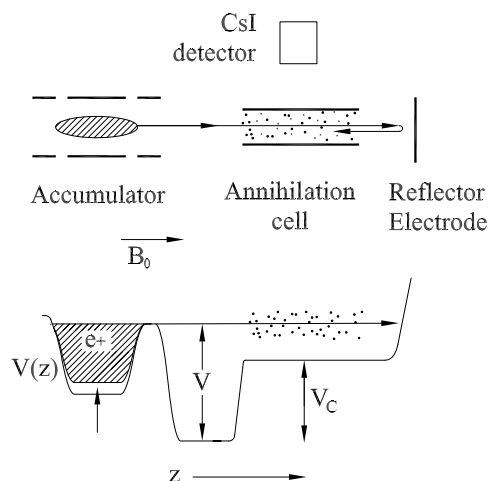


**Figure 15.** Experimental arrangement used to study positron annihilation using a trap-based positron beam. Above: arrangement of the positron accumulator, annihilation cell and gamma-ray detector. Below: corresponding potential profile. The positron energy in the cell is given by  $E = e(V - V_C)$ .

cycles of positron accumulation, cooling and pumping out the buffer gas, followed by measurement in the presence of the test gas using an intrinsic germanium detector. Typical runs take  $\sim 12$  h for  $\sim 10^6$  gamma-ray counts. The positron temperature was measured separately and confirmed to be the ambient temperature of 300 K.

**3.7.3. Energy-resolved studies using a trap-based beam.** The apparatus for these experiments is shown in figure 15 [46, 47]. A trap-based beam is guided magnetically through a gas cell. Annihilation radiation from the interaction of the positrons with the test gas is detected using a CsI scintillator and photodiode located in close proximity to the gas cell. The positron beam is operated in a pulsed mode to minimize space-charge effects on the beam energy spread, with  $\sim 10^4$  positrons per pulse at a repetition rate of 4 Hz. The energy distribution in the positron beam is approximately Gaussian with a width of  $\sim 25$  meV (FWHM).

Due to the low expected gamma-ray signal, the gas cell and the detector were carefully shielded. Experiments are run either in a single- or multiple-pass mode. In the latter case, the beam is reflected from a potential applied to an electrode on the opposite side of the scattering cell. The positron pulse bounces back and forth through the cell (typically a total of  $\sim 2$ – $5$  passes), with the positrons confined between this repulsive potential and the exit gate of the positron trap.

The uniformity of the potential in the annihilation region is verified using a time-of-flight technique and found to be constant to within  $\sim 10$  meV [228]. This degree of uniformity was found to be even greater here than in the scattering experiments described above. Likely, this is due to the fact that the detector acceptance angle defines the interaction region and no material was required close to the positron beam.

Positron energies are measured using the cell electrode as an RPA and are corrected for the calculated perpendicular energy in the cell [46, 47]. The average positron energy can be varied from 0.05 to  $\sim 100$  eV. Measurements are precluded below 50 meV due to elastic scattering in the region before the gas cell [47]. The detection apparatus is gated to count only those events detected within the time interval (e.g.,  $\sim 15$   $\mu$ s) during which the positrons are kept in flight. The background amounted to only  $\sim 1$  count per  $10^9$  positrons. The test-gas pressure is set so as to avoid scattering greater than  $\sim 10\%$  per pass. The linearity of signal intensity as a function of test-gas pressure was also checked. The gamma-ray collection and detector efficiency were calibrated using a radioactive source of known activity.

## 4. Positron scattering

### 4.1. Grand total cross sections

Most measurements of total scattering cross sections,  $\sigma_T$ , were made before 1990 and many of them have been reviewed previously [2, 3, 5]. Here we concentrate on a number of specific examples, including what might be considered benchmark cases such as H, H<sub>2</sub> and He. We also discuss an example from the large body of work on polyatomic systems, done mainly by the Yamaguchi group.

The only measurements of  $\sigma_T$  for positron scattering from atomic hydrogen are those of the Detroit group [189, 190, 244]. These authors also provided direct measurements of the total electron scattering cross section. The cross sections for both e<sup>+</sup> and e<sup>−</sup> impact are compared in figure 16. Below 10 eV the electron scattering cross section is about ten times larger than that for the positrons, (partly because of the presence of the Ramsauer–Townsend minimum for the positron), although at higher energies the positron cross section exceeds that for electrons. The rapid increase of the positron cross section above 7 eV is almost exclusively due to positronium formation. At energies above 200 eV the two cross sections merge, as expected, based on calculations using the first Born approximation.

In figure 16, we also show the corresponding cross sections calculated using the convergent close-coupling (CCC) approach [245, 246] of Bray and collaborators; the pseudostate coupled-channel method for the positron [103] of Walters *et al*; a coupled-channel approach, again for positrons, by Mitroy [247, 248]; and a Kohn variational calculation [83] by Humberston *et al*. In the case of positrons, the agreement of all four theories with experiment is excellent above the positronium-formation threshold. Below this energy, the theories are in excellent agreement with each other (i.e., essentially indistinguishable), but the experiment has considerably smaller values. While it remains an open question, it may be that the problems here lie largely with the experimental measurements, which are extremely difficult to make. For the electron case, the theory [246] is in good agreement with experiment at all energies.

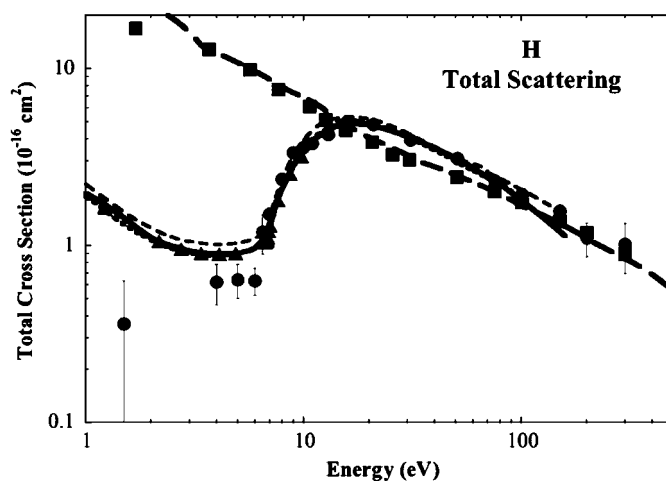


**Figure 16.** Total cross sections for positrons and electrons scattered from atomic hydrogen. The measurements (( $\blacksquare$ ) electrons, ( $\bullet$ ) positrons) [190] are compared with the convergent close-coupling calculation [245, 246] for positrons (—) and electrons (---) respectively, and with the coupled-channel plus pseudostates model (- - -) for positrons [103], a close-coupling calculation (- - -) for positrons [247, 248], and a Kohn variational approach [83] ( $\blacktriangle$ ) (see text for details).

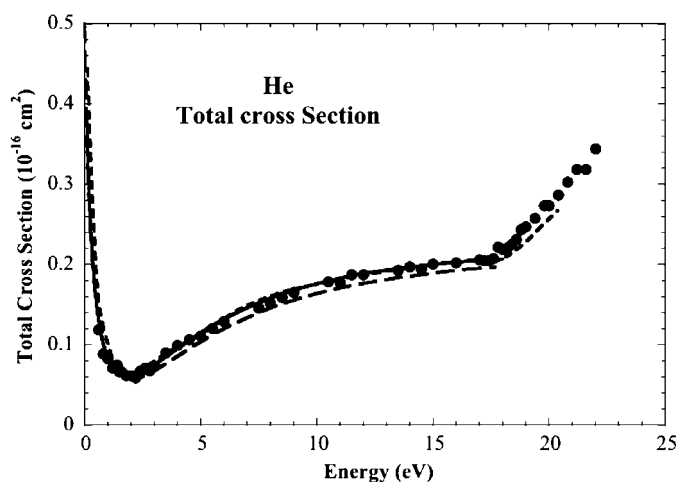


**Figure 17.** Total cross section for positron scattering from helium. The experimental results of Mizogawa *et al* ( $\bullet$ ) [249] are compared with a convergent close-coupling calculation (—) [104], a many-body theory calculation (---) [58, 59], and a Kohn variational calculation (- - -) [84].

There have been many measurements of the total scattering cross section for helium, and this work is well summarized in [5]. Here we contrast the most recent measurements of [249] with the Kohn variational calculations [84], recent convergent close-coupling calculations [104], and many-body theory calculations [58, 59]. As can be seen in figure 17, the agreement both between different theories and with experiment is excellent below the positronium-formation threshold (i.e., in helium,  $\varepsilon_{\text{thr}} = 17.8 \text{ eV}$ ). The Kohn calculation also provides a good description of the total cross section in the region immediately above the positronium threshold.

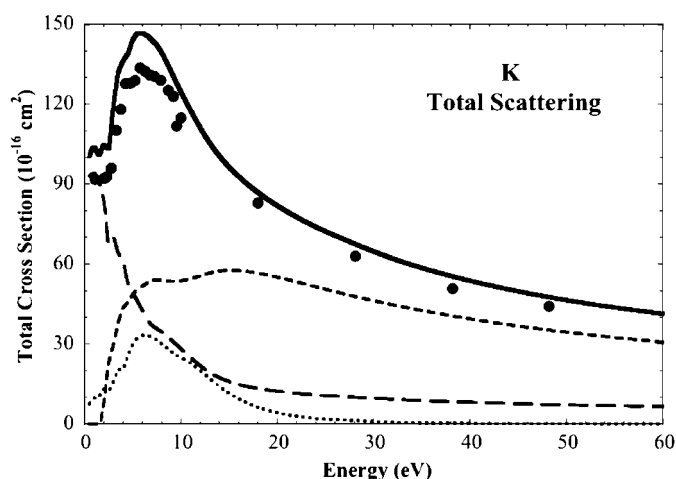


**Figure 18.** Total cross section for positron scattering from potassium. The experimental results (●) [187] (corrected and renormalized—see text) are compared with a coupled-state calculation (—) [101]. The various contributions to the calculated cross section are also shown: (— —) total elastic, (- - -) 4s-4p excitation, (···) positronium formation.

Total cross sections for several of the alkali-metal atoms have been measured by the Wayne State group. An example of these data for potassium [187] is shown in figure 18 and is compared with the coupled-state calculations of McAlinden *et al* [101]. Note that the experimental data are the measured cross sections, corrected by McAlinden *et al* to account for forward elastic scattering contributions in the original measurements. This, together with an upward scaling of the corrected cross section by a factor of 1.1, results in an experimental cross section which is between 5–30% higher than the original measurements, depending on the incident energy. The resulting agreement between experiment and theory is clearly quite satisfactory.

Another benchmark example is that of molecular hydrogen. Recent measurements using two different techniques [190, 228, 250] are shown in figure 19. The results of Zhou *et al* cover an extensive energy range while the high-resolution data of Sullivan *et al* were obtained on a dense energy grid over a span of 2.5 eV in a search for possible resonance features. Although the overlapping energy range is small, the agreement in the energy dependence and the absolute magnitude of the two measurements is excellent. We also compare with the *R*-matrix calculations of Danby and Tennyson [118], a Kohn variational method of Armour *et al* [117], and a Schwinger variational calculation of Lino *et al* [128], all of which neglect the Ps-formation channel. At energies below the Ps threshold the *R*-matrix results probably suffer from a lack of convergence, while the two variational calculations are almost identical and provide a reasonable description of the experiment.

The Yamaguchi group has measured total scattering cross sections for a large number of molecules; and in recent years, they have compared these cross sections with the corresponding electron scattering measurements. We refer the reader to [185] and references therein for further discussion of this work. A consistent feature of these comparisons is that, while the positron measurements contain structures that can be assigned to positronium or ionization thresholds, they bear none of the significant resonant structures that are ubiquitous in electron–molecule scattering cross sections. An example of such a comparison is shown in figure 20 for scattering from methyl chloride (CH<sub>3</sub>Cl) [185]. Not only is the electron scattering cross

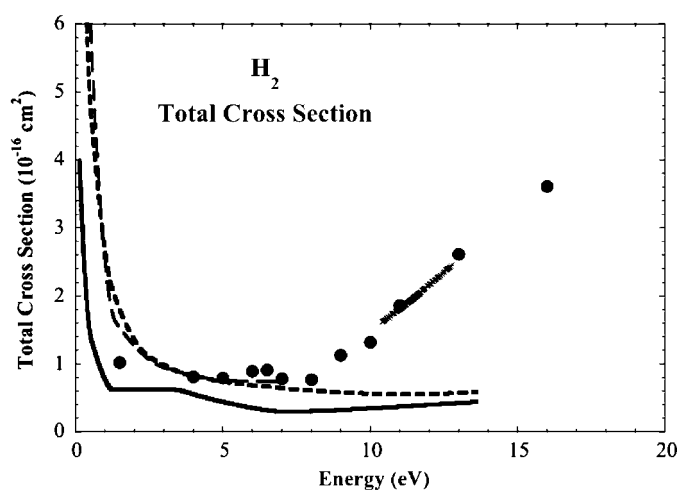


**Figure 19.** Total cross section for positron scattering from  $\text{H}_2$ . The experimental results of Zhou *et al.* (●) [190] and Sullivan *et al.* (×) [250] are compared with the theoretical calculations of Danby and Tennyson (—) [118], Armour *et al.* (---) [117] and Lino *et al.* (- - -) [128].

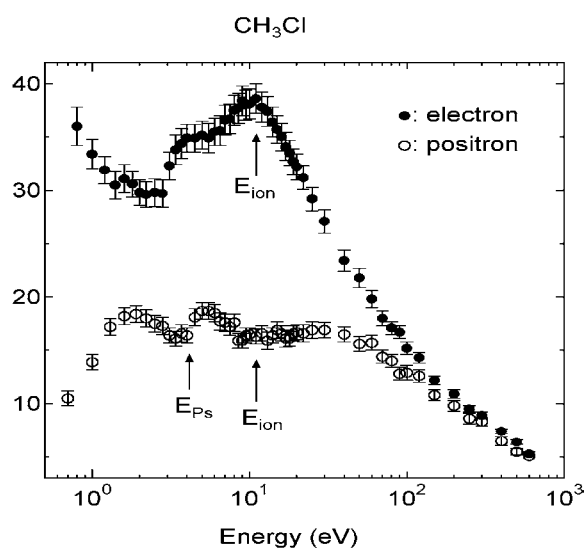


**Figure 20.** Total cross section for positron (○) and electron (●) scattering from methyl chloride. Reprinted with permission from [185]; copyright 2001 by Institute of Physics Publishing.

section substantially larger than that for the positron, but there are also structures in the electron cross section below 10 eV. These features are due to intermediate negative-ion resonances that both enhance the cross section and lead, in some cases, to fragmentation via dissociative attachment.

Finally, we note that the Trento group [251] have investigated the convergence of positron and electron scattering cross sections for noble-gas atoms at intermediate and high energies.



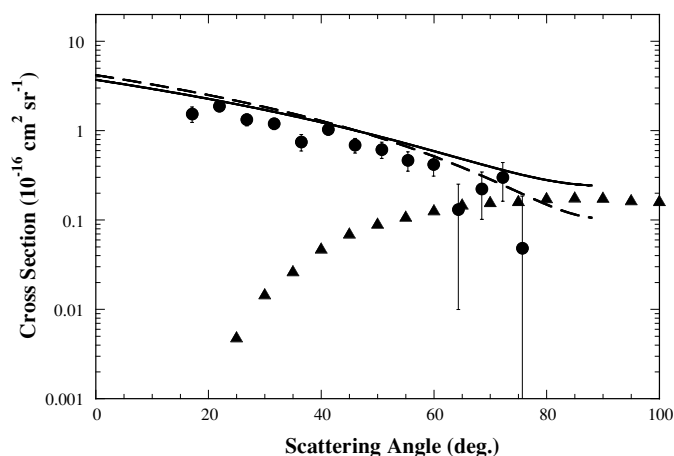


**Figure 21.** Absolute elastic DCS for positron scattering from argon (●) at an incident energy of 1.0 eV (from [228]): (—) polarized-orbital calculation of McEachran *et al* [252], and (---) the many-body theory result of Ludlow and Gribakin [58, 59]. This is compared with recent electron scattering data (▲) [253]. The theoretical results are ‘folded’ around 90° (see text for details). The electron scattering results are not folded.

Their measurements indicate that cross sections for argon converge by an incident energy of 5 keV, while those for Kr still show slight differences.

#### 4.2. Elastic differential cross sections

As discussed in section 3.4.2, an extensive set of relative elastic differential cross sections (DCS) has been obtained by the Detroit group for a large range of atoms and molecules. In addition, the DCS have been measured at a number of fixed angles by the UCL group, and recently absolute DCS measurements have been made by the San Diego group using a trap-based beam. Interestingly, there are no contemporary experimental data for elastic DCS for helium, a target where very accurate, low-energy calculations might be expected from recent close-coupling treatments.

There have been a number of measurements for argon, and a recent example is shown in figure 21. One can see that the absolute DCS for positrons from [228] at an energy of 1.0 eV are in good agreement with the polarized-orbital and many-body calculations of [252] and [58, 59]. The theoretical calculations for positrons have been ‘folded’ around 90°, in order to compare with the DCS measured using the magnetized, trap-based beam (see section 3.6.2 and equation (22)). It is interesting to contrast the positron cross section at this energy with the corresponding electron scattering measurements shown in figure 21 [253]. Due mainly to the presence of the Ramsauer–Townsend (RT) minimum below 1 eV for electrons in Ar, the positron cross section is considerably larger than the electron cross section at smaller scattering angles. Note that positron scattering cross sections for rare-gas atoms also possess RT minima. However, the *s*-wave cross section minimum tends to be ‘filled in’ by the contributions of higher partial waves (see figure 17). This is particularly true in the heavier rare gases where the minimum occurs at higher energies.

In figure 22 we show the absolute elastic DCS for positron and electron scattering from Xe at 5.0 eV. The positron results are from the trap-based beam at UCSD [254], while the electron results are those of Gibson *et al* [255]. At incident energies well above the electron RT

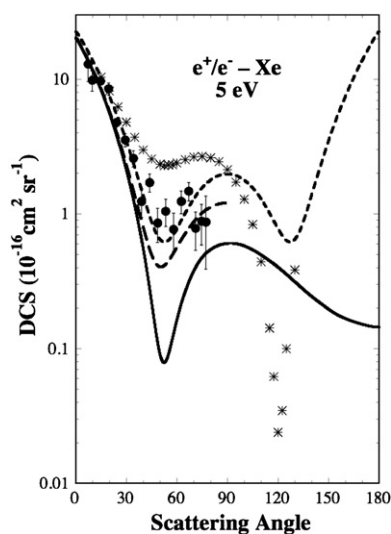


**Figure 22.** Absolute elastic DCS for positrons (●) and electrons (\*) from xenon at an incident energy of 5.0 eV [254]: (—) theory of McEachran [256]; (---) same theory, and (- · -) the many-body theory calculation of Ludlow and Gribakin [58, 59], both folded about 90°. The electron scattering data are from Gibson *et al* [255].

minimum, the two cross sections are comparable in magnitude. The theoretical curves from the polarized-orbital calculation [256] show the effect of folding of the DCS around 90° on the magnitude of the cross section near the minimum at around 50°. The agreement between experiment and the folded theoretical cross section is good. Also shown is a many-body theory calculation [58, 59] which again shows good agreement with the experiment.

Two final examples of recent DCS measurements are shown in figures 23 and 24 for H<sub>2</sub> and CO respectively [257]. The H<sub>2</sub> measurements were taken using the trap-based beam at an incident energy of 0.5 eV, which is just below the first vibrational excitation threshold. The measurements are compared with a Kohn variational calculation of e<sup>+</sup>-H<sub>2</sub> elastic scattering [117] and a calculation using a so-called ‘distributed positron model’ [258]. While there is reasonable agreement between experiment and theory regarding the absolute magnitude of the cross section, there are clear differences between the two for the shape of the angular distribution. One possible reason for the disagreement in the case of the Kohn calculation is that only three symmetries were included in the calculation. The strong forward scattering observed in the experiment is no doubt the result of polarization effects and many partial waves and symmetries may need to be included to account for this.

Shown in figure 24 are absolute DCS results for CO (folded around 90°), measured using a trap-based beam at an energy of 6.75 eV [257]. They are compared with the earlier work of the Detroit group [259] which covers a larger angular range. In both cases, the measurements represent ‘quasi-elastic’ scattering in that there are likely contributions from both vibrational and rotational excitation of the ground state of the CO molecule. However, as pointed out in [225], these contributions are likely to be small (less than 5%), and the measurements provide a reasonable estimate of the elastic DCS in this energy range. In figure 24, the relative measurements of Przybyla *et al* have been normalized to the UCSD data at an angle of 45°. There is a general agreement over the range of overlap of the two sets of data (in spite of the fact that trap-based beam DCS are folded). The shape of the DCS with a forward peak and a minimum is similar to that calculated for CO at 5 eV [135].

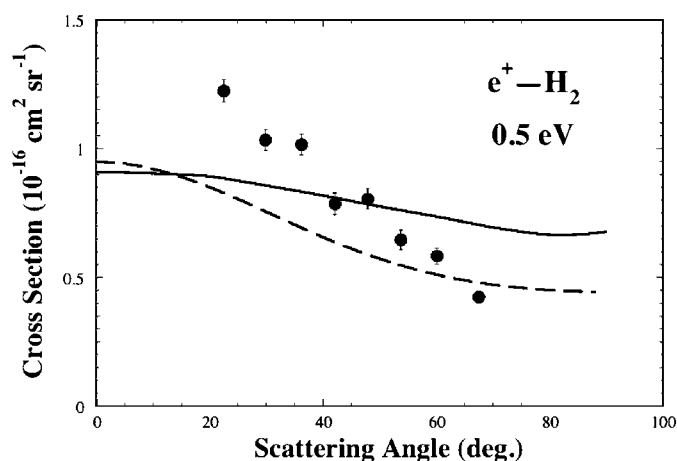


**Figure 23.** Elastic differential cross section for positron scattering from  $\text{H}_2$  at an energy of 0.5 eV: (●) data by Sullivan *et al* [257]. The results of a Kohn variational calculation (—) [117] and one using the distributed positron method (DPM) (---) [258] are also shown.

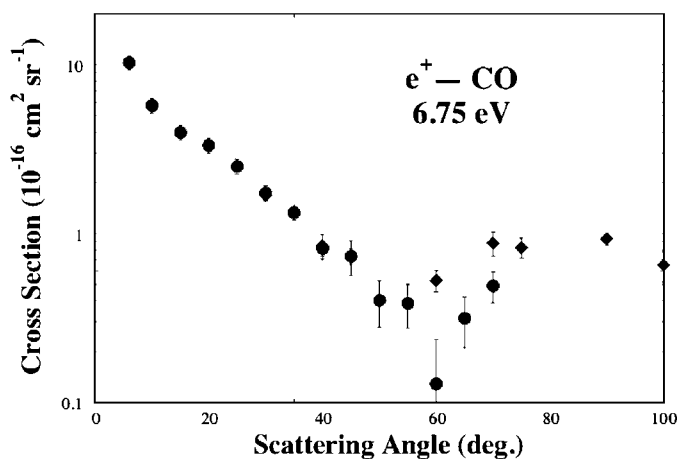


**Figure 24.** Elastic differential cross section for positron scattering from CO at an energy of 6.75 eV: (●) Sullivan *et al* (folded about  $90^\circ$ ) [257], and (◆) Przybyla *et al* [259].

#### 4.3. Vibrational excitation

Measurements of state-resolved excitation cross sections have posed considerable difficulties for conventional, moderator-based positron beams, due mainly to the limitations of energy resolution. This is particularly true for rotational and vibrational excitation of molecules where the spacing of energy levels can lie anywhere in the range from 0.1 to 500 meV. Nonetheless there have been a few attempts over the years at measuring vibrational excitation cross sections with conventional beams using time-of-flight detection techniques discussed briefly in section 3.4.3. For example, Kimura *et al* [137] and Kawada *et al* [199] measured the vibrational excitation cross sections for the sums of all the modes of  $\text{CO}_2$  and OCS respectively.

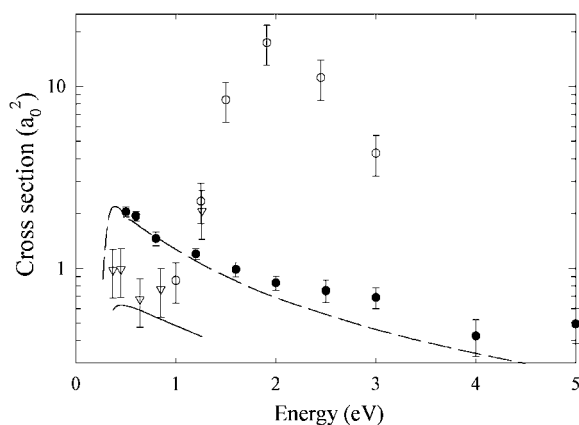


**Figure 25.** Absolute cross sections for the vibrational excitation in CO by electron ( $\circ$ ,  $\nabla$ ) and ( $\bullet$ ) positron impact [228]; (---) a calculation for positron scattering [135], and (—) a Born-dipole calculation for electron scattering [260].

The first, fully state-resolved vibrational excitation measurements were carried out by Gilbert *et al* [227], using the trap-based beam. They measured the integral cross section for exciting the  $\nu_3$  asymmetric stretch mode of  $\text{CF}_4$  which has an excitation energy of 157 meV at energies between 0.2 and 1 eV, using a beam with energy resolution  $\Delta\varepsilon \sim 20$  meV. Experimental data have now been obtained for the vibrational excitation of CO,  $\text{H}_2$ ,  $\text{CO}_2$ ,  $\text{CH}_4$  and  $\text{CF}_4$  using this technique [227, 229, 257].

In figure 25 the cross section is shown for the first vibrational excitation measurements of CO by positron impact [228]. The experimental cross section, which peaks just above threshold with a magnitude of around  $2a_0^2$ , compares favourably with the vibrational close-coupling calculation of [135]. Also shown in this figure are results for vibrational excitation of CO by electron impact [261], and a number of interesting conclusions can be drawn from the comparison. First, in the near-threshold region, the positron cross section exceeds that of the electrons by about a factor of 2. At higher energies the well-known  $\pi_g$  shape resonance dominates the electron scattering cross section from 1.5 to 3 eV and yields an integral cross section about a factor of 10 higher than the positron cross section. This illustrates one of the major differences between low-energy electron and positron scattering—the dominant role that resonances play in the former as compared with the latter. Second, it is apparent that the absolute uncertainty of the positron scattering data is comparable to, or smaller than, that of the electron data. This highlights the advantage of the trap-based experiment which provides a *direct* measurement of the integral inelastic cross sections, as compared with the electron cross sections that have been derived from differential scattering measurements.

Figure 26 shows the excitation cross sections for the three vibrational modes of the  $\text{CO}_2$  molecule measured with the trap-based beam [229, 262]. These modes have excitation energies of 82 meV (bend), 165 meV (symmetric stretch) and 291 meV (asymmetric stretch). The two dipole-allowed excitations exhibit the largest cross sections, while the symmetric stretch cross section is much smaller. There is reasonably good agreement with cross sections for the bend and asymmetric stretch modes which have been calculated using the continuum multiple scattering approximation, and given in [137, 199]. Also, as shown in figure 26, measurements of the cross section for the sum of all three vibrational modes at energies above 4 eV [137] are consistent with the individual mode measurements.

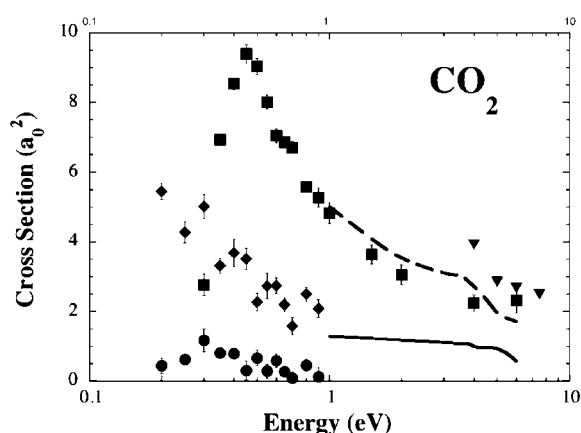


**Figure 26.** Integral excitation cross sections for the bending ( $\blacklozenge$ ), asymmetric stretch ( $\blacksquare$ ) and symmetric stretch ( $\bullet$ ) modes of the  $\text{CO}_2$  molecule [229, 262]. Also shown ( $\blacktriangledown$ ) are the cross sections for the sum of the three modes measured by Kawada, *et al* [199] and Kimura *et al* [137]; (---) and (—), the continuum multiple scattering calculations by the same authors for the two dipole-allowed transitions [137].

#### 4.4. Electronic excitation

For reasons similar to those advanced in the previous section, there have been few measurements of state-resolved *electronic* excitation cross sections for atoms and molecules by positron impact. A few earlier attempts, where inelastically scattered positrons were detected using time-of-flight techniques, usually involved a sum over a range of excited states or a sum of excitation and ionization processes. It was not until the recent development of trap-based beams that the possibility of state-resolved measurements has been realized.

The first experiments of this type were conducted by Sullivan *et al* [225], on Ar,  $\text{H}_2$  and  $\text{N}_2$  at energies from near threshold to 20–30 eV, as outlined in section 3.6.2 These spectra are similar to conventional, integral energy-loss spectra. For molecules they show clear steps in the transmitted signal corresponding to the excitation of the vibrational manifold of the electronic states involved. Such a spectrum for  $\text{N}_2$  is shown in figure 27. In this case, the steps correspond to vibrational levels of the  $a^1\Sigma$  and  $a^1\Pi$  electronic states lying 8.42 and 8.56 eV above the molecular ground state, respectively.

The absolute cross sections for these two states were extracted by fitting the spectrum shown in figure 27 using the known Franck–Condon factors (see [225]) for the vibrational transitions in  $\text{N}_2$ . They are shown in figure 28. The cross section for the  $a^1\Pi$  state is quite large ( $\sim 3a_0^2$  at 11 eV), and it appears as if it may be resonantly enhanced in the energy region immediately above threshold. The only available calculation, done using the Schwinger multichannel method [264], does not reproduce this feature. As seen in the figure, the corresponding electron scattering cross sections [263] are similar in magnitude. However, they have substantially larger uncertainties compared with the positron data as they have been derived from differential scattering data.

A second example is the excitation of the  $\text{B}^1\Sigma$  state of  $\text{H}_2$ , measured by Sullivan *et al* [225] between threshold and 30 eV. In figure 29 these results are compared with the calculations using a close-coupling approach [266] and the Schwinger multichannel (SMC) technique [125]. The close-coupling calculation predicts a cross section that is too high by about a factor of 4. The SMC prediction made a decade ago is in good agreement, both in magnitude

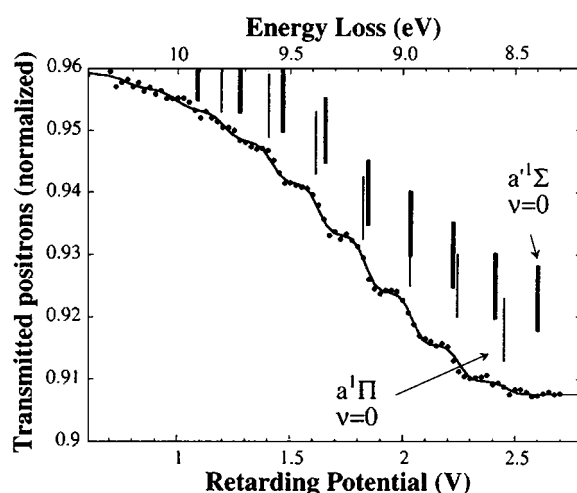


**Figure 27.** Retarding potential data (●) for the energy distribution of positrons (with incident energy 11 eV) transmitted through a gas cell containing  $N_2$  [225]. Thin and thick vertical bars show the positions of vibrational excitations of the  $a^1\Pi$  and  $a^1\Sigma$  electronic states, respectively.

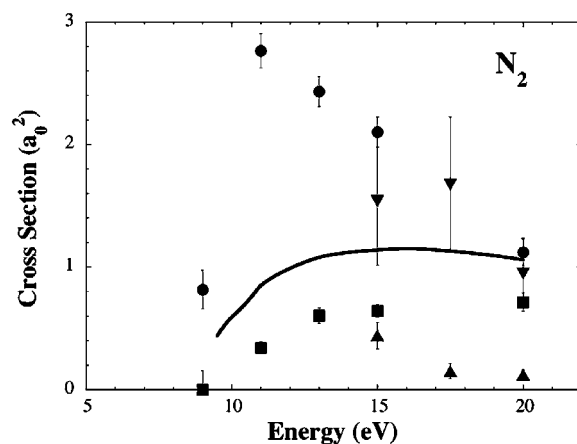


**Figure 28.** Absolute cross sections for (●, ■) positron [225] and (▼, ▲) electron [263] excitation of  $N_2$ :  $a^1\Pi$  (●, ▼) and  $a^1\Sigma$  states (■, ▲). The solid line is a Schwinger multichannel calculation for the  $a^1\Pi$  state [264].

and energy dependence, with the experimental result. Note that, at lower energies, the corresponding excitation cross section by electron impact [265] is similar but smaller.

The final example of electronic excitation is the measurement of Sullivan *et al* [225, 250] of the  $3p^5 4s$  states of argon, shown in figure 30. This excited state manifold consists of four levels, but only two of these, namely  $3p^5(^2P_{3/2})4s$  and  $3p^5(^2P_{1/2})4s$ , with total angular momenta  $J = 1$  and excitation energies of 11.63 and 11.83 eV, are accessible by positron impact. In the  $LS$ -coupling scheme, these two states would be described as  $3p^5 4s^3P_1$  and  $3p^5 4s^1P_1$ , and only one of them (the latter) would be excited if the electron spin-orbit interaction (which mixes them) was neglected or weak. The other two states with  $J = 0$  and  $2$ , are of triplet,  $3p^5 4s^3P_{0,2}$  nature and were not observed. In their experiment, Sullivan *et al* were able to resolve the two  $J = 1$  states, and to measure the cross sections between threshold and 30 eV.



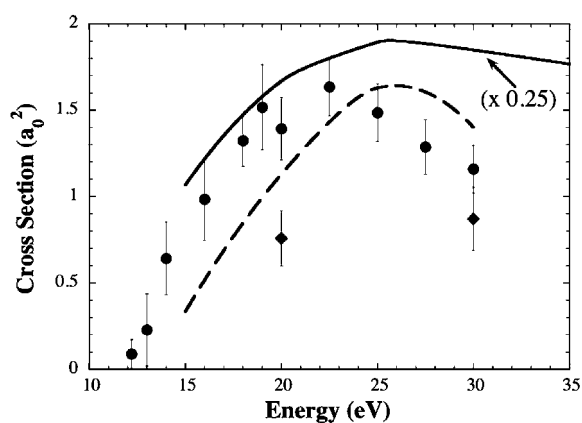


**Figure 29.** Excitation cross section for the  $B^1\Sigma$  state of  $H_2$  by positron (●) [225] and electron (◆) [265] impact. Also shown are the theoretical calculations: (---) [125] and (—) [266].

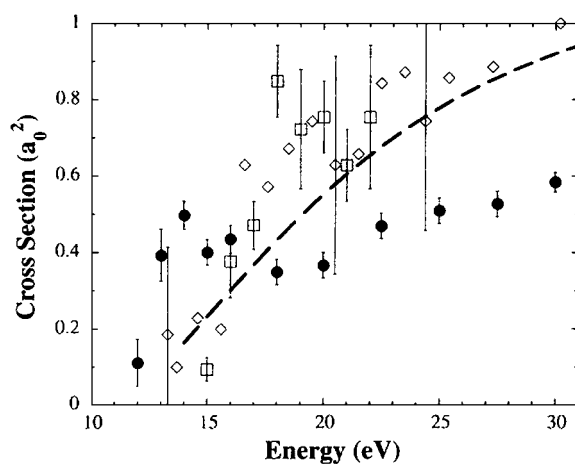


**Figure 30.** Excitation of the two  $3p^5 4s$  ( $J=1$ ) states of argon by positron impact. The results of Sullivan *et al* [225] (●) are compared with previous data for the excitation of all excited states: (□) [267] and (◇) [198]; and (---) the calculation of [269].

These results showed a remarkable similarity in magnitude to the excitation cross sections by electron impact [225]. In figure 30 we compare the total excitation cross section for the two  $J=1$  states obtained by Sullivan *et al* with the results of Coleman *et al* [267] and Mori and Sueoka [198], and with the distorted-wave calculation for these two states by McEachran and coworkers [268, 269]. The earlier experiments measured the summed cross section for all excited states, and thus one might expect them to be larger than the result of Sullivan *et al*, as shown in the figure. The calculated cross section has a reasonable energy dependence and size, but fails to reproduce the sharp onset of the cross section near the threshold.

#### 4.5. Direct ionization

The technique to study direct ionization using an electrostatic positron beam is described in section 3.4.5. An alternative method based on a magnetized, trap-based beam is described in section 3.6.2. Figure 31 presents an example of measurements for positron impact on argon

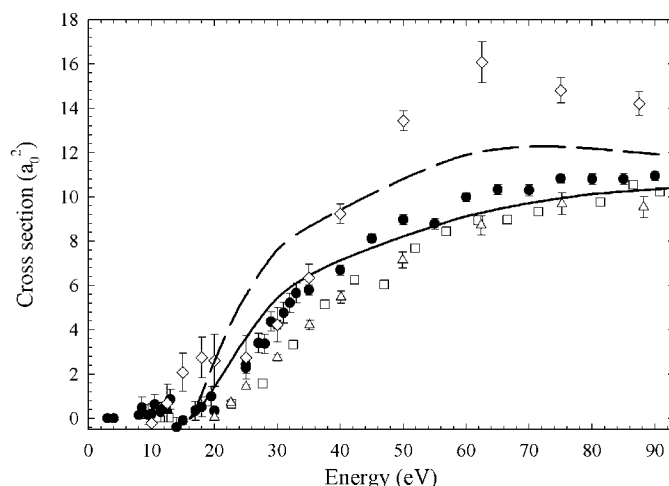


**Figure 31.** Cross section for direct ionization of argon by positron impact using a trap-based beam (●) [272]; and electrostatic beams (□) [207], (Δ) [216], (◇) [273]. Also shown are the results of calculations (---) and (—) by Campeanu *et al* [270, 271]. See [272] for details.

using both techniques. Recent measurements made using the two different techniques are in reasonably good, quantitative agreement with each other and with a recent distorted-wave calculation by Campeanu *et al* [270, 271].

#### 4.6. Positronium formation

Techniques to measure positronium-formation cross sections using electrostatic beams and a trap-based beam were both described in sections 3.4.4 and 3.6.2. Experimentally, Ps formation has been studied most extensively for noble-gas atoms, and a summary of earlier results for neon, argon, krypton and xenon is shown in figure 32. However, agreement between various experiments is modest at best. The most comprehensive set of measurements using an electrostatic beam was done by Laricchia and coworkers [207]. They obtained the Ps-formation cross sections by measuring the total number of ions produced, and subtracting from it the direct ionization signal, which was measured by correlating the ion signal with the simultaneous detection of a positron. Up to the peak in the cross section there is good absolute agreement with previous measurements made by Jin *et al* [274].

Recently, Ps formation in Ne, Ar, Kr and Xe was studied by Marler and coworkers, using a magnetized, trap-based beam [272, 280, 281] (see section 3.6.2). A comparison of the new data for argon with those of Laricchia *et al* [207] is shown in figure 33. The two measurements are in good agreement up to and including the peak in the cross section, but differ at higher energies. In particular, the data from [207] show a second peak, not present in the data obtained with the trap-based beam.

Another determination of the positronium-formation cross section, which we call method III [272, 280], is done by subtracting the direct ionization cross section measured with a trap-based beam [280] from the total ionization cross section from [207]. Figure 33 shows that the results obtained using method III are in agreement with the direct trap-based beam measurements of Ps formation from [280]. Similar agreement between method III and the directly measured positronium-formation cross sections of Marler *et al* is found for krypton, and all three methods yield similar results for xenon [272]. In neon, which has the

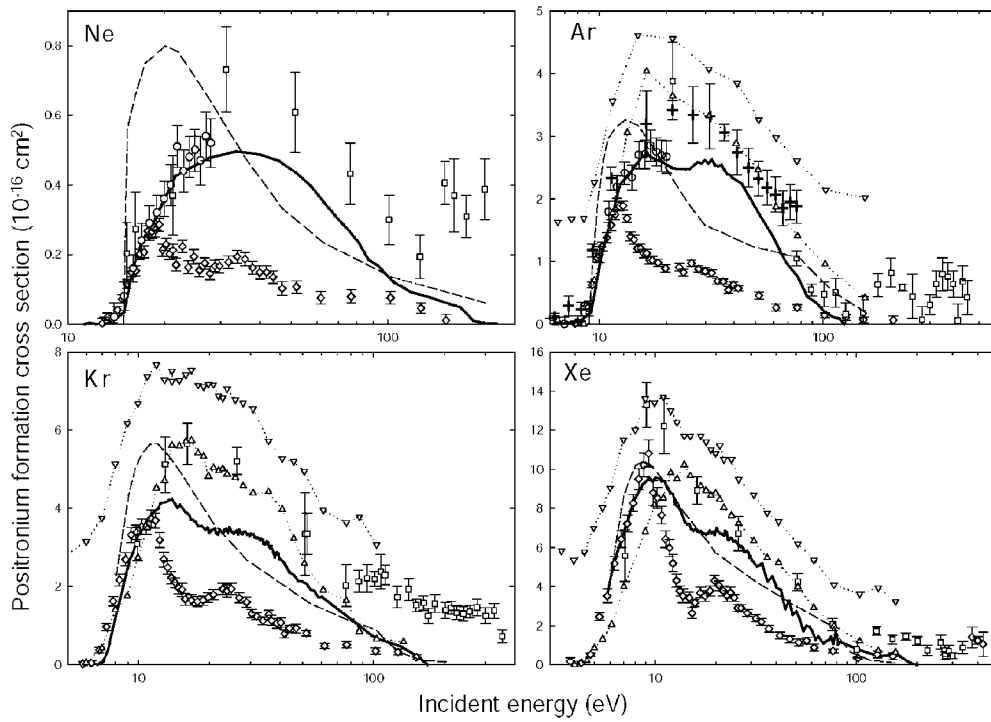


**Figure 32.** Compilation of earlier positronium-formation cross sections for neon, argon, krypton and xenon as a function of positron energy: figure reprinted with permission from [207]; copyright 2002 by the Institute of Physics: (—) from [207]; ( $\diamond$ ) [201]; ( $\circ$ ) [274]; ( $\square$ ) [275–278]; (+) [202]; ( $\nabla$ ) and ( $\Delta$ ), upper and lower limits [206]; and (— · —) theory of [279].

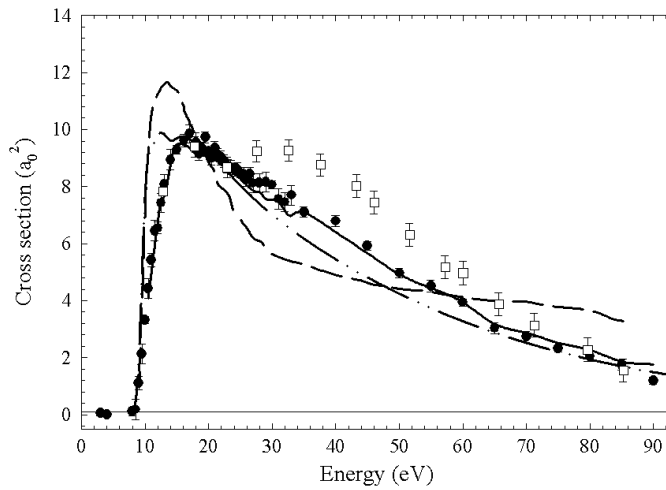


**Figure 33.** Positronium-formation cross section measurements for argon: (●) using a magnetized, trap-based beam [280]; ( $\square$ ) [207]; and (—) using the technique of [207] but with direct ionization cross sections from [280]. Theoretical predictions: (—) static exchange approximation, neglecting exchange between the Ps atom and the ion [279]; (- · -) distorted-wave Born approximation, scaled by 0.5 [282].

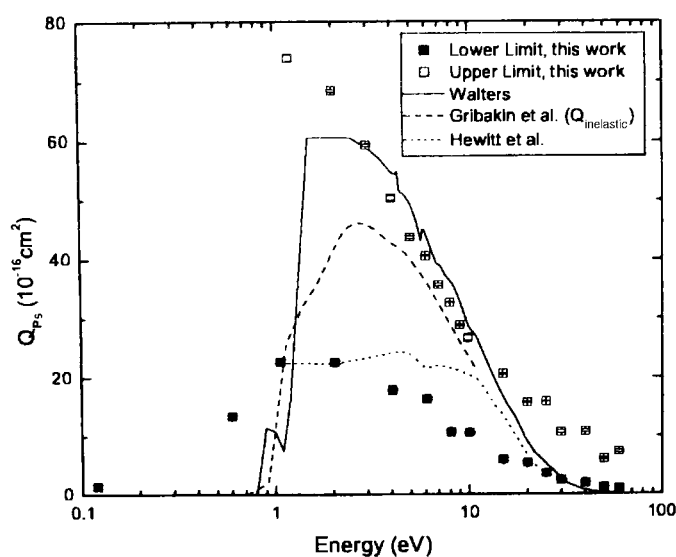


**Figure 34.** Positronium-formation cross section for magnesium. Reprinted with permission from [286]; copyright 2003 by the American Physical Society. The upper and lower limit cross sections are compared with theoretical calculations: (—) [286], (---) [288] and (· · · ·) [287].

smallest Ps-formation cross section (about  $2a_0^2$  at the maximum), there is a fair agreement between the measurements of [207] and [272], and the alternative procedure of method III does not improve the situation.

As seen in figure 32, the cross sections of Laricchia *et al* [207] for Ar and Xe exhibit a second peak at energies higher than the main peak. The authors suggest that this may be due to positronium formation in excited states. This feature is not observed in the measurements of Marler *et al* [272] (e.g., see figure 33). The cross sections for neon, argon, krypton and xenon measured by Marler *et al* decrease monotonically after the main peak, except for a shoulder in xenon beginning at an energy  $\sim 15$  eV, which is close to, but lower than the threshold for positronium formation involving the inner shell (5s) electrons of xenon. The origin of this shoulder is unclear at present.

In figure 33, the results of Marler *et al* are compared with two theoretical predictions for Ps formation in argon [279, 282]. Note that for the purpose of comparison with experiment, the cross section from [282] has been multiplied by 0.5. Thus, the coupled-static calculation [279] produces a reasonable estimate of the peak cross section. On the other hand, the distorted-wave Born cross section [282] (which also contains the contributions of excited state Ps at the level not exceeding 15%) exhibits an energy dependence which is closer to experiment. A similar picture is found for the other noble gases. Given the high quality of the experimental data now available, further theoretical effort on this problem would be most welcome.

The Wayne State group has carried out an extensive set of measurements of Ps-formation cross sections for atomic H [190] and a number of metal vapour atoms: Na, K [283], Li [284], Rb [285], Cs [105] and Mg [286]. A general comparison of these and other atomic systems is presented in [206]. As an example of this work, in figure 34, we show the most recent results for Mg [286]. This atom has a low Ps-formation threshold,  $\varepsilon_{\text{thr}} \approx 0.84$  eV, and the cross section for positronium formation is very large at near-threshold energies. The measured upper and lower limit cross sections (see section 3.4.4) are compared with a coupled-state calculation by Walters (see [286]), a close-coupling approach by Hewitt *et al* [287], and a many-body

correlation potential calculation by Gribakin and King [288]. The latter is an estimate of the total inelastic scattering cross section and contains contributions from electronic excitation and direct ionization above 4.3 eV. Compared with noble gases, Mg is a much ‘softer’ target and an accurate account of electron–positron correlations is more difficult. At present there is a fair accord between theory and experiment. However, accurate determination of the true magnitude and energy dependence of these and other positronium-formation cross sections, for which only upper and lower limit measurements are available, awaits further work.

## 5. Positron annihilation

In this section, we discuss the process of positron annihilation on atoms and molecules for the case in which the positronium-formation channel is closed—so-called ‘direct’ annihilation. This is an important process for systems with ionization potentials,  $E_i > E_{\text{Ps}}$ , where  $E_{\text{Ps}} = (1/2)$  Ryd is the binding energy of a positronium atom, for positron energies below the positronium-formation threshold,  $\varepsilon < E_i - E_{\text{Ps}}$ . When the positronium channel is open, the positronium-formation cross section is larger than that of direct annihilation by many orders of magnitude; and so the signal from positron annihilation in the Ps atoms masks that due to the direct annihilation. As mentioned above, study of the annihilation on atoms and molecules began with the seminal work of Deutsch and coworkers [25] and Paul and Saint-Pierre [28]. The experiments involved measuring the rate,  $\lambda$ , of annihilation of positrons in amagat-density gases at temperatures  $\sim 300$  K. This technique is described briefly in section 3.7 and in more detail in the reviews by Griffith and Heyland [1] and by Charlton and Humberston [5].

As discussed in section 2.3, it is natural to compare measured annihilation rates with those predicted by equation (1) for a positron in a free electron gas. This comparison motivated the definition [141], now standard in the field, of a normalized annihilation rate,

$$Z_{\text{eff}} = \lambda / (\pi r_0^2 c n_m), \quad (26)$$

where  $n_m$  is the density of atoms or molecules. In a crude sense,  $Z_{\text{eff}}$  can be regarded as the effective number of electrons participating in the annihilation process per target atom or molecule. For no correlation of the electrons and the positron,  $Z_{\text{eff}} = Z$ . However, Paul and Saint-Pierre showed that, for hydrocarbon molecules,  $Z_{\text{eff}}$  increases rapidly with molecular size and becomes much greater than the actual number of electrons for larger molecules. This phenomenon was subsequently investigated, in numerous experiments, for a wide variety of chemical species. The development of positron trapping techniques enabled study of positron annihilation at lower molecular densities (e.g.,  $n_m \leq 10^{-6}$  amagat). This helped to ensure that the positrons were truly thermalized and to rule out the possibility that the large rates measured in amagat-density gases were due to molecular clustering or other many-particle effects. Experiments in positron traps also enabled the study of low-vapour-pressure materials, such as those that are liquid and solid at room temperature. Figure 35 shows a summary of data from a wide variety of chemical species [148]. Recent experimental results (discussed below) indicate that the values of  $Z_{\text{eff}} \gg Z$  are due to the formation of temporary positron–molecule bound states, a phenomenon hypothesized by Paul and Saint-Pierre and Smith and Paul [28, 30] and discussed subsequently in the context of a number of models.

### 5.1. Annihilation on atoms

While there have been theoretical calculations of positron annihilation on atomic hydrogen and a number of other atoms, experimental studies of atoms to date have been confined to the noble gases. Measurements began with the work of Shearer and Deutsch on argon [25]

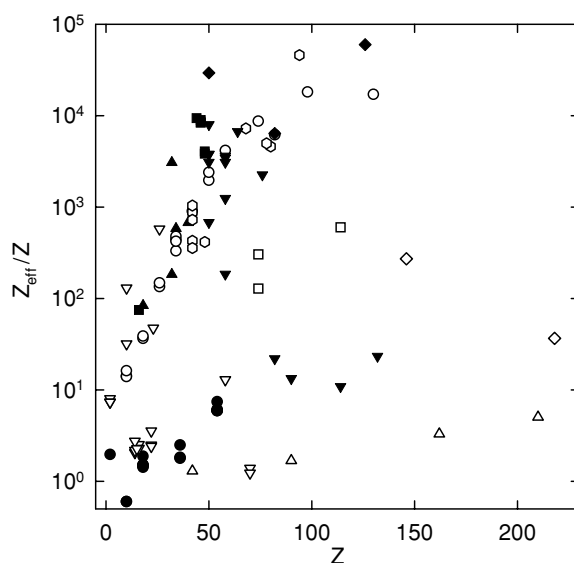


**Figure 35.** Experimental values of  $Z_{\text{eff}}/Z$  plotted as a function of  $Z$  for target species interacting with a 300 K Maxwellian distribution of positrons. From [148]. The data indicate the strong dependence of  $Z_{\text{eff}}$  on chemical effects: (●) noble gases, (▽) simple molecules, (○) alkanes, (△) perfluorinated alkanes, (□) perchlorinated alkanes, (◇) perbrominated and periodated alkanes, (■) alkenes, (▲) oxygen-containing hydrocarbons, (⊙) ring hydrocarbons, (▼) substituted benzenes, and (◆) large organic molecules.

and have been refined and expanded in many subsequent works [1, 5, 148, 289]. With few exceptions, experiments in amagat-density gases have been restricted to measuring  $Z_{\text{eff}}$  for positrons with a thermal Maxwellian velocity distribution in the case where both the target species and the positrons are at ambient temperature (i.e.,  $\sim 300$  K).

In table 3 these measurements are compared with the corresponding data for argon, krypton and xenon that were obtained in a positron trap with a thermal distribution of positrons at 300 K. For argon, the measurements are in reasonable agreement to within the experimental accuracy of the techniques. In the case of krypton, measurements in high-density gases yielded a value of 65.7 [150], while measurements in the trap find a value of 90.1. This discrepancy is unresolved; but as shown in table 3, theoretical predictions favour the lower number. Finally, in xenon previous measurements showed a difference between  $Z_{\text{eff}} = 320$  obtained in pure Xe versus  $Z_{\text{eff}} = 400\text{--}450$  for Xe with a small amount of  $\text{H}_2$  added to accelerate positron thermalization [150]. The trap measurements confirmed the value of 400 [289]. These results support the current understanding that positrons in amagat-density Xe do not thermalize before annihilating.

The use of a positron trap also provided the capability to study the dependence of the annihilation rate on *positron temperature*. This was accomplished by heating the positrons using radio-frequency noise. Kurz *et al* studied annihilation in noble gases from room temperatures, i.e.,  $k_{\text{B}}T = 0.025$  eV (300 K), up to  $\sim 0.5$  eV [241]. The annihilation rates normalized to unity at room temperature are shown in figure 36. These results are compared with the theoretical predictions of Van Reeth and Humberston for He and McEachran *et al* for heavier targets by folding the theoretical values with a Maxwellian positron energy distribution. The curves shown in figure 36 are due to an analysis by Mitroy and Ivanov [142] that corrects an error in the earlier, and similar, analysis of Kurz *et al*.



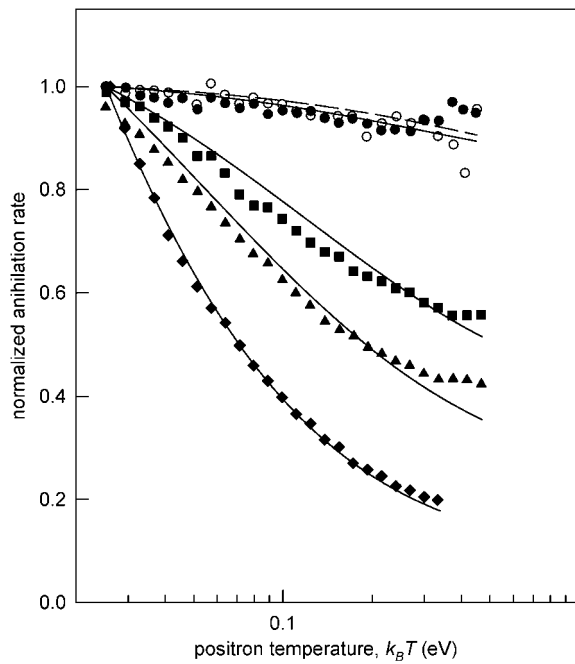


**Figure 36.**  $Z_{\text{eff}}$  for noble-gas atoms measured as a function of positron temperature in a positron trap: (○), He; (●), Ne; (■), Ar; (▲), Kr; (◆), Xe [241]. The data are compared with (—) the polarized-orbital calculations of McEachran *et al* for Ne, Ar, Kr and Xe [67, 76, 252, 290], and (---) theory by Van Reeth and Humberston for He using variational wavefunctions [151]. Figure courtesy of J Mitroy, following the analysis of [142, 241].

Good agreement between theory and experiment is found for the dependence of  $Z_{\text{eff}}$  on positron temperature. The fact that the observed temperature dependence becomes stronger from He and Ne to Xe is directly related to the presence of the positron virtual levels, whose energy decreases as the atomic number increases, as shown in table 2. The success of the polarized-orbital method in describing the temperature dependence is related to the fact that it gives a good description of low-energy scattering, and the scattering lengths, in particular. However, the absolute values of  $Z_{\text{eff}}$  predicted by the polarized-orbital method of McEachran *et al*, do not agree well with the measurements (see table 3).

Recently,  $Z_{\text{eff}}(\varepsilon)$  was measured as a function of positron energy for argon and xenon [280]. These results are shown in figure 37 for  $0.1 \leq \varepsilon \leq 3$  eV, and compared with three calculations for these targets. The agreement is generally good to excellent.

Additional information about the process of sub-positronium annihilation of positrons on neutral targets can be obtained by measuring the Doppler broadening of the annihilation gamma-ray spectrum. As discussed in section 3.2, the Doppler width is dominated by the momentum distribution of the annihilating electrons. Such experiments have been conducted using 300 K thermal positrons in a trap. Shown in figure 38 are measurements of the gamma-ray spectrum for helium and comparison with a calculation by Van Reeth *et al* [151] which used the Kohn variational approach. Theory and experiment are in good agreement over three orders of magnitude in spectral intensity.

Similar Doppler-broadening measurements were also made in the heavier noble gases [243]. The experiments confirm that the spectra are dominated by positron annihilation with

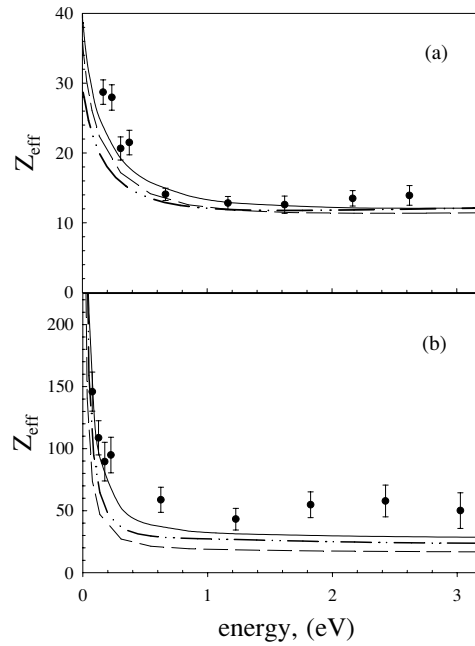


**Figure 37.** (●)  $Z_{\text{eff}}$  as a function of incident positron energy  $\varepsilon$ , measured for argon (a) and xenon (b), using a tunable, trap-based positron beam. From [280]. Also shown are  $Z_{\text{eff}}(\varepsilon)$  from the polarised-orbital theory, (– –) [252], many-body theory, (– · – ·) [58, 59], and a model-potential calculation (—) [142], tuned to reproduce the polarised-orbital scattering results and experimental room-temperature  $Z_{\text{eff}}$  values.

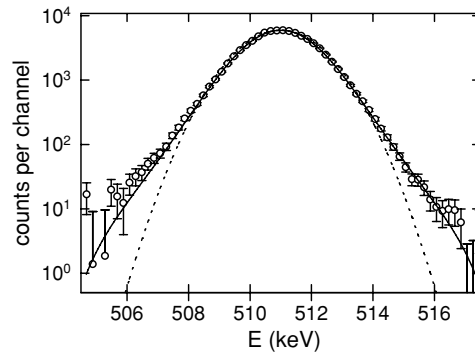


**Figure 38.** (○) Doppler-broadened gamma-ray spectrum from positron annihilation on helium atoms, and comparison with (—) theoretical predictions using a variational wavefunction, and (– –) a Gaussian fit. From [151].

the valence electrons, while the wings of the Doppler-broadened line provide a measure of annihilation on inner-shell electrons. The measurements were analysed in terms of annihilation from the valence and next-inner-shell orbitals (i.e., the 4s, 4p, 4d electrons in Xe; 3s, 3p, 3d in Kr; and 2s and 2p electrons in Ar). The fraction,  $\xi$ , of annihilation on inner-shell electrons was found to increase with atomic size, from  $\xi \approx 0$  for Ar to 1.3% for Kr and 2.4% for Xe. While not measured in experiments to date, the likely fate of ions following inner-shell annihilation is the Auger decay of the vacancy accompanied by the emission of an Auger electron. This

process is central to the technique of positron-induced Auger-electron analysis [291]. In this case, the inner-shell ionization by annihilation with a low-energy positron eliminates the unwanted signal of secondary electrons, which are produced in conventional, electron-induced Auger emission studies.

We conclude that the process of positron annihilation in noble gases below the threshold for positronium formation is reasonably well understood. Following the partial success of polarized-orbital calculations [67, 76], recent theoretical works [52, 56, 58, 59] fully explain the origin of large  $Z_{\text{eff}}$  values for heavier noble-gas atoms. The main physical effects are (i) virtual positron levels due to long-range positron–atom attraction (which are also responsible for the rapid variation of  $\sigma_{\text{el}}$  and  $Z_{\text{eff}}$  at low energies), and (ii) short-range electron–positron correlation which enhances the contact density and has a weak energy dependence. This physics underpins the success of model-potential calculations of [142]. One important process yet to be investigated is that of annihilation on inner-shell electrons as a function of positron energy. In particular, this would provide a quantitative measure of the (expected) increase in penetration of positrons into the atomic core as the positron energy is increased.

## 5.2. Annihilation on molecules

The first study of annihilation on molecules below the threshold for positronium formation was conducted by Shearer and Deutsch on  $\text{N}_2$  and  $\text{CH}_4$  [25]. The work of Paul and Saint-Pierre expanded the range of molecules studied and provided unambiguous evidence that, for broad classes of molecules, positron annihilation with molecules could not be described in terms of simple ‘annihilation in flight’ model, since these molecules exhibited values of  $Z_{\text{eff}} \gg Z$  [28]. We now understand that, for molecules such as large hydrocarbons, these large annihilation rates are due to positron capture in vibrational Feshbach resonances, as discussed in section 2.4 [46, 47, 152, 156]. The situation for small molecules and many other chemical species is less clear. Thus, we first discuss alkane molecules and some fluorinated and partially fluorinated analogues. A qualitative picture of the annihilation process has been developed for these molecules and aspects of the theory have now been confirmed.

**5.2.1. Large alkane molecules.** As shown in figure 39, the ratio of room-temperature  $Z_{\text{eff}}$  to  $Z$  for alkane molecules,  $\text{C}_n\text{H}_{2n+2}$ , increases exponentially with  $Z$  for molecules with up to 10 carbon atoms and then tends to saturate, with  $Z_{\text{eff}}/Z \geq 10^4$  observed for  $n \geq 10$ . In order to gain insight into the underlying physics, Iwata *et al* investigated the dependence of  $Z_{\text{eff}}$  on positron temperature,  $T_{\text{e}^+}$ , for methane ( $\text{CH}_4$ ), deuterated methane ( $\text{CD}_4$ ), fluoromethane ( $\text{CH}_3\text{F}$ ), and butane ( $\text{C}_4\text{H}_{10}$ ) by radio-frequency heating positrons in a trap in the presence of the test molecules [240]. For all molecules except fluoromethane,  $Z_{\text{eff}}$  showed a rapid decrease with increasing  $T_{\text{e}^+}$ , in the range from 0.025 eV to  $\sim 0.05$  eV, and then a slower decrease in the range of temperatures from 0.1 eV up to  $\sim 0.35$  eV, which was the highest temperature that could be investigated. It was speculated that this slower decrease in  $Z_{\text{eff}}$  at higher energies might be due to interaction of the positrons with the molecular vibrations.

With the development of the tunable trap-based positron beam, more definitive measurements have been made in this range of energies that highlight the role of molecular vibrations. Figure 40 shows the dependence of  $Z_{\text{eff}}$  on the positron energy for butane, obtained using the cold beam and the technique described in section 3.7 [46]. As seen in figure 40(a), the values of  $Z_{\text{eff}}$  are not much greater than  $Z$  for energies from 0.4 eV up to the positronium-formation threshold, but there are strong enhancements in  $Z_{\text{eff}}$  at lower energies. As shown in figure 40(b), the energy dependence of  $Z_{\text{eff}}$  is very similar for butane and deuterated butane when the energies are scaled to account for the change in vibrational

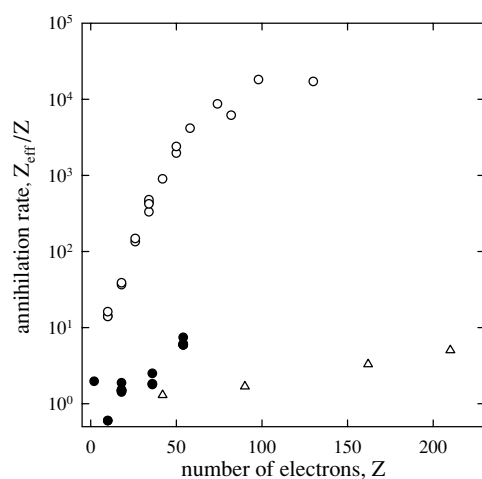


**Figure 39.** Comparison of  $Z_{\text{eff}}/Z$  as a function of  $Z$  for (●) noble gases, (○) alkanes and (△) perfluoroalkanes for a 300 K Maxwellian, as measured using a positron trap. From [148].

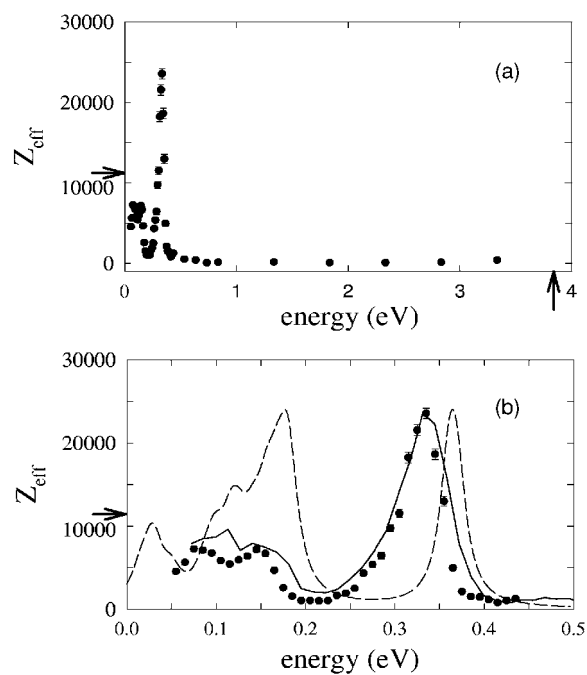


**Figure 40.**  $Z_{\text{eff}}$  for butane (●) as a function of positron energy: (a) 0 to 5 eV, and (b) 0 to 0.5 eV. From [46, 47]. The arrow on the abscissa in (a) is the threshold for positronium formation. Also shown in (b) is the  $Z_{\text{eff}}$  spectrum for fully deuterated butane,  $\text{C}_4\text{D}_{10}$  (solid line), with the amplitude scaled to match the C–H peak and the energies scaled by the appropriate reduced mass factor. The vibrational-mode spectrum of butane is also shown in (b) for comparison (dashed line, arbitrary vertical  $Z_{\text{eff}}$  scale), with each mode broadened by 25 meV [162]. Arrows on the ordinate indicate values of  $Z_{\text{eff}}$  for a 300 K Maxwellian.

frequencies due to the substitution of the hydrogens by the deuterium atoms. This experiment provided unambiguous evidence that enhancement of the  $Z_{\text{eff}}$  at low positron energies in these

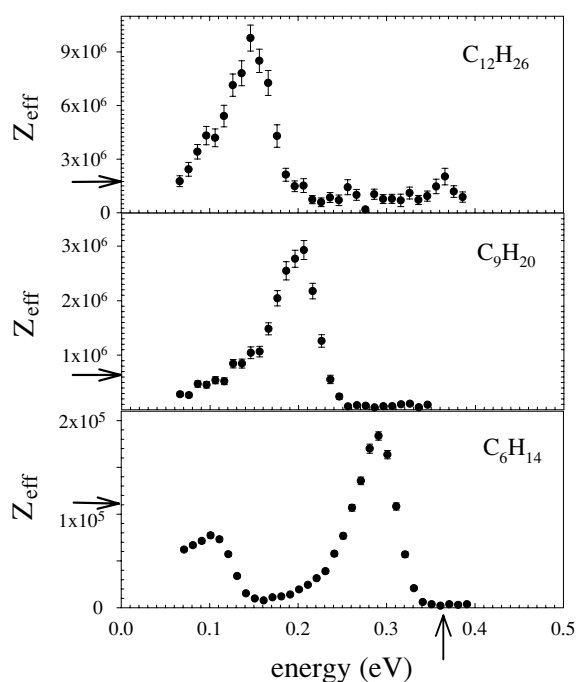


**Figure 41.** The  $Z_{\text{eff}}$  spectra for  $\text{C}_{12}\text{H}_{26}$ ,  $\text{C}_9\text{H}_{20}$  and  $\text{C}_6\text{H}_{14}$ . Arrows on the ordinate indicate the value of  $Z_{\text{eff}}$  for thermal positrons at 300 K. The arrow on the abscissa indicates the energy of the C–H vibrational mode. Note the large increase in  $Z_{\text{eff}}$  and the progressive increase in  $\Delta\varepsilon$  with increasing molecular size. From [47].

molecules is due to excitation of the molecular vibrations. Comparison with the shape of the spectrum of the molecular vibrational modes, also shown in figure 40(b), confirms this. The peaks in  $Z_{\text{eff}}$  match to those of the vibrational mode spectrum. The most prominent peak in the spectrum corresponds to the C–H stretch vibrational modes, which are located near 0.36 eV. At the same time, a comparison of the measured energy dependence of  $Z_{\text{eff}}$  with that of the vibrational modes indicates that the peaks in the former are downshifted by an amount  $\Delta\varepsilon \sim 30$  meV in butane.

Figure 41 shows the  $Z_{\text{eff}}$  spectra for larger alkane molecules [47]. Consistent with the experiments done with thermal positrons at 300 K, the resonant enhancement of  $Z_{\text{eff}}$  in the range of energies of the molecular vibrations increases very rapidly with molecular size. The spectra exhibit increasing downshifts of the C–H peak as the number of carbon atoms,  $n$ , increases;  $\Delta\varepsilon = 220$  meV for dodecane, ( $\text{C}_{12}\text{H}_{26}$ ), which was the largest molecule studied. This experiment provides unambiguous evidence that the large values of  $Z_{\text{eff}}$  in the range of energies studied (i.e., 50–400 meV) are due to vibrational Feshbach resonances. The downshift,  $\Delta\varepsilon$ , is a measure of the positron–molecule binding energy. Data for  $\Delta\varepsilon$  for the alkanes as a function of molecular size are shown in figure 42. Apart from the systematic downshift in energy, the annihilation rates,  $Z_{\text{eff}}(\varepsilon)$ , for the alkanes from propane to dodecane (i.e.,  $n = 3$ –12) appear to be very similar in shape over the range of energies of the molecular vibrations [47]. The C–H peak is asymmetric, with more spectral weight towards lower energies.

The magnitudes of the measured  $Z_{\text{eff}}$  spectra increase rapidly with molecular size, similar to the behaviour observed earlier with room-temperature positrons. In particular, the

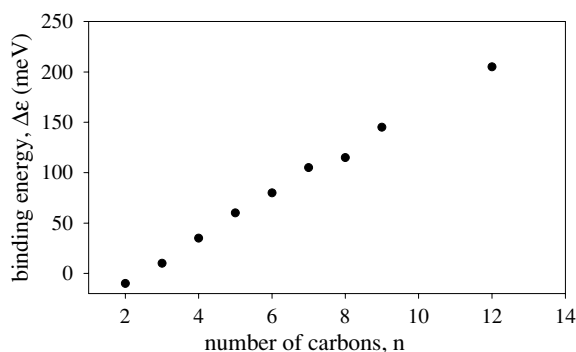


**Figure 42.** The energy shift,  $\Delta\varepsilon$ , of the C–H stretch peak in the  $Z_{\text{eff}}$  spectra as a function of the number of carbon atoms,  $n$ , for alkane molecules. Interpreted in the framework of the vibrational Feshbach resonance model,  $\Delta\varepsilon$  is the positron binding energy to the molecule. From [47].

energy-resolved  $Z_{\text{eff}}$  spectra are proportional to the thermal  $Z_{\text{eff}}$  values for  $n \leq 9$  carbons, with  $Z_{\text{eff}}$  at the C–H stretch peak about twice that at 300 K. For  $9 \leq n \leq 12$ , values of  $Z_{\text{eff}}$  at the C–H peak are  $\sim 5$ – $6$  times larger than the value at 300 K [47]. This latter effect appears to be due to the fact that the vibrational-mode spectrum in the alkanes, for  $9 \leq n \leq 12$ , is downshifted so that the gap in the mode spectrum below the C–H stretch peak occurs at thermal energies (i.e.,  $\sim 25$  meV) [292]. Thus, there are fewer modes available to mediate the Feshbach resonances, or they are further away in energy, and consequently the room-temperature  $Z_{\text{eff}}$  values are expected to be smaller than those at higher positron energies. The close correspondence between the large values of  $Z_{\text{eff}}$  observed in alkane molecules with thermal positrons at 300 K and those observed for positron energies in the range of the molecular vibrations indicates that they arise from the same basic mechanism.

As shown in figure 39, fluorinated alkanes have much smaller values of thermal  $Z_{\text{eff}}$  than the alkanes. Gribakin has pointed out that this is likely to signify that the vibrational mechanism is switched off for the fluorinated alkanes [152]. He argued that, due to a relatively weak positron attraction to fluorine atoms (cf, positron interaction with Ne), fully fluorinated alkanes do not form bound states with the positron, and hence, do not capture the positrons in VFR [152]. However, as we discuss below, *partial* fluorination of alkanes *can* produce large changes in  $Z_{\text{eff}}$  with complex dependence on the number of fluorine atoms and positron energy. These effects are not yet understood.

The question arises as to which electron orbitals participate in the annihilation process. As discussed in section 3.2, the Doppler spectrum of the annihilation gamma rays provides a measure of the momentum distribution of the bound electrons. In the case of alkanes, Iwata *et al* measured the gamma-ray spectrum as a function of molecular size for a thermal 300 K positron distribution [240]. They were able to analyse the data for hydrocarbons in terms of the fraction of annihilation on valence electrons on C–C bonds as opposed to in C–H bonds, and concluded that the positrons annihilate with electrons in both C–C and C–H bonds. Similar measurements on partially and fully fluorinated alkanes showed that positrons annihilate with approximately equal probability on electrons in the C–H bonds and on the fluorine atoms. The results of these studies indicate that, whatever the nature of the positron states in molecules, the positron density appears to be delocalized rather than localized at a specific molecular site. This may be responsible for the density dependence of  $Z_{\text{eff}}$  observed in annihilation experiments in dense gases [48].

In summary, the energy-resolved measurements of  $Z_{\text{eff}}$  for alkanes provide strong evidence for positron–molecule binding and prove that vibrations are responsible for the very large values of  $Z_{\text{eff}}$  observed in molecules. However, the exact nature of the positron coupling to molecular vibrations is still an open question. In particular, to account for the observed  $Z_{\text{eff}}$  values, the level density,  $\rho$ , in the VFR equation (15) must be much greater than the density of the (fundamental) vibrational modes. The rapid increase of  $Z_{\text{eff}}$  with molecular size is also incompatible with the linear growth of the spectral density of the fundamentals. On the other hand, the energy dependence of  $Z_{\text{eff}}$  reproduces the (shifted) spectrum of modes. To reconcile these facts, Gribakin and Gill [162] have proposed that positron–molecule states formed by single-quantum excitations of the fundamentals play the role of vibrational *doorway* states for positron capture. Due to nonlinear interactions, these states couple to more complex multi-mode high-density vibrational resonances, in a process of intramolecular vibrational energy redistribution. In the context of this model, there are a number of open questions. It is unclear as to whether the energy spreads statistically into all accessible combination vibrations, or there is a selective coupling between particular modes. Also, unlike the typical annihilation time, the time scale of vibrational energy redistribution is unknown. Finally another unknown, at present, is the branching ratio of VFR decay by positron *detachment* as opposed to annihilation.

**5.2.2. Small molecules.** There have been a number of energy-resolved measurements of  $Z_{\text{eff}}$  for smaller molecules. Shown in figure 43 are results for hydrocarbons containing two carbon atoms [46, 47]. The C–H stretch peak exhibits little or no downshift and decreases in amplitude as the number of electrons in the C–C bond increases from 2 to 6. In contrast with the larger alkanes, the room-temperature values of  $Z_{\text{eff}}$  (660 for ethane, 1200 for ethylene and 3160 for acetylene) are larger than those at higher energies for all three molecules.

Following [29], Gribakin proposed that bound or virtual states close to zero energy could explain values of  $Z_{\text{eff}}$  in the range  $\leq 10^3$ , such as those observed in these small hydrocarbons [152]. Marler *et al* [280] have fit data for CH<sub>4</sub> and CF<sub>4</sub> to the form for  $Z_{\text{eff}}$  predicted by the model, namely

$$Z_{\text{eff}}(\varepsilon) = \frac{A}{\varepsilon + |\varepsilon_0|} + B, \quad (27)$$

where  $A$  and  $B$  are constants and  $\varepsilon_0$  is the energy of the resonance or bound state. Shown in figure 44 is the fit for CH<sub>4</sub>. The values of  $\varepsilon_0$  resulting from this procedure are 10 meV for CH<sub>4</sub> and 72 meV for CF<sub>4</sub>. Note that this analysis cannot distinguish whether the states are virtual or bound, however it likely indicates a weaker positron attraction to the fluorinated molecule. Values of  $Z_{\text{eff}}$  as a function of positron energy have been measured for a few other small molecules [47], but there are no systematic conclusions from these studies thus far.

**5.2.3. Chemical effects, including fluorination of hydrocarbons.** In a comparison of isomers, it was found that the  $Z_{\text{eff}}$  spectra appear to be relatively insensitive to molecular shape. The dependences of  $Z_{\text{eff}}$  on positron energy for the isomers pentane and isopentane were found to be identical to within the accuracy of the measurements in the range of the C–H stretch peak, while  $Z_{\text{eff}}$  for pentane was smaller than for isopentane (by  $\sim 15\%$ ) at lower energies [47].

In contrast, figure 39 shows that changes in chemical composition can produce very large changes in annihilation rates. In hydrocarbons, substitution of fluorines for hydrogen atoms can have particularly profound effects. While the complete substitution of fluorines for hydrogen atoms produces a systematic decrease in  $Z_{\text{eff}}$ , the results for annihilation rates and their dependence on positron energy for *partially fluorinated* compounds are more complicated.



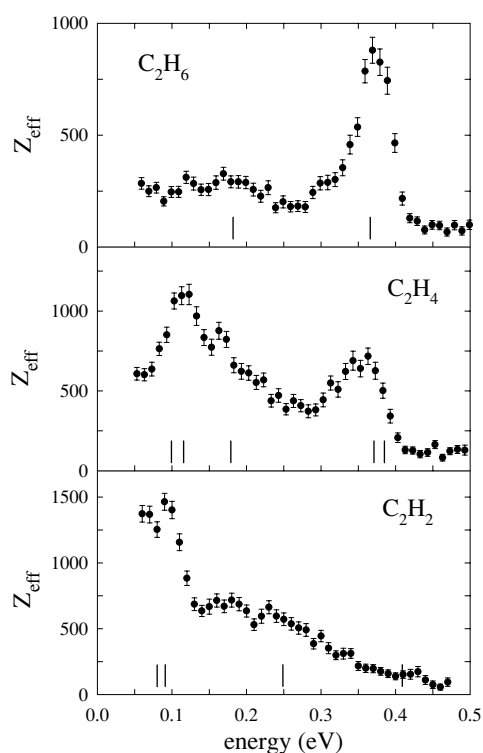


**Figure 43.**  $Z_{\text{eff}}$  spectra for the two-carbon alkanes, ethane ( $\text{C}_2\text{H}_6$ ), ethylene ( $\text{C}_2\text{H}_4$ ) and acetylene ( $\text{C}_2\text{H}_2$ ). From [46, 47].

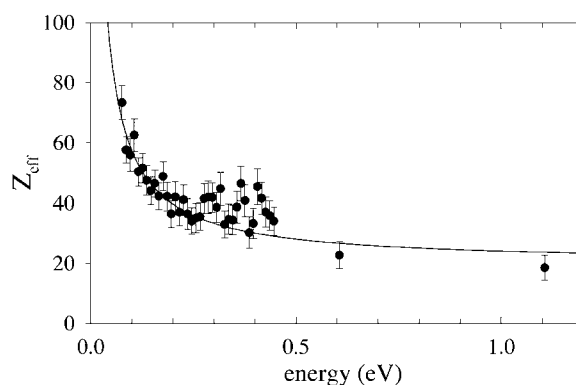


**Figure 44.** (●)  $Z_{\text{eff}}$  for methane ( $\text{CH}_4$ ) and (—) best fit of the form given by equation (27) for the weakly bound/virtual level model. From [280].

Figure 45 shows  $Z_{\text{eff}}(\varepsilon)$  for the partially and fully fluorinated methanes. In partially fluorinated molecules, there is a peak at  $\sim 0.14$  eV, which is in the region of a number of modes (i.e., the C–F stretch, C–H rock and C–H deformation). Neither methane nor tetrafluoromethane have any prominent features (e.g., such as a C–H stretch peak in large alkanes). It is interesting to note that the thermal values of  $Z_{\text{eff}}$  at 300 K (142 for  $\text{CH}_4$ , 1390 for  $\text{CH}_3\text{F}$ , 799 for  $\text{CH}_2\text{F}_2$  and 247 for  $\text{CHF}_3$ ) are larger than the values at higher energies shown in figure 45. The exception

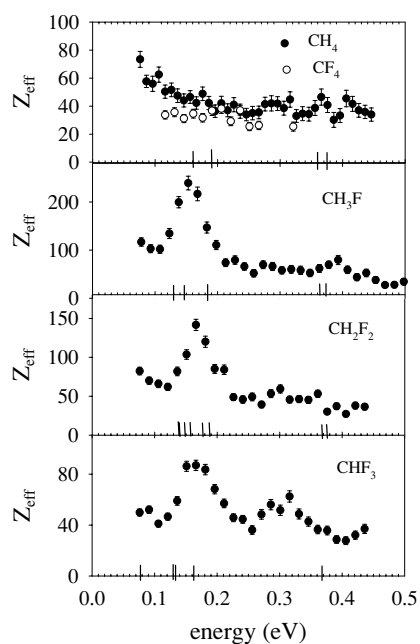


**Figure 45.**  $Z_{\text{eff}}$  spectra for the fluorinated methane series,  $\text{CH}_x\text{F}_{4-x}$ . From [47].

is  $\text{CF}_4$ , for which  $Z_{\text{eff}} = 42$  at 300 K. The large increase in  $Z_{\text{eff}}$  observed with partial fluorination has been discussed in terms of low-lying virtual or weakly bound states [152]. This model is discussed in the previous section for  $\text{CH}_4$  (figure 44) and  $\text{CF}_4$  [280].

The substitution of a single hydrogen atom by a fluorine in larger hydrocarbons produces dramatic changes in  $Z_{\text{eff}}$ . Shown in figure 46 are the  $Z_{\text{eff}}$  spectra for hexane and nonane and their 1-fluorine analogues [47]. The resonant C–H stretch peak is greatly reduced (and all but disappears in hexane) with the addition of just one fluorine, while the positions of the peaks are not shifted. The fact that the peak position is unchanged indicates that the positron–molecule binding energy is the same as in the unsubstituted alkane. As mentioned above, gamma-ray Doppler-broadening measurements on partially and fully fluorinated alkanes indicate that positrons annihilate with equal probability on electrons in the C–H bonds and on the fluorine atoms, so the changes illustrated in figure 46 do not appear to be due to changes in the annihilation site. Whether the changes in  $Z_{\text{eff}}$  shown in figure 46 are due to a change in the symmetry of the molecule is as yet unclear. Note that, in contrast to the behaviour illustrated in figure 46 at higher energies, the addition of one fluorine to hydrocarbons quite generally leads to an *increase* in thermal room-temperature  $Z_{\text{eff}}$ . Both effects may be related to the changes in the vibrational spectrum of the molecule, i.e. the emergence of a few low-energy modes involving the heavy fluorine atom. One may speculate that the energy of a C–H vibration excited by positron capture can be transferred quickly to a similar but lower lying C–F vibration, releasing enough energy for the positron to detach. This would mean that the suppression of the C–H peak is caused by increased probability of C–F vibrational excitation of the molecule.

**5.2.4. Ionization and molecular fragmentation.** Passner *et al* conducted the first experiment to study the ionization of molecules by positrons with energies below the Ps-formation

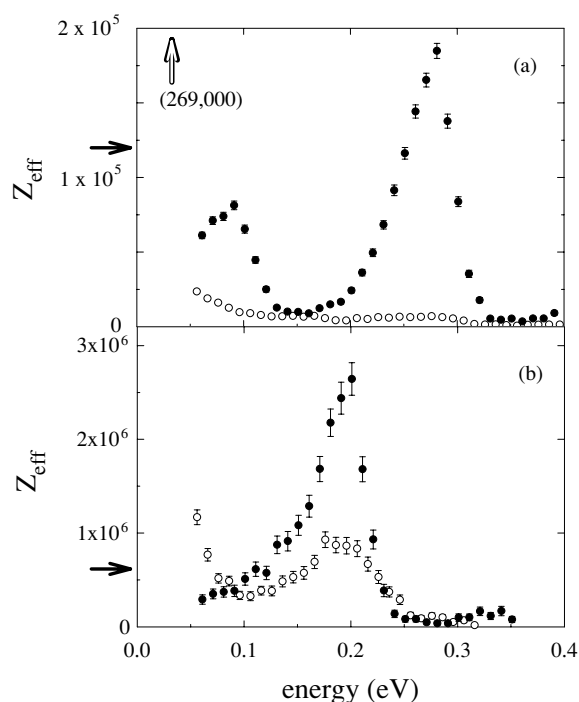


**Figure 46.** The effect of substituting one fluorine for a hydrogen in larger alkanes: shown are the  $Z_{\text{eff}}$  spectra for (a) hexane (●) and 1-fluorohexane (○), and (b) nonane (●) and 1-fluorononane (○). From [47].

threshold [293, 294]. They showed that for thermal 300 K positrons interacting with alkane molecules, this process produces a broad spectrum of ions. Hulett and collaborators conducted detailed studies of many aspects of this phenomenon [22, 223, 295–298]. One of the most important results of their research was the discovery that, while molecular fragmentation is large at low positron energies (as in the Passner *et al* experiments) and also at energies far above the positronium threshold, there is comparatively little fragmentation just above the Ps-formation threshold. An example of this is shown in figure 47. This offers the possibility that positrons might be used to selectively ionize and fragment ions, for example, in mass spectroscopic analysis. Crawford developed a model of this process that appears to explain the effect [299]. This model asserts that annihilation occurs statistically with all valence electrons, and not just with those in the highest occupied molecular orbital. This results in an excess energy that can break bonds and induce fragmentation of the molecular cation.

## 6. Summary and a look to the future

There is no doubt that the positron will always retain its significance as a fundamental particle of antimatter. On the other hand, one can expect that, in the future, it will be viewed less as an exotic particle and more as a useful tool in research and technology. Obtaining the full advantages of this tool requires a better understanding of the elementary processes of positron interactions with matter. We have presented a review of studies of the interaction of low-energy positrons with atoms and molecules, with the emphasis on the developments over the last decade and a half. It is fair to say that progress has been made in many facets of

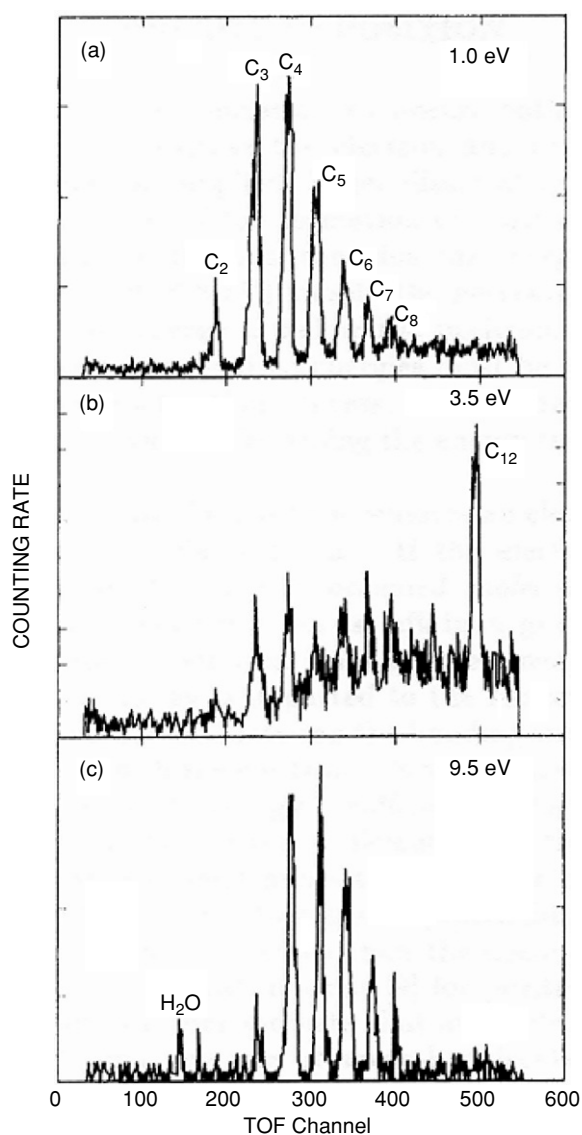


**Figure 47.** Positron-induced ion mass spectrum of dodecane ( $C_{12}H_{24}$ ) for three values of incident positron energy: (a) below the positronium-formation threshold; (b) just above the threshold; and (c) farther above threshold. The dominant ionization processes at the three energies are: (a) positron annihilation, statistically on all valence electrons; (b) Ps formation with the highest lying molecular orbital; and (c) positron-impact ionization. Reprinted with permission from [297]; copyright 1994 by the American Physical Society.

this research—from new experimental and theoretical tools to improved agreement between theory and experiment. A useful benchmark for progress in the area of positron scattering (i.e., excluding for the moment annihilation processes) is comparison with low-energy electron interactions with similar targets.

Experimental studies of positron phenomena were clearly behind analogous electron studies in almost all areas at the beginning of this period. While positron physics remains

behind in many areas, with a few notable exceptions, the gap has closed considerably. In experimental studies, the period has seen an increase in the energy resolution of positron beams by more than an order of magnitude. Positron beams still trail the resolution available with electron sources by another order of magnitude or more (i.e., 20 meV as compared to a fraction of an meV). Nevertheless, one is now able to study state-resolved vibrational processes and to investigate possible resonance phenomena at a new level of precision. State-resolved study of electronic excitations by positron impact has also begun, albeit with a technique limited to low-lying electronic states, at least for the near future. Efforts are underway to make even higher resolution positron beams, using cryogenic positron plasmas. For example, a 10 K plasma could be used to create a positron beam with  $\sim 1$  meV energy resolution. This, in turn would provide new insights into the details of positron–atom and positron–molecule interactions, including such phenomena as resonances and the excitation of molecular rotations.

A new scattering technique has been developed that exploits the properties of positron orbits in a strong magnetic field. This technique was crucial in measuring state-resolved integral cross sections and yields data at least comparable in accuracy to the best measurements done to date with electrons. It is likely that many other measurements can be made with this technique, such as measurement of differential *inelastic* scattering cross sections. The improved resolution provided by this technique is close to that required to make other fundamental measurements including the study of positron-impact excitation of rotational transitions in molecules. For example, the study of rotations in molecular hydrogen is now within reach. Investigation of other targets would be enabled by the development of colder positron beams such as those described above.

On the theoretical front, the period covered by the review saw a development of new approaches to the positron–atom problem. Many-body theory has provided insights into the relative importance of electron–positron correlation effects such as target polarization and virtual Ps formation. It quantified the size of the short-range electron–positron correlation effects in annihilation. The latter is especially difficult to account for theoretically, which partly explains the lack of reliable theoretical results on positron–molecule annihilation rates. On the other hand, *ab initio* Schwinger multichannel and correlation–polarization potential calculations are often in good accord with positron–molecule scattering data, which means that the important long-range correlations effects are described adequately. Many-body theory calculations also highlighted the special role of low-lying virtual states and weakly bound states in positron interactions with atoms and molecules. New computational approaches, such as the stochastic variational method, have greatly expanded our knowledge about positron–atom binding. At the same time, coupled-channel methods with pseudostates achieved convergence and provided information on positron scattering both below and above the Ps-formation and ionization thresholds. On the whole, the positron problem provides healthy and stimulating challenges to atomic theorists.

One outstanding and important problem is the study of positron interactions with helium. This is the simplest atomic system that can be handled relatively well *both* experimentally and theoretically. However for technical reasons, that can be circumvented, there is as yet no comprehensive set of absolute cross section measurements available for this target. Studies of interest include differential elastic scattering, inelastic scattering, positronium formation and ionization. Such measurements would provide a benchmark for the state-of-the-art theoretical methods such as the convergent close coupling and *R*-matrix with pseudostates. In particular, efforts to include the positronium formation channel in such calculations are critical to the correct treatment of positron scattering problems. These calculations would likely benefit greatly from such measurements. The lack of established results is even more glaring for H<sub>2</sub>, the simplest of the molecules.

An area where exciting prospects lie in the near future is in the study of both bound and quasi-bound states of positrons with atoms and molecules. As discussed above, there is now an extensive literature of *ab initio* calculations of bound states of positrons with atoms. These theoretical predictions have, however, not been accompanied by complementary experimental studies. The experiments presently proposed to study positron binding to atoms are likely to be very difficult. Nonetheless, many opportunities exist in this area and, as the recent low-energy annihilation experiments in hydrocarbons have demonstrated, evidence of binding can be gleaned from a wide range of experimental approaches.

The question of the existence of quasi-bound states or resonances, which are ubiquitous in electron scattering, is another of the 'holy grails' in positron physics. While evidence for the existence of vibrational Feshbach resonances and positron binding in the low-energy annihilation cross section measurements is compelling, regular scattering techniques have been unable to provide insight into this phenomenon. There is evidence in several of the recent near-threshold vibrational and electronic excitation measurements that resonant states may be involved in these phenomena, and such measurements should be pursued in the future with higher resolution and sensitivity. Another candidate for possible resonance structures is the positronium-formation channel, where high-resolution measurements near the positronium excitation thresholds could prove interesting.

Much progress on the experimental front has been made in studying positron annihilation and positronium formation, areas that, by definition, do not have electron-impact analogues. In the case of positronium formation on atomic targets, experiments are converging, at least in noble gases which are most amenable to experiment. A number of theoretical challenges remain, however, such as determining the cross sections near threshold, the possible production of Ps atoms with inner-shell electrons, and the production of Ps atoms in excited states.

The development of positron traps permitted the study of positron annihilation below the threshold for positronium formation in a dilute gas (i.e., essentially in an isolated environment). Many-atom and many-molecule effects were eliminated to a new level of certainty, and study of binary interaction with a thermalized distribution of room-temperature positrons was guaranteed. Later, annihilation was studied with a thermal distribution of positrons at elevated temperatures, up to a fraction of an electron volt for molecules and to higher temperatures for atoms. Doppler-broadening studies provided insight into the annihilation sites on molecules and a better quantification of the fraction of annihilation in atomic targets that occurs on inner-shell electrons.

Finally the advent of the tunable, cold positron beam permitted the first energy-resolved studies of positron annihilation. The principal conclusion of this work is that the very large values of  $Z_{\text{eff}}$  observed in molecules (i.e.,  $Z_{\text{eff}} \gg 10^3$ ) are due to positron capture in vibrational Feshbach resonances. In turn, the signature of these Feshbach resonances was used to infer the values of the positron–molecule binding energies in alkanes. Experiments are now beginning to distinguish the specific vibrational modes responsible for the resonant positron capture. Vibrational Feshbach resonances are, of course, an important feature of electron–molecule collisions. There is hope that the information provided by the annihilation signal from positron–molecule vibrational resonances will be able to elucidate the dynamics of vibrational coupling and intramolecular vibrational relaxation effects common to such systems.

From the theoretical viewpoint, this question of positron annihilation below the Ps-formation threshold has proven to be difficult, particularly in molecules. In atoms, experiment and theory are generally in good, quantitative agreement regarding the magnitude of the annihilation rate, its dependence on positron energy, and the (small) fraction of annihilation occurring on inner-shell electrons, although it is fair to say that quantitative tests have been

restricted to noble-gas targets. A qualitative understanding of sub-positronium annihilation in molecules has improved in the last decade, but a quantitative theory has yet to be developed. There is mounting evidence that low-lying resonances and weakly bound states greatly enhance  $Z_{\text{eff}}$  in small molecules, and there is convincing evidence that vibrational Feshbach resonances underlie the huge enhancements in  $Z_{\text{eff}}$  observed in large hydrocarbons. Nevertheless, quantitative agreement between theory and experiment has yet to be demonstrated by first-principles calculations, so this remains an important, but as yet unsolved problem.

While the experimental techniques described above have been developed to study atoms and molecules, they may well find broader utility. In particular, these techniques are likely to be more or less directly applicable to the study of atomic clusters and nanoscale-size particles, *in situ*, *in vacuo*. Such studies would help bridge the gap between atomic and molecular systems, for which we have arguably the most detailed understanding, and solid surfaces and bulk materials, where our knowledge is less complete. A variety of cluster properties could be investigated in this way, including particle size (by elastic scattering) and vibrational and electronic structure. One challenging, but potentially important research direction would be to develop positron-induced Auger spectroscopy to study the *surfaces* of clusters. This is a very important property of clusters and nanoparticles for which, at present, relatively little information is available and few techniques can address. Furthermore, if predictions of novel trapped positron states in cage-like clusters systems, such as  $C_{60}$ , are confirmed, positrons might provide a method to study the interior of such caged structures via positron annihilation in these cages.

From a broader perspective, low-energy antimatter is finding increasing use in science and technology. Examples range from fundamental studies of antihydrogen atoms and efforts to create Bose-condensed gases of positronium atoms, to the use of positrons as probes of materials. Other applications are planned, such as the use of positrons to selectively fragment molecules, including those of biological interest, and study of electron-positron plasmas. On a longer time horizon, possibilities include the use of positrons to catalyze reactions and the creation of annihilation gamma-ray laser. The progress in the area of positron interactions with simple targets, discussed here, is important not only to advance our fundamental understanding. It will be important in many, if not most, of these applications, either directly or in providing new tools for this research.

## Acknowledgments

We wish to acknowledge our collaborators in recent aspects of this research, J Ludlow, J P Sullivan, J P Marler, L D Barnes, and we thank J Winstead for extensive assistance in the preparation of the manuscript. We acknowledge helpful conversations with R Campeanu, R McEachran, H R J Walters; and thank J Mitroy and P Van Reeth for providing data in numerical form. Finally we are grateful to M Charlton, M Lima and J Mitroy for carefully reading the manuscript and many useful suggestions. The research at the University of California, San Diego was supported by the U.S. National Science Foundation.

## References

- [1] Griffith T C and Heyland G R 1978 *Phys. Rep.* **39** 169
- [2] Stein T S and Kauppila W E 1982 *Adv. At. Mol. Phys.* **18** 53
- [3] Kauppila W E and Stein T S 1990 *Adv. At. Mol. Opt. Phys.* **26** 1



- [4] Charlton M 2001 *New Directions in Antimatter Chemistry and Physics, Perspectives on Physics with Low Energy Positrons: Fundamentals, Beams and Scattering* ed C M Surko and F A Gianturco (Dordrecht: Kluwer) p 223
- [5] Charlton M and Humberston J W 2001 *Positron Physics* (Cambridge: Cambridge University Press)
- [6] Amoretti M *et al* 2002 *Nature* **419** 456
- [7] Gabrielse G *et al* 2002 *Phys. Rev. Lett.* **89** 233401
- [8] Gabrielse G *et al* 2002 *Phys. Rev. Lett.* **89** 213401
- [9] Mitroy J, Bromley M W J and Ryzhikh G G 2002 *J. Phys. B: At. Mol. Opt. Phys.* **35** R81
- [10] Mills A P Jr 2002 *Nucl. Instrum. Methods B* **192** 107
- [11] Tsytochik V and Wharton C B 1978 *Comments Plasma Phys. Control. Fusion* **4** 91
- [12] Zhao J, Nishikawa K I, Sakai J I and Neubert T 1994 *Phys. Plasmas* **1** 103
- [13] Sakai J, Eda M and Shiratori W 1998 *Phys. Scr. T* **75** 67
- [14] Greaves R G and Surko C M 1997 *Phys. Plasmas* **4** 1528
- [15] Greaves R G and Surko C M 2002 *Non-Neutral Plasma Physics IV, Practical Limits on Positron Accumulation and the Creation of Electron-Positron Plasmas* ed F Anderegg, L Schweikhard and C Driscoll (New York: AIP) p 10
- [16] Surko C M and Greaves R G 2004 *Phys. Plasmas* **11** 2333
- [17] Guessoum N, Ramaty R and Lingenfelter R E 1991 *Astrophys. J.* **378** 170
- [18] Wahl R L 2002 *Principles and Practice of Positron Emission Tomography* (Philadelphia, PA: Lippincott, Williams and Wilkins)
- [19] Schultz P J and Lynn K G 1988 *Rev. Mod. Phys.* **60** 701
- [20] See articles Xu J and Moxom J (ed) 2003 *Proc. 7th Int. Conf. on Positron and Positron Chemistry, Radiation Physics and Chemistry* vol 68 (Amsterdam: Pergamon) pp 329–680
- [21] Surko C M, Leventhal M, Crane W S, Passner A and Wysocki F 1986 *Rev. Sci. Instrum.* **57** 1862
- [22] Hulet L D, Donohue D L, Xu J, Lewis T A, McLuckey S A and Glish G L 1993 *Chem. Phys. Lett.* **216** 236
- [23] Dirac P A M 1930 *Proc. R. Soc. Lond.* **126** 360
- [24] Anderson C D 1933 *Phys. Rev.* **43** 491
- [25] Shearer J W and Deutsch M 1949 *Phys. Rev.* **76** 462
- [26] Deutsch M 1951 *Phys. Rev.* **82** 866
- [27] Dirac P A M 1930 *Proc. Camb. Phil. Soc.* **26** 361
- [28] Paul D A L and Saint-Pierre L 1963 *Phys. Rev. Lett.* **11** 493
- [29] Goldanskii V I and Sayasov Y S 1964 *Phys. Lett.* **13** 300
- [30] Smith P M and Paul D A L 1970 *Can. J. Phys.* **48** 2984
- [31] Orth P H R and Jones G 1969 *Phys. Rev.* **183** 7
- [32] McNutt J D, Summerour V B, Ray A D and Huang P H 1975 *J. Chem. Phys.* **62** 1777
- [33] Mao A C and Paul D A L 1977 *Can. J. Phys.* **55** 235
- [34] Heyland G R, Charlton M, Griffith T C and Clark G 1985 *Chem. Phys.* **95** 157
- [35] Sharma S C, Hyatt S D, Ward M H and Dark C A 1985 *J. Phys. B: At. Mol. Phys.* **18** 3245
- [36] Davies S A, Charlton M and Griffith T C 1989 *J. Phys. B: At. Mol. Opt. Phys.* **22** 327
- [37] Cherry W 1958 *PhD Thesis* Princeton University, unpublished
- [38] Groce D E, Costello D G, McGowan J W and Herring D F 1968 *Bull. Am. Phys. Soc.* **13** 1397
- [39] Canter K F, Coleman P G, Griffith T C and Heyland G R 1972 *J. Phys. B: At. Mol. Phys.* **5** L167
- [40] Lynn K G, Nielsen B and Quateman J H 1985 *Appl. Phys. Lett.* **47** 239
- [41] Mills A P Jr and Gullikson E M 1986 *Appl. Phys. Lett.* **49** 1121
- [42] Greaves R G and Surko C M 1996 *Can. J. Phys.* **51** 445
- [43] Surko C M, Gilbert S J and Greaves R G 1999 *Non-Neutral Plasma Physics III* ed J J Bollinger, R L Spencer and R C Davidson (New York: AIP) p 3
- [44] Gilbert S J, Kurz C, Greaves R G and Surko C M 1997 *Appl. Phys. Lett.* **70** 1944
- [45] Greaves R G and Surko C M 2002 *Nucl. Instrum. Methods B* **192** 90
- [46] Gilbert S J, Barnes L D, Sullivan J P and Surko C M 2002 *Phys. Rev. Lett.* **88** 043201
- [47] Barnes L D, Gilbert S J and Surko C M 2003 *Phys. Rev. A* **67** 032706
- [48] Charlton M, van der Werf D P and Al-Qaradawi I 2002 *Phys. Rev. A* **65** 042716
- [49] Laricchia G, Armitage S and Leslie D E 2004 *Nucl. Instrum. Methods B* **221** 60
- [50] Bransden B H 1969 *Case Studies in Atomic Collision Physics American* (New York: Elsevier) p 171
- [51] Dzuba V A, Flambaum V V, Gribakin G F and King W A 1995 *Phys. Rev. A* **52** 4541
- [52] Dzuba V A, Flambaum V V, Gribakin G F and King W A 1996 *J. Phys. B: At. Mol. Opt. Phys.* **29** 3151
- [53] Feynman R P 1949 *Phys. Rev.* **76** 769
- [54] Migdal A B 1967 *Theory of Finite Fermi Systems and Applications to Atomic Nuclei* (New York: Interscience)

- [55] Amusia M Y, Cherepkov N A, Chernysheva L V and Shapiro S G 1976 *J. Phys. B: At. Mol. Phys.* **9** L531
- [56] Dzuba V A, Flambaum V V, King W A, Miller B N and Sushkov O P 1993 *Phys. Scr. T* **46** 248
- [57] Gribakin G F and King W A 1994 *J. Phys. B: At. Mol. Opt. Phys.* **27** 2639
- [58] Ludlow J 2003 *PhD Thesis* Queens University, Belfast, unpublished
- [59] Ludlow J and Gribakin G F 2004 unpublished
- [60] Gribakin G F and Ludlow J 2004 *Phys. Rev. A* **70** 032720
- [61] Amusia M Y, Cherepkov N A, Chernysheva L V, Davidov D M and Radojevic V 1982 *Phys. Rev. A* **25** 219
- [62] Johnson W R and Guet C 1994 *Phys. Rev. A* **49** 1041
- [63] Johnson W R and Guet C 2001 *Phys. Rev. A* **64** 019901
- [64] Buckman S J and Mitroy J 1989 *J. Phys. B: At. Mol. Opt. Phys.* **22** 1365
- [65] Radtsig A A and Smirnov B M 1985 *Reference Data on Atoms, Molecules and Ions Chemical Physics* vol 31 (Berlin: Springer)
- [66] Miller T M 1995 *CRC Handbook of Chemistry and Physics* vol 76, ed D R Lide and H P R Frederikse (Boca Raton, FL: CRC Press) p 10
- [67] McEachran R P, Stauffer A D and Campbell L E M 1980 *J. Phys. B: At. Mol. Phys.* **13** 1281
- [68] Schwartz C 1961 *Phys. Rev.* **124** 1468
- [69] Campeanu R I and Humberston J W 1977 *J. Phys. B: At. Mol. Phys.* **10** L153
- [70] Dzuba V A, Flambaum V V, Gribakin G F and Harabati C 1999 *Phys. Rev. A* **60** 3641
- [71] Ryzhikh G G and Mitroy J 1997 *Phys. Rev. Lett.* **79** 4124
- [72] Mitroy J and Ryzhikh G G 1999 *J. Phys. B: At. Mol. Opt. Phys.* **32** L411
- [73] Mitroy J and Ivanov I A 2001 *J. Phys. B: At. Mol. Opt. Phys.* **34** L121
- [74] Bromley M W J and Mitroy J 2002 *Phys. Rev. A* **65** 062506
- [75] Temkin A 1957 *Phys. Rev. A* **107** 1004
- [76] McEachran R P, Morgan D L, Ryman A G and Stauffer A D 1977 *J. Phys. B: At. Mol. Phys.* **10** 663
- [77] McEachran R P and Stauffer A D 1983 *J. Phys. B: At. Mol. Phys.* **16** 255
- [78] Szymkowski R 1994 *Acta Phys. Pol. A* **86** 309
- [79] Humberston J W and Wallace J B G 1972 *J. Phys. B: At. Mol. Phys.* **5** 1138
- [80] Humberston J W 1973 *J. Phys. B: At. Mol. Phys.* **6** L305
- [81] Humberston J W 1982 *Can. J. Phys.* **60** 591
- [82] Brown C J and Humberston J W 1985 *J. Phys. B: At. Mol. Phys.* **18** L401
- [83] Humberston J W, Van Reeth P, Watts M S T and Meyerhof W E 1997 *J. Phys. B: At. Mol. Opt. Phys.* **30** 2477
- [84] Van Reeth P and Humberston P 1999 *J. Phys. B: At. Mol. Opt. Phys.* **32** 3651
- [85] Van Reeth P and Humberston J W 1998 *J. Phys. B: At. Mol. Opt. Phys.* **31** L231
- [86] Bhatia A K, Temkin A, Drachman R J and Eiserike H 1971 *Phys. Rev. A* **3** 1328
- [87] Bromley M W J and Mitroy J 2002 *Phys. Rev. A* **67** 062709
- [88] Novikov S A, Bromley J W J and Mitroy J 2004 *Phys. Rev. A* **69** 052702
- [89] Wakid S E A and LaBahn R W 1972 *Phys. Rev. A* **6** 2039
- [90] Higgins K and Burke P G 1991 *J. Phys. B: At. Mol. Opt. Phys.* **24** L343
- [91] McAlinden M T, Kernoghan A A and Walters H R J 1994 *Hyperfine Interact.* **89** 161
- [92] Basu M, Mukherjee M and Ghosh A S 1989 *J. Phys. B: At. Mol. Opt. Phys.* **22** 2195
- [93] Hewitt R N, Noble C J and Bransden B H 1990 *J. Phys. B: At. Mol. Opt. Phys.* **23** 4185
- [94] Mitroy J 1993 *Aust. J. Phys.* **46** 751
- [95] Higgins K and Burke P G 1993 *J. Phys. B: At. Mol. Opt. Phys.* **26** 4269
- [96] Mitroy J, Berge L and Stelbovics A T 1994 *Phys. Rev. Lett.* **73** 2966
- [97] Kernoghan A A, McAlinden M T and Walters H R J 1995 *J. Phys. B: At. Mol. Opt. Phys.* **28** 1079
- [98] Bray I and Stelbovics A T 1993 *Phys. Rev. A* **48** 4787
- [99] Kernoghan A A, McAlinden M T and Walters H R J 1996 *J. Phys. B: At. Mol. Opt. Phys.* **29** 3971
- [100] Ryzhikh G and Mitroy J 1997 *J. Phys. B: At. Mol. Opt. Phys.* **30** 5545
- [101] McAlinden M T, Kernoghan A A and Walters H R J 1996 *J. Phys. B: At. Mol. Opt. Phys.* **29** 555
- [102] Bray I and Stelbovics A T 1994 *Phys. Rev. A* **49** R2224
- [103] Campbell C P, McAlinden M T, Kernoghan A A and Walters H R J 1998 *Nucl. Instrum. Methods B* **143** 41
- [104] Wu H, Bray I, Fursa D V and Stelbovics A T 2004 *J. Phys. B: At. Mol. Opt. Phys.* **37** L1
- [105] Surdutovich E, Kauppila W E, Kwan C K, Miller E G, Parikh S P, Price K A and Stein T S 2004 *Nucl. Instrum. Methods B* **221** 97
- [106] Ivanov I A, Mitroy J and Varga K 2001 *Phys. Rev. Lett.* **87** 063201
- [107] Mitroy J and Bromley M W J 2003 *Phys. Rev. A* **67** 034502
- [108] Platzman P M and Mills A P Jr 1994 *Phys. Rev. B* **49** 454

- [109] Cassidy D B and Golovchenko J A 2001 *New Directions in Antimatter Chemistry and Physics* ed C M Surko and F A Gianturco (Dordrecht: Kluwer) p 83
- [110] Crawford O H 1967 *Proc. Phys. Soc.* **91** 279
- [111] Tachikawa M, Buenker R J and Kimura M 2003 *J. Chem. Phys.* **119** 5005
- [112] Bressanini D, Mella M and Morosi G 1998 *J. Chem. Phys.* **109** 1716
- [113] Mitroy J and Ryzhikh G G 2000 *J. Phys. B: At. Mol. Opt. Phys.* **33** 3495
- [114] Strasburger K 1999 *J. Chem. Phys.* **111** 10555
- [115] Kurtz H A and Jordan K D 1981 *J. Chem. Phys.* **72** 493
- [116] Armour E A G 1988 *Phys. Rep.* **169** 1
- [117] Armour E A G, Baker D J and Plummer M 1990 *J. Phys. B: At. Mol. Opt. Phys.* **23** 3057
- [118] Danby G and Tennyson J 1990 *J. Phys. B: At. Mol. Opt. Phys.* **23** 1005
- [119] Armour E A G and Plummer M 1991 *J. Phys. B: At. Mol. Opt. Phys.* **24** 4463
- [120] Danby G and Tennyson J 1991 *J. Phys. B: At. Mol. Opt. Phys.* **24** 3517
- [121] Germano J S E and Lima M A P 1993 *Phys. Rev. A* **47** 3976
- [122] daSilva E P, Germano J S E and Lima M A P 1996 *Phys. Rev. Lett.* **77** 1028
- [123] deCarvalho C R C, Varella M T do N, Lima A P, daSilva E P and Germano J S E 2000 *Nucl. Instrum. Methods B* **171** 33
- [124] Sanchez S d A, Arretche F, Varella M T do N and Lima M A P 2004 *Phys. Scr. T* **110** 276
- [125] Lino J L S, Germano J S E and Lima M A P 1994 *J. Phys. B: At. Mol. Opt. Phys.* **27** 1881
- [126] Chadhuri P, Varella M T do N, deCarvalho C R C and Lima M A P 2004 *Nucl. Instrum. Methods B* **221** 69
- [127] daSilva E P, Germano J S E and Lima M A P 1994 *Phys. Rev. A* **49** R1527
- [128] Lino J L S, Germano J S E, daSilva E P and Lima M A P 1998 *Phys. Rev. A* **58** 3502
- [129] Carvalho C R C, Varella M T do N and Lima M A P 2003 *Phys. Rev. A* **67** 062706
- [130] Jain A and Thompson D G 1983 *J. Phys. B: At. Mol. Opt. Phys.* **16** 1113
- [131] Jain A 1990 *J. Phys. B: At. Mol. Opt. Phys.* **23** 863
- [132] Jain A and Gianturco F A 1991 *J. Phys. B: At. Mol. Opt. Phys.* **24** 2387
- [133] Gianturco F A, Mukherjee T and Occhigrossi A 2001 *Phys. Rev. A* **64** 032715/1
- [134] Occhigrossi A and Gianturco F A 2003 *J. Phys. B: At. Mol. Opt. Phys.* **36** 1383
- [135] Gianturco F A, Mukherjee T and Paoletti P 1997 *Phys. Rev. A* **56** 3638
- [136] Gianturco F A, Mukherjee T and Paoletti P 1997 *Phys. Rev. A* **55** 1044
- [137] Kimura M, Takekawa M, Itakawa Y, Takaki H and Sueoka O 1998 *Phys. Rev. Lett.* **80** 3936
- [138] Connerade J P and Ipatov A 1998 *J. Phys. B: At. Mol. Opt. Phys.* **31** L273
- [139] Gianturco F A and Lucchese R R 1999 *Phys. Rev. A* **60** 4567
- [140] Berestetskii V B, Lifshitz E M and Pitaevskii L P 1982 *Quantum Electrodynamics* (Oxford: Pergamon)
- [141] Fraser P A 1968 *Adv. At. Mol. Phys.* **4** 63
- [142] Mitroy J and Ivanov I A 2002 *Phys. Rev. A* **65** 042705
- [143] Igarashi A, Kimura M and Shimamura I 2002 *Phys. Rev. Lett.* **89** 123201
- [144] Igarashi A, Kimura M, Shimamura I and Toshima N 2003 *Phys. Rev. A* **68** 042716
- [145] Ludlow J and Gribakin G F 2002 *Phys. Rev. A* **66** 012713
- [146] Heyland G R, Charlton M, Griffith T C and Wright G L 1982 *Can. J. Phys.* **60** 503
- [147] Surko C M, Passner A, Leventhal M and Wysocki F J 1988 *Phys. Rev. Lett.* **61** 1831
- [148] Iwata K, Greaves R G, Murphy T J, Tinkle M D and Surko C M 1995 *Phys. Rev. A* **51** 473
- [149] Coleman P G, Griffith T C, Heyland G R and Killeen T L 1975 *J. Phys. B: At. Mol. Phys.* **8** 1734
- [150] Wright G L, Charlton M, Griffith T C and Heyland G R 1985 *J. Phys. B: At. Mol. Phys.* **18** 4327
- [151] Van Reeth P, Humberston J W, Iwata K, Greaves R G and Surko C M 1996 *J. Phys. B: At. Mol. Opt. Phys.* **29** L465
- [152] Gribakin G F 2000 *Phys. Rev. A* **61** 22720
- [153] Humberston J W 1979 *Adv. At. Mol. Opt. Phys.* **15** 101
- [154] Griffith T C 1986 *Adv. At. Mol. Opt. Phys.* **22** 37
- [155] Ryzhikh G G and Mitroy J 2000 *J. Phys. B: At. Mol. Opt. Phys.* **33** 2229
- [156] Gribakin G 2001 *New Directions in Antimatter Chemistry and Physics* ed Surko C M and Gianturco F A (Dordrecht: Kluwer) p 366
- [157] Laricchia G, Charlton M, Beling C D and Griffith T C 1987 *J. Phys. B: At. Mol. Phys.* **20** 1865
- [158] Armour E A G and Baker D J 1986 *J. Phys. B: At. Mol. Phys.* **19** L871
- [159] Varella M T N, deCarvalho C R C and Lima M A P 2002 *Nucl. Instrum. Methods B* **192** 225
- [160] Gianturco F A and Mukherjee T 1999 *Euro Phys. Lett.* **48** 519
- [161] Gianturco F A and Mukherjee T 2000 *Nucl. Instrum. Methods B* **171** 17
- [162] Gribakin G F and Gill P M W 2004 *Nucl. Instrum. Methods B* **221** 30

- [163] Gribakin G F 2002 *Nucl. Instrum. Methods B* **192** 26
- [164] Nishimura T and Gianturco F A 2003 *Phys. Rev. Lett.* **90** 183201
- [165] Hotop H, Ruf M-W, Allan M and Fabrikant I I 2003 *Adv. At. Mol. Opt. Phys.* **49** 85
- [166] Mills A P Jr 1995 *Atomic, Molecular and Optical Physics: Charged Particles* ed F B Dunning and R G Hunt (New York: Academic) p 39
- [167] Krause-Rehberg R, van der Walt N, Buttner L and Borner F 2004 *Nucl. Instrum. Methods B* **221** 165
- [168] Hirose M, Washio M and Takahashi K 1995 *Appl. Surf. Sci.* **85** 111
- [169] Saito F *et al* 2000 *Nucl. Instrum. Methods A* **450** 491
- [170] Fujiwara I, Itoh Y, Iwata R, Saito F and Goto A 1999 *Appl. Surf. Sci.* **149** 30
- [171] Hunt A W, Pilant L, Cassidy D B, Tjossem R, Shurtliff M, Weber M H and Lynn K G 2002 *Appl. Surf. Sci.* **194** 296
- [172] Howell R H, Rosenberg I J and Fluss M J 1987 *Appl. Phys. A* **43** 247
- [173] Hugenschmidt C, Kogel G, Repper R, Schreckenbach K, Sperr P and Triftshauser W 2002 *Nucl. Instrum. Methods B* **198** 220
- [174] Stein T S, Kauppila W E and Roellig L O 1974 *Rev. Sci. Instrum.* **45** 951
- [175] Charlton M 1985 *Rep. Prog. Phys.* **48** 737
- [176] Hyder G M A, Dababneh M S, Hsieh Y-F, Kauppila W E, Kwan C K, Mahdavi-Hezadeh M and Stein T S 1986 *Phys. Rev. Lett.* **57** 2252
- [177] Floeder K, Honer P, Raith W, Schwab A, Sinapius G and Spicher G 1988 *Phys. Rev. Lett.* **60** 2363
- [178] Kover A, Laricchia G and Charlton M 1994 *J. Phys. B: At. Mol. Opt. Phys.* **27** 2409
- [179] Gao H, Garner A J, Moxom J, Laricchia G and Kover A 1998 *Nucl. Instrum. Methods B* **143** 184
- [180] Bluhme H, Knudsen H, Merrison J P and Nielsen K A 1999 *J. Phys. B: At. Mol. Opt. Phys.* **32** 5237
- [181] Bluhme H, Knudsen H, Merrison J P and Nielsen K A 1999 *J. Phys. B: At. Mol. Opt. Phys.* **32** 5835
- [182] Bluhme H, Frandsen N P, Jacobsen F M, Knudsen H, Merrison J P, Mitchell R, Paludan K and Poulsen M R 1999 *J. Phys. B: At. Mol. Opt. Phys.* **32** 5825
- [183] Kimura M, Sueoka O, Hamada A and Itikawa Y 2000 *Adv. Chem. Phys.* **111** 537
- [184] Sueoka O, Mori S and Hamada A 1994 *J. Phys. B: At. Mol. Opt. Phys.* **27** 1453
- [185] Kimura M, Sueoka O, Makochekanwa C, Kawate H and Kawada M 2001 *J. Chem. Phys.* **115** 7442
- [186] Hoffman K R, Dababneh M S, Hsieh Y, Kauppila W E, Smart J H and Stein T S 1982 *Phys. Rev. A* **25** 1393
- [187] Kwan C K, Kauppila W E, Lukaszew R A, Parikh S P, Stein T S, Wan Y J and Dababneh M S 1991 *Phys. Rev. A* **44** 1620
- [188] Parikh S P, Kauppila W E, Kwan C K, Lukaszew R A, Stein T S and Zhou S 1993 *Phys. Rev. A* **47** 1535
- [189] Zhou S, Kauppila W E, Kwan C K and Stein T S 1994 *Phys. Rev. Lett.* **72** 1443
- [190] Zhou S, Li H, Kauppila W E, Kwan C K and Stein T S 1997 *Phys. Rev. A* **55** 361
- [191] Zecca A, Karwasz G, Brusa R S and Grisenti R 1991 *J. Phys. B: At. Mol. Opt. Phys.* **24** 2737
- [192] Coleman P G and McNutt J D 1979 *Phys. Rev. Lett.* **42** 1130
- [193] Dou L, Kauppila W E, Kwan C K and Stein T S 1992 *Phys. Rev. Lett.* **68** 2913
- [194] Gao H, Garner A J, Moxom J, Laricchia G and Kover A 1999 *J. Phys. B: At. Mol. Opt. Phys.* **32** L693
- [195] Griffith T C, Heyland G R, Lines K S and Twomey T R 1979 *J. Phys. B: At. Mol. Phys.* **12** L747
- [196] Coleman P G and Hutton J T 1980 *Phys. Rev. Lett.* **45** 2017
- [197] Katayama Y, Sueoka O and Mori S 1987 *J. Phys. B: At. Mol. Phys.* **20** 1645
- [198] Mori S and Sueoka O 1994 *J. Phys. B: At. Mol. Opt. Phys.* **27** 4349
- [199] Kawada M I, Sueoka O and Kimura M 2000 *J. Chem. Phys.* **112** 7057
- [200] Charlton M, Griffith T C, Heyland G R, Lines K S and Wright G L 1980 *J. Phys. B: At. Mol. Phys.* **13** L757
- [201] Charlton M, Clark G, Griffith T C and Heyland G R 1983 *J. Phys. B: At. Mol. Phys.* **16** L465
- [202] Fornari L S, Diana L M and Coleman P G 1983 *Phys. Rev. Lett.* **51** 2276
- [203] Diana L M, Coleman P G, Brooks D L, Pendleton P K and Norman D M 1986 *Phys. Rev. A* **34** 2731
- [204] Fromme D, Kruse G, Raith W and Sinapius G 1986 *Phys. Rev. Lett.* **57** 3031
- [205] Sperber W, Becker D, Lynn K G, Raith W, Schwab A, Sinapius G, Spicher G and Weber M 1992 *Phys. Rev. Lett.* **68** 3690
- [206] Stein T S, Harte M, Jiang J, Kauppila W E, Kwan C K, Li H and Zhou S 1998 *Nucl. Instrum. Methods B* **143** 68
- [207] Laricchia G, Van Reeth P, Szluinska M and Moxom J 2002 *J. Phys. B: At. Mol. Opt. Phys.* **35** 2525
- [208] Moxom J, Laricchia G and Charlton M 1995 *J. Phys. B: At. Mol. Opt. Phys.* **28** 1331
- [209] Sueoka O 1982 *J. Phys. Soc. Japan* **51** 3757
- [210] Spicher G, Olsson B, Raith W, Sinapius G and Sperber W 1990 *Phys. Rev. Lett.* **64** 1019
- [211] Jones G O, Charlton M, Slevin J, Laricchia G, Kover A, Poulsen M R and Chormaic S N 1993 *J. Phys. B: At. Mol. Opt. Phys.* **26** L483

- [212] Weber M, Hofmann A, Raith W, Sperber W, Jacobsen F M and Lynn K G 1994 *Hyperfine Interact.* **89** 221
- [213] Hofmann A, Falke T, Raith W, Weber M, Becker D and Lynn K G 1997 *J. Phys. B: At. Mol. Opt. Phys.* **30** 3297
- [214] Kruse G, Quermann A, Raith W, Sinapius G and Weber M 1991 *J. Phys. B: At. Mol. Opt. Phys.* **24** L33
- [215] Moxom J, Laricchia G and Charlton M 1993 *J. Phys. B: At. Mol. Opt. Phys.* **26** L367
- [216] Jacobsen F M, Frandsen N P, Knudsen H, Mikkelsen U and Schrader D M 1995 *J. Phys. B: At. Mol. Opt. Phys.* **28** 4691
- [217] Kara V, Paludan K, Moxom J, Ashley P and Laricchia G 1997 *J. Phys. B: At. Mol. Opt. Phys.* **30** 3933
- [218] Paludan K *et al* 1997 *J. Phys. B: At. Mol. Opt. Phys.* **30** L581
- [219] Kover A, Finch R M, Charlton M and Laricchia G 1997 *J. Phys. B: At. Mol. Opt. Phys.* **30** L507
- [220] Moxom J, Schrader D M, Laricchia G, Xu L and Hulett L D 1999 *Phys. Rev. A* **60** 2940
- [221] Kover A, Paludan K and Laricchia G 2001 *J. Phys. B: At. Mol. Opt. Phys.* **34** L219
- [222] Bluhme H, Frandsen N P, Jacobsen F M, Knudsen H, Merrison J P, Paludan K and Poulsen M R 1998 *J. Phys. B: At. Mol. Opt. Phys.* **31** 4631
- [223] Moxom J, Schrader D M, Laricchia G, Xu J and Hulett L D 2000 *Phys. Rev. A* **62** 052708
- [224] Murphy T J and Surko C M 1991 *Phys. Rev. Lett.* **67** 2954
- [225] Sullivan J P, Marler J P, Gilbert S J, Buckman S J and Surko C M 2001 *Phys. Rev. Lett.* **87** 073201
- [226] Greaves R G and Surko C M 2000 *Phys. Rev. Lett.* **85** 1883
- [227] Gilbert S J, Greaves R G and Surko C M 1999 *Phys. Rev. Lett.* **82** 5032
- [228] Sullivan J P, Gilbert S J, Marler J P, Greaves R G, Buckman S J and Surko C M 2002 *Phys. Rev. A* **66** 042708
- [229] Sullivan J, Gilbert S J and Surko C M 2001 *Phys. Rev. Lett.* **86** 1494
- [230] Young J *et al* unpublished
- [231] Gribakin G F and Ludlow J 2002 *Phys. Rev. Lett.* **88** 163202
- [232] Deutsch M 1951 *Phys. Rev.* **83** 455
- [233] Coleman P G, Griffith T C, Heyland G R and Killeen T L 1974 *Appl. Phys.* **3** 271
- [234] MacKenzie I K 1983 *Positron Solid-State Physics, Proc. Int. School of Physics 'Enrico Fermi' Course 83* ed W Brandt and A Dupasquier (Amsterdam: North-Holland) p 196
- [235] Rutenberg A H, Tawel R and Canter K F 1985 *Solid State Commun.* **53** 63
- [236] Tawel R and Canter K F 1986 *Phys. Rev. Lett.* **56** 2322
- [237] Heinberg M and Page L A 1957 *Phys. Rev.* **107** 1589
- [238] Coleman P G, Rayner S, Jacobsen F M, Charlton M and West R N 1994 *J. Phys. B: At. Mol. Opt. Phys.* **27** 981
- [239] Iwata K, Greaves R G and Surko C M 1997 *Phys. Rev. A* **55** 3586
- [240] Iwata K, Gribakin G F, Greaves R G, Kurz C and Surko C M 2000 *Phys. Rev. A* **61** 022719
- [241] Kurz C, Greaves R G and Surko C M 1996 *Phys. Rev. Lett.* **77** 2929
- [242] Tang S, Tinkle M D, Greaves R G and Surko C M 1992 *Phys. Rev. Lett.* **68** 3793
- [243] Iwata K, Gribakin G F, Greaves R G and Surko C M 1997 *Phys. Rev. Lett.* **79** 39
- [244] Stein T S, Jiang J, Kauppila W E, Kwan C K, Li H, Surdutovich A and Zhou S 1996 *Can. J. Phys.* **74** 313
- [245] Kadyrov A S and Bray I 2002 *Phys. Rev. A* **66** 012710
- [246] Bray I and Stelbovics A T 1992 *Phys. Rev. A* **46** 6995
- [247] Mitroy J 1995 *J. Phys. B: At. Mol. Opt. Phys.* **28** 645
- [248] Mitroy J 1996 *Aust. J. Phys.* **49** 919
- [249] Mizogawa T, Nakayama Y and Karawatani T 1985 *Phys. Rev. Lett.* **31** 2171
- [250] Sullivan J P, Gilbert S J, Buckman S J and Surko C M 2001 *J. Phys. B: At. Mol. Opt. Phys.* **34** L467
- [251] Karwasz G P, Barozzi M, Brusa R S and Zecca A 2002 *Nucl. Instrum. Methods B* **192** 157
- [252] McEachran R P, Ryman A G and Stauffer A D 1979 *J. Phys. B: At. Mol. Phys.* **12** 1031
- [253] Gibson J C, Gulley R J, Sullivan J P, Buckman S J, Chan V and Burrow P D 1996 *J. Phys. B: At. Mol. Opt. Phys.* **29** 3177
- [254] Marler J Private communication
- [255] Gibson J C, Lun D R, Allen L J, McEachran R P, Parcell L A and Buckman S J 1998 *J. Phys. B: At. Mol. Opt. Phys.* **31** 3949
- [256] McEachran R 2001 Private communication
- [257] Sullivan J P, Gilbert S J, Marler J P, Barnes L D, Buckman S J and Surko C M 2002 *Nucl. Instrum. Methods B* **192** 3
- [258] Gibson T L 1992 *J. Phys. B: At. Mol. Opt. Phys.* **25** 1321
- [259] Przybyla D A, Addo-Asah W, Kauppila W E, Kwan C K and Stein T S 1999 *Phys. Rev. A* **60** 359
- [260] Jain A 1986 *J. Phys. B: At. Mol. Phys.* **19** L379
- [261] Gibson J C, Morgan L A, Gulley R J, Brunger M J, Bundschu C T and Buckman S J 1996 *J. Phys. B: At. Mol. Opt. Phys.* **29** 3197



- [262] Sullivan J P, Marler J P, Buckman S J and Surko C M unpublished
- [263] Campbell L *et al* 2001 *J. Phys. B: At. Mol. Opt. Phys.* **34** 1185
- [264] Chaudhuri P, Varella M T do N, deCarvalho C R C and Lima M A P 2004 *Phys. Rev. A* **69** 042703
- [265] Khakoo M and Trajmar S 1986 *Phys. Rev. A* **34** 146
- [266] Mukherjee T, Sur S and Ghosh A 1991 *J. Phys. B: At. Mol. Opt. Phys.* **24** 1449
- [267] Coleman P G, Hutton J T, Cook D R and Chandler C A 1982 *Can. J. Phys.* **60** 584
- [268] McEachran R P and Stauffer A D 2002 *Phys. Rev. A* **65** 034703
- [269] Parcell L A, McEachran R P and Stauffer A D 2000 *Nucl. Instrum. Methods B* 171
- [270] Campeanu R I, McEachran R P and Stauffer A D 2002 *Nucl. Instrum. Methods B* **192** 146
- [271] Campeanu R I, Nagy L and Stauffer A D 2003 *Can. J. Phys.* **81** 919
- [272] Marler J P, Sullivan J P and Surko C M 2004 *Phys. Rev. A* **71** 022701
- [273] Knudsen H, Brum-Nielsen L, Charlton M and Poulsen M R 1990 *J. Phys. B: At. Mol. Opt. Phys.* **23** 3955
- [274] Jin B, Miyamoto S, Sueoka O and Hamada A 1994 *At. Collision Res. Japan* **20** 9
- [275] Diana L M 1985 *Positron Annihilation* ed P Jain, R M Singru and K P Gopinathan (Singapore: World Scientific) p 428
- [276] Diana L M, Coleman P G, Brooks D L, Pendleton P K and Norman D M 1986 *Positron (Electron)—Gas Scattering* ed W E Kauppila, T S Stein and J Wadehra (Singapore: World Scientific) p 296
- [277] Diana L M, Coleman P G, Brooks D L and Chaplin R L 1987 *Atomic Physics with Positrons* ed J W Humberston and E A G Armour (New York: Plenum) p 55
- [278] Diana L M, Brooks D L, Coleman P G, Chaplin R L and Howell J P 1989 *Positron Annihilation* ed L Dorokins-Vanpraet, M Dorikins and D Segers (Singapore: World Scientific) p 311
- [279] McAlinden M T and Walters H R J 1992 *Hyperfine Interact.* **73** 65
- [280] Marler J, Barnes L D, Gilbert S J, Sullivan J P, Young J A and Surko C M 2004 *Nucl. Instrum. Methods B* **221** 84
- [281] Barnes L D, Marler J P, Sullivan J P and Surko C M 2004 *Phys. Scr. T* **110** 280
- [282] Gilmore S, Blackwood J E and Walters H R J 2004 *Nucl. Instrum. Methods B* **221** 129
- [283] Zhou S, Parikh S P, Kauppila W E, Kwan C K, Lin D, Surdutovich A and Stein T S 1994 *Phys. Rev. Lett.* **73** 236
- [284] Surdutovich E, Johnson J M, Kauppila W E, Kwan C K and Stein T S 2002 *Phys. Rev. A* **65** 032713
- [285] Surdutovich A, Jian J, Kauppila W E, Kwan C K, Stein T S and Zhou S 1996 *Phys. Rev. A* **53** 2861
- [286] Surdutovich E, Harte M, Kauppila W E, Kwan C K and Stein T S 2003 *Phys. Rev. A* **68** 022709
- [287] Hewitt R N, Noble C J, Bransden B H and Joachain C J 1996 *Can. J. Phys.* **74** 559
- [288] Gribakin G F and King W A 1996 *Can. J. Phys.* **74** 449
- [289] Murphy T J and Surko C M 1990 *J. Phys. B: At. Mol. Opt. Phys.* **23** L727
- [290] McEachran R P, Ryman A G and Stauffer A D 1978 *J. Phys. B: At. Mol. Phys.* **11** 551
- [291] Weiss A, Mayer R, Jibaly M, Lei C, Mehl D and Lynn K G 1988 *Phys. Rev. Lett.* **61** 2245
- [292] Barnes L D 2005 *PhD Thesis* University of California, San Diego, unpublished
- [293] Passner A, Surko C M, Leventhal M and Mills A P J 1989 *Phys. Rev. A* **39** 3706
- [294] Glish G L, Greaves R G, McLuckey S A, Hulett L D, Surko C M, Xu J and Donohue D L 1994 *Phys. Rev. A* **49** 2389
- [295] Donohue D L, Hulett L D Jr, Eckenrode B A, McLuckey S A and Glish G L 1990 *Chem. Phys. Lett.* **168** 37
- [296] Xu J, Hulett L D Jr, Lewis T A, Donohue D L, McLuckey S A and Glish G L 1993 *Phys. Rev. A* **47** 1023
- [297] Xu J, Hulett L D, Lewis T A, Donohue D L, McLuckey S A and Crawford O H 1994 *Phys. Rev. A* **49** R3151
- [298] Xu J, Hulett L D Jr, Lewis T A and McLuckey S A 1995 *Phys. Rev. A* **52** 2088
- [299] Crawford O H 1994 *Phys. Rev. A* **49** R3147